AD-A255 001

②

COMPACT BLUE-GREEN LASERS

S DTIC
ELECTE
AUG 12 1992
A D

Sponsored by
Air Force Office of Scientific Research
National Science Foundation

For
Optical Society of America

In cooperation with
IEEE Lasers and Electro-Optics Society

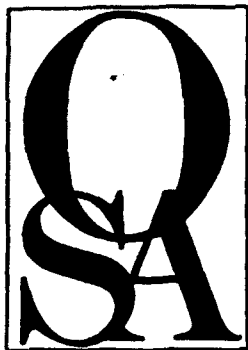992 TECHNICAL DIGEST
ERIES VOLUME 6

FEBRUARY 20–21, 1992
SANTA FE, NEW MEXICO

92   8   7   104

92-22466

392813   1793

Compact Blue-Green Lasers

Summaries of papers presented at the
Compact Blue-Green Lasers Topical Meeting

February 20–21, 1992
Santa Fe, New Mexico

1992 Technical Digest Series
Volume 6

CONFERENCE EDITION

DTIC QUALITY INSPECTED 5

Accesion For

NTIS CRA&I	☑	
DTIC TAB	☐	
Unannounced	☐	
Justification		

By

Distribution /

Availability Codes

Dist	Avail and/or Special
A-1	

Articles in this publication may be cited in other publications. In order to facilitate access to the original publication source, the following form for the citation is suggested:

Name of Author(s), "Title of Paper," in Compact Blue-Green Lasers Technical Digest, 1992 (Optical Society of America, Washington, D.C., 1992), Vol. 6, pp. xx–xx.

REPORT DOCUMENTATION PAGE

Public reporting burden for this collection of information is estimated to average 1 hour per response, including the time for reviewing instructions, searching existing data sources, gathering and maintaining the data needed, and completing and reviewing the collection of information. Send comments regarding this burden estimate or any other aspect of this collection of information, including suggestions for reducing this burden, to Washington Headquarters Services, Directorate for Information Operations and Reports, 1215 Jefferson Davis Highway, Suite 1204, Arlington, VA 22202-4302. and to the Office of Management and Budget, Paperwork Reduction Project (0704-0188). Washington, DC 20503.

1. AGENCY USE ONLY (Leave blank)	2. REPORT DATE	3. REPORT TYPE AND DATES COVERED
		Quarterly 19 Feb - 12 Feb 92

4. TITLE AND SUBTITLE

COMPACT BLUE-GREEN LASER

5. FUNDING NUMBERS

F49620-92-J-0264

6. AUTHOR(S)

Dr Quinn

7. PERFORMING ORGANIZATION NAME(S) AND ADDRESS(ES)

Optical Society of America
2010 Massachusetts Ave N. W.
Washington, DC 20036

AFOSR-TR·

8. PERFORMING ORGANIZATION REPORT NUMBER

92 0736

9. SPONSORING/MONITORING AGENCY NAME(S) AND ADDRESS(ES)

AFOSR/NE
Bldg 410
Bolling AFB, DC 20332-6448

10. SPONSORING/MONITORING AGENCY REPORT NUMBER

2301/AS

11. SUPPLEMENTARY NOTES

12a. DISTRIBUTION/AVAILABILITY STATEMENT

UNLIMITED

12b. DISTRIBUTION CODE

13. ABSTRACT (Maximum 200 words)

CONFERENCE WAS HELD

14. SUBJECT TERMS

15. NUMBER OF PAGES

16. PRICE CODE

17. SECURITY CLASSIFICATION OF REPORT	18. SECURITY CLASSIFICATION OF THIS PAGE	19. SECURITY CLASSIFICATION OF ABSTRACT	20. LIMITATION OF ABSTRACT
UNCLASS	UNCLASS	UNCLASS	UL.

Standard Form 298 (Rev. 2-89)

CONTENTS

ANASAZI NORTH

7:15 am–8:25 am BREAKFAST

CONCOURSE

7:30 am–7:30 pm REGISTRATION/SPEAKER CHECK-IN

ANASAZI SOUTH

8:30 am–10:00 am
ThA, APPLICATIONS
Donald L. Sipes, *Amoco Laser Co., Presider*

8:30 am—ThA1 (Invited)
Application of blue–green diode laser sources to optical recording, Donald B. Carlin, *David Sarnoff Research Center.* The performance characteristics required of blue–green diode laser sources for application in optical data storage systems are discussed. (p. 2)

9:00 am—ThA2 (Invited)
Lasers in flow cytometry and biotechnology, Larry A. Sklar, *Los Alamos National Laboratory.* Flow cytometry and various fluorescent analytical techniques are widely based, laser-dependent technologies with clinical and basic science applications. The instrumentation takes advantage of laser lines spanning the ultraviolet, visible, and near infrared. I discuss prospects for laser developments and their importance in future directions of flow cytometry and biotechnology. (p. 5)

9:30 am—ThA3 (Invited)
Compact visible lasers in reprographics, James C. Owens, *Eastman Kodak Company.* This review outlines the system requirements for visible lasers and their advantages and problems, for a wide variety of hard-copy electronic imaging applications. (p. 8)

10:00 am–10:30 am COFFEE BREAK

ANASAZI SOUTH

10:30 am–12:00 m
ThB, IR PUMPED VISIBLE LASERS
Jeff Dixon, *University of Central Florida/CREOL, Presider*

10:30 am—ThB1 (Invited)
Visible upconversion fiber lasers, Anne C. Tropper, *Univ. Southampton, U.K.* Fluorozirconate glass fiber is an advantageous upconversion laser host. Praseodymium-doped fluoride fiber has operated as a blue-green laser pumped at diode-compatible infrared wavelengths. (p. 12)

11:00 am—ThB2 (Invited)
Bulk crystal upconversion lasers, William F. Krupke, *Lawrence Livermore National Laboratory.* Prompted by recent achievements, research on upconversion lasers using impurity doped bulk crystals is accelerating. These advances are critically reviewed, and research trends are described. (p. 14)

11:30 am—ThB3
Tm^{3+} room temperature upconversion laser, R. J. Thrash, *Amoco Technology Company;* L. F. Johnson, *Laser Consulting.* Room temperature upconversion laser operation from Tm^{3+} at 455, 510, 649, and 799 nm has been observed. The transition at 649 nm can run cw and has been diode laser pumped. (p. 17)

11:45 am—ThB4 (Invited)
Rare-earth-doped waveguide devices: the potential for compact blue–green lasers, N. A. Sanford, K. J. Malone, D. R. Larson, M. J. McCollum, *National Institute of Standards and Technology.* Rare-earth-doped channel waveguide devices have been demonstrated to lase in the infrared. The possibility for upconversion visible lasing is also being explored. (p. 20)

12:00 m–1:30 pm LUNCH (on your own)

ANASAZI SOUTH

1:30 pm–3:00 pm
ThC, BLUE–GREEN DIODE EMITTERS
Peter S. Zory, *University of Florida, Presider*

1:30 pm—ThC1 (Invited)
II–VI blue–green diode lasers, Jim DePuydt, *3M Company.* Our recent demonstration of blue–green laser diodes from wide band gap II–VI semiconductors introduces a new era of laser research. Devices emitting at 490–535 nm have been operated in the pulsed mode up to room temperature. I review the development of these devices and present the current status of II–VI laser diodes and obstacles that must be overcome before cw, room-temperature operation can be realized. (p. 22)

2:00 pm—ThC2 (Invited)
Blue–green semiconductor LED/laser work in Japan, Hiroshi Kukimoto, *Tokyo Institute of Technology, Japan.* Current research in Japan on the wide-gap materials for blue–green LEDs and lasers is reviewed with emphasis on the growth of high-quality layers, impurity doping, and device applications. (p. 25)

2:30 pm—ThC3
Versatile blue–green laser diodes and LEDs in ZnSe-based quantum wells, H. Jeon, J. Ding, A. V. Nurmikko, *Brown Univ.;* W. Xie, D. Grillo, M. Kobayashi, R. L. Gunshor, *Purdue Univ.* Diode laser action in the blue–green up to room temperature has been achieved in strained (Zn, Cd)Se/ZnSe single and multiple quantum wells of a number of different designs. High pulsed output powers (>0.5 W) and external differential quantum efficiencies (60%) are especially evident at lower temperatures where excitonic component to gain dominates, allowing, for example, picosecond pulse generation. (p. 28)

2:45 pm—ThC4
Perspective of GaN/GaAlN based ultraviolet/blue lasers, H. Amano, I. Akasaki, K. Itoh, H. Murakami, *Nagoya Univ., Japan.* GaN/GaAlN heterostructures are promising for the realization of UV/blue lasers. Results on the fabricated P-$Ga_{0.9}Al_{0.1}N/n$ – $GaN/Ga_{0.9}Al_{0.1}N/n$ – GaN double heterostructures or P-$Ga_{0.9}Al_{0.1}GaN/n$ – GaN/N – $Ga_{0.95}Al_{0.05}N/$ N-$Ga_{0.9}Al_{0.1}N/n$ – GaN separate confinement heterostructures are discussed. (p. 32)

3:00 pm-3:30 pm   COFFEE BREAK

ANASAZI SOUTH

3:30 pm-5:30 pm
ThD, MATERIALS
John D. Bierlein, *E. I. du Pont de Nemours & Co., Presider*

3:30 pm—ThD1   (Invited)
Inorganic crystals for frequency conversion, Peter Bordui, *Crystal Technology, Inc.* Bulk inorganic crystals, including KTP, $KNbO_3$, $Mg:LiNbO_3$, and periodically poled $LiNbO_3$, are known to offer attractive potential for frequency conversion devices. Although problems remain, significant progress has been made in developing these materials for practical application. (p. 36)

4:00 pm—ThD2   (Invited)
Organic nonlinear materials for frequency conversion: property trade-off and recent applications, L.-T. Cheng, *E. I. du Pont de Nemours & Co., Inc.* Structure-property trends that govern the quadratic optical polarizabilities of donor-acceptor-substituted conjugated organic molecules are summarized. Nonlinearity and transparency trade-off and its implication on material availability for frequency conversion are highlighted. Molecular designs, microscopic organizational approaches, phase-matching schemes, and recent frequency conversion experiments are reviewed. (p. 37)

4:30 pm—ThD3
Large second-order nonlinearity in poled fused silica, R. A. Myers, N. Mukherjee, S. R. J. Brueck, *Univ. New Mexico.* A large second-order $\chi^{(2)}$ nonlinearity, comparable to that of $LiNbO_3$, is induced in fused silica by a temperature and electric field process. Potential applications are discussed. (p. 41)

4:45 pm—ThD4
Self-frequency-doubled high δn proton exchange Nd:LiNbO₃ waveguide lasers, Q. He, M. P. De Micheli, D. B. Ostrowsky, *Univ. Nice, France;* E. Lallier, J. P Pocholle, M. Papuchon, F. Armani, D. Delacourt, *Thomson-CSF, Laboratoire Centrale de Recherches, France;* C. Grezes-Besset, E. Pelletier, *Domaine Univ. Saint Jerome, France.* We report the realization of the first self-frequency-doubled waveguide laser. The structure is based on a high δn proton exchange waveguide in Z-cut Nd:MgO:LiNbO₃. (p. 44)

5:00 pm—ThD5
Periodically poled lithium niobate crystals for efficient frequency-doubling, D. H. Jundt, M. M. Fejer, R. L. Byer, *Stanford Univ.* Periodically poled lithium miobate with periods as short as 2 μm has been grown by laser-heated pedestal growth, suitable for quasi-phase-matching (QPM) frequency doubling. A conversion efficiency of 65% was achieved in a 1.25-mm-long sample at 532 nm. (p. 47)

5:15 pm—ThD6
High-efficiency frequency doubling around 430 nm, E. S. Polzik, H. J. Kimble, *California Institute of Technology.* Conversion efficiency of 70% has been demonstrated for cw frequency doubling in potassium niobate. Cw blue power up to 0.65 W has been achieved. (p. 50)

ANASAZI NORTH

6:00 pm-7:30 pm
ThE, POSTER SESSION/POSTDEADLINE PAPERS

ThE1
Narrow band iso-index filters for blue-green laser communications, Roger F. Belt, Mark Randles, John Creamer, *Litton Systems, Inc.;* Oscar M. Stafsudd, *UC-Los Angeles.* Single crystals of β-Al_2O_3 ($Na_2$0.11 Al_2O_3) were grown by the Czochralski method. Ion exchange of Na^+ with other ions after growth modifies the refractive index. These materials permit construction of iso-index filters for fixed laser sources. (p. 54)

ThE2
Application of blue-green lasers to high data rate underwater communications, Judith B. Snow, Jacob R. Longacre, *Naval Underwater Systems Center.* Advances in blue-green lasers make high data rate underwater laser communications feasible, but system capabilities are strongly dependent on characteristics of the marine environment. (p. 57)

ThE3
Characteristics of ZnSe light-emitting diodes as a function of temperature, Y. Guan, L. Calhoun, R. M. Park, P. S. Zory, *Univ. Florida.* Temperature dependence of the electroluminescence and current-voltage characteristics of ZnSe homojunction light-emitting diodes in the temperature range of 80-300 K. (p. 60)

ThE4
Two-dimensional modal analysis of blue-green lasers using ZnSe-based p-n and metal-insulator-semiconductor (MIS) heterostructures, C. Chung, F. Jain, *Univ. Connecticut.* The modal analysis of p-n double-heterojunction and MIS laser structures using ZnSe-ZnSSe and ZnSe-ZnCdSe systems is presented. Confinement factor Γ and threshold current density J_{TH} are computed. Injection luminescence data of MIS devices at high current densities is also presented. (p. 63)

ThE5
High peak and average power diode-pumped NYAB green laser, R. E. Stone, S. C. Wang, *Lockheed Palo Alto Research Laboratory.* We report a diode-pumped NYAB green laser with a peak output power of 55 W and an average power of 30 mW under Q-switched and cw operations. (p. 66)

ThE6
Diode-pumped self-doubling laser of modified neodymium yttrium aluminum borate crystal, Yujing Huo, Jinxing Cai, Qinqing Zhang, Bingkun Zhou, *Tsinghua Univ., China;* Pu Wang, Hengfu Pan, Jing Xue, Baosheng Lu, *Shandong Univ., China.* We report the first diode-pumped self-doubling laser of modified neodymium yttrium aluminum borate crystal with lower threshold pumping power and fundamental transverse mode operation. (p. 69)

ThE7
Second harmonic generation (SHG) and degradation in critically phase-matched KNbO₃, using diode-pumped, Q-switched Nd:lasers, W. Seelert, P. Kortz, *ADLAS GmbH, Germany;* D. Rytz, B. Zysset, D. Ellgehausen, G. Mizell, *Centre de Recherche en Optoelectronique, France.* We report on critically phase matched SHG of diode-pumped Nd Q-switched lasers in KNbO₃. Conversion efficiencies and long-term degradation effects will be discussed. (p. 72)

ThE8
Novel thermal poling technique for fabricating QPM SHG structures in X-cut lithium tantalate, R. A. Rubino, D. E. Bossi, J. D. Farina, *United Technologies Research Center.* A novel laser-based thermal poling process for writing sign-reversed domains in x-cut LiTaO₃ has been developed. This technique allows for optimum profile quasi-phase-matched waveguide frequency doublers. (p. 75)

ThE9
Simultaneous blue and green second harmonic generation (SHG) in quasi-phase-matched LiNbO₃ waveguide, Xiaofan Cao, Ramakant Srivastava, Ramu V. Ramaswamy, *Univ. Florida.* We report the first simultaneous quasi-phase-matched (QPM) generation of blue (433 nm) and green (532 nm) light by SHG in LiNbO₃ channel waveguides. (p. 78)

ThE10
Novel organic nonlinear optical materials for second harmonic generation (SHG) devices of semiconductor lasers, Yuzo Itoh, Yasuo Imanishi, Masakazu Sagawa, Hiroyuki Kagawa, Tomoyuki Hamada, Atsushi Kakuta, *Hitachi, Ltd., Japan.* We developed novel organic nonlinear optical materials (xanthone derivatives) using molecular design methods. The cut-off wavelength is around 420 nm short enough to be used for SHG devices of common semiconductor lasers. (p. 82)

ThE11
Blue-green injection laser made of nitride semiconductors, Jacques I. Pankove, *Univ. Colorado at Boulder.* A new laser is proposed comprising a superlattice of InN layers forming quantum wells in GaN. An asymmetric barrier provides hole injection without electron extraction. (p. 84)

ThE12
Investigation of compact S₂ vapor blue-green laser, Yu Jun-hua, Zhang Zhong hua, Zhang hua, Zhu Zhong wei, Ma Zu guang, *Harbin Institute of Technology, China.* Eleven blue-green spectral bands of S₂ laser excited by laser were obtained. Compact S₂ blue-green laser using transverse pulse fast discharge pumping and corresponding kinetics were investigated. (p. 86)

ANASAZI NORTH

7:15 am-8:25 am   BREAKFAST

CONCOURSE

7:30 am-5:30 pm   REGISTRATION/SPEAKER CHECK-IN

ANASAZI SOUTH

8:30 am-10:00 am
FA, FREQUENCY CONVERSION IN BULK DEVICES
William P. Risk, *IBM Almaden Research Center, Presider*

8:30 am—FA1   (Invited)
80% nonlinear conversion efficiency: when?, Robert L. Byer, *Stanford Univ.* Improvements in the efficiency of cw second harmonic generation (SHG) and cw optical parametric oscillation depend on the ratio of the nonlinearity to the loss in the nonlinear medium. External resonant SHG in monolithic lithium niobate crystals has now reached 69% conversion efficiency. Progress for SHG to the ultraviolet in barium borate and for cw OPO operation will be reviewed. (p. 90)

9:00 am—FA2   (Invited)
Frequency-doubled diode lasers, W. J. Kozlovsky, *IBM Almaden Research Center.* Progress in efficient frequency conversion of single-mode diode lasers using a buildup resonator containing a nonlinear crystal is described. Techniques for pulsing and frequency-locking are also discussed. (p. 91)

9:30 am—FA3
Miniature integrated SHG green laser, Hisashi Masuda, Fumisada Maeda, Michio Oka, Yushi Kaneda, Minako Sugiura, Shigeo Kubota, *Sony Corp., Japan.* Temperature-controlled diode-pumped SHG green lasers were constructed in 28 x 38 x 16 mm packages with output powers of 5 mW. Resonator length including QWP, Nd:YAG, and KTP was 7.5 mm. (p. 94)

9:45 am—FA4
Seventy percent conversion efficiency for frequency-doubling of a diode-pumped cw single-frequency Nd:YAG laser, D. C. Gerstenberger, T. E. Olson, G. E. Tye. R. W. Wallace, *LIGHTWAVE Electronics Corp.* Five hundred milliwatts of cw single-frequency 532 nm light was generated using a diode-pumped 700 mW Nd:YAG laser and a monolithic magnesium-oxide-doped lithium niobate resonant frequency-doubler. (p. 97)

10:00 am—FA5
Harmonic generation from 1.079 to 0.54 μm with 85% efficiency, Z. Y. Ou, S. F. Pereira, E. S. Polzik, H. J. Kimble, *California Institute of Technology.* Nonlinear conversion efficiency of 85% for cw frequency doubling has been achieved with KTP inside a passive ring cavity. (p. 100)

10:15 am—FA6
Resonantly pumped 459 nm sum-frequency upconversion laser, P. N. Kean, *Amoco Laser Co.;* G. J. Dixon, *CREOL.* Sum-frequency upconversion in a resonantly pumped Nd:YAG laser has produced 1.2 mW at 459 nm for 50 mW incident pump power. Theoretical calculations show that with lower intracavity losses and an optimized Nd concentration, a significant improvement on this result is expected. (p. 103)

10:30 am-11:00 am   COFFEE BREAK

ANASAZI SOUTH

11:00 am-12:00 m
FB, GAS LASERS
J. Gary Eden, *University of Illinois, Urbana-Champaign, Presider*

11:00 am—FB1   (Invited)
Air-cooled noble gas ion lasers—operating properties, construction techniques, and applications, S. M. Jarrett, *Spectra-Physics Lasers, Inc.* Air-cooled noble gas ion lasers have been continuously improved in operating characteristics, reliability, and lifetime. We discuss their operation, construction, and applications. (p. 108)

11:30 am—FB2   (Invited)
He-Cd lasers—present and future, Mark W. Dowley, *LiCONIX.* A brief history of He-Cd laser development is followed by a discussion of current technology. Recent refinement in performance is explored, and the remaining outstanding problems of the technology are discussed. Current OEM applications are reviewed with emphasis on unique contributions of He-Cd lasers, followed by a word about the future and an attempt to assess the competition from solid-state rivals. (p. 111)

12:00 m-1:30 pm   LUNCH (on your own)

ANASAZI SOUTH

1:30 pm-3:30 pm
FC, FREQUENCY CONVERSION IN GUIDED-WAVE DEVICES
Martin M. Fejer, *Stanford University, Presider*

1:30 pm—FC1   (Invited)
Second harmonic generation (SHG) in quasi-phase-matching waveguides, Gunnar Arvidsson, *Institute of Optical Research, Sweden.* Quasi-phase-matching waveguides have recently been fabricated in several different materials and used for efficient generation of blue light by SHG. (p. 116)

2:00 pm—FC2   (Invited)
Second harmonic and sum-frequency generation in optical waveguides, John D. Bierlein, *E. I. du Pont de Nemours & Co., Inc.* Several waveguide systems have been demonstrated that can efficiently generate short-wavelength outputs from various IR laser inputs. This paper reviews these systems and compares recent results achieved in $LiNbO_3$, $LiTaO_3$, and $KTiOPO_4$. (p. 119)

2:30 pm—FC3
Blue second harmonic generation (SHG) with low Cerenkov angles from Ta$_2$O$_5$/KTiOPO$_4$ waveguides, Hitoshi Tamada, Chiharu Isobe, Takaaki Murakami, Masaki Saitoh, *Sony Corp. Research Center, Japan*. The conditions for efficient blue SHG with low Cerenkov angles from Ta$_2$O$_5$/KTiOPO$_4$ channel waveguides are investigated theoretically and experimentally. (p. 120)

2:45 pm—FC4
Efficient direct diode laser frequency doubling in quasi-phase-matched LiNbO$_3$ waveguide, Xiaofan Cao, Ramu V. Ramaswamy, Ramakant Srivastava, *Univ. Florida*. We report efficient (22%/W) blue light generation by direct diode laser frequency doubling in second order quasi-phase-matched LiNbO$_3$ channel waveguides. (p. 123)

3:00 pm—FC5
Second harmonic generation from diode lasers in KTP waveguides, M. G. Roelofs, J. D. Bierlein, *E. I. du Pont de Nemours & Co.*; F. Laurell, *Institute of Optical Research, Sweden.* Segmented optical waveguides in KTiOPO$_4$ were coupled to single-mode diode lasers for blue light generation using QPM. The reflected light was used to lock the diode laser, forcing it to remain narrow-band even in the presence of reflected light from the end faces of the waveguide. (p. 127)

3:15 pm—FC6
Blue-green light generation from a neodymium fiber laser, K. S. Buritskii, E. M. Dianov, V. A. Maslov, V. A. Chernykh, E. A. Shcherbakov, *General Physics Institute, U.S.S.R.*; V. P. Gapontsev, I. E. Samartsev, *IRE-Polus, U.S.S.R.* Blue and green light has been observed by phase-matched second-harmonic and sum-frequency generation in channel KTP waveguides pumped with a neodymium fiber laser. (p. 128)

3:30 pm–4:00 pm   COFFEE BREAK

ANASAZI SOUTH

4:00 pm–6:00 pm
FD, PANEL DISCUSSION ON DEVICE AND APPLICATION ISSUES
Gary T. Forrest, *FYI Reports, Presider*

Applications

ThA 8:30am–10:00am
Anasazi South

Donald L. Sipes, *Presider*
Amoco Laser Company

APPLICATION OF BLUE-GREEN DIODE LASER SOURCES
TO OPTICAL RECORDING

Donald B. Carlin

David Sarnoff Research Center

Princeton, NJ 08543-5300

A primary motivation for the original development of optical recording was that the technique allowed a much smaller area for the storage of a bit of information than did the magnetic techniques of that time. Most early data recording was by ablative effects, the formation of "pits" in an optical media. Today, storage may be by ablation, magneto-optic effects, or phase-changes. The basic optical principles remain the same for all recording techniques. In general, recording laser light that has a gaussian-like spatial beam profile is expanded to fill the optics to the $1/e^2$ intensity points of the beam profile and to focus the light onto the recording medium. The recorded spots are formed with a diameter of approximately equal to the full-width-at-half-power (FWHP) of the primary central lobe of the diffraction pattern on the medium. Under these assumptions, the diameter (d_0) of the recorded spot is given by:

$$d_0 = 0.56\, \lambda/_{NA},$$

where NA is the numerical aperture of the focussing objective. This basic equation drove early systems to the shortest wavelength lasers having adequately powerful cw emission from practical sources[1]. Consequently, much of the early results were obtained at wavelengths of 488 and 514 nm from the Ar$^+$ laser or at 442 nm from He-Cd. While these lasers sufficed

for laboratory demonstrations and prototype systems, they were large and inefficient, had relatively modest expected lifetimes, often required water cooling, and definitely required external modulators to encode data on the recording beam.

In contrast, semiconductor diode lasers are plagued by none of the above deficiencies. Consequently, when the first AlGaAs lasers of sufficient power were available in the late 70's and early 80's, they were used almost immediately[2,3] despite their considerably longer emission wavelength of $\approx$ 830 nm. The last decade was characterized by remarkable improvement in the output power capabilities of such devices, as well as their spatial mode properties and lifetimes. In addition, lasers made of AlGaInP have been developed to emit in the red region of the spectrum. Despite the fact that the data capacity for optical storage is inversely proportional to d_0^2 and the data transfer rate is inversely proportional to d_0, no commercial systems have been announced that make use of a red diode laser source. The data rate and capacity advantages are just not sufficient to overcome the inertia of a market that has already developed standard formats and materials. A blue semiconductor diode laser source, however, would allow twice the data rate and four times the capacity on the storage medium. The prevailing wisdom is that this would be more than sufficient to generate whole new lines of products to take advantage of these attributes.

A blue or blue-green diode laser must possess other attributes, however, in order to be practical as the recording source in optical data storage systems. A minimum power of 10 mW cw must be avaiable, and the emission must be in a stable, fundamental lowest-order mode in order to be focussed to a diffraction limited spot. The ratio of the beam

divergences parallel and perpendicular to the epitaxial layers of the device must not be very large, as focussing by practical (inexpensive) optics becomes difficult. In addition, the light must be linearly polarized if the system is based on magneto-optic effects. Of course, the projected lifetime must be typically at least 10,000 hours for commercial systems and possibly greater than 100,000 hours for some memories.

It should be noted that data retrieval is optimized when the readout beam has a full-width at its $1/e2$ intensity point equal to d_0. Thus, in principle, it is advantageous to have a shorter wavelength for data retrieval than for data writing.

Recent work on blue-green sources has focussed on doubling of infrared diode laser emission by in non-linear crystals and waveguides, and the direct emission of short wavelength light by injection of high-bandgap materials such as the II-VI compounds. Either can be configured for integration in optical recording systems. In addition, either can be configured as linear independently addressable arrays for multichannel, high-speed systems. Depending on the rate at which these technologies advance, on or more types of blue or blue-green diode laser sources may be incorporated into practical memory systems by the end of the decade.

[1]D. Maydan, "Micromachining and image recroding in thin filmes by laser beams," Bell Syst. Tech. J., July-Aug 1971, 1761.

[2]P. M. Asbeck, D. A. Commack, J. J. Daniele, D. Lou, J. P. Heemskerk, W. J. Kleuters, and W. H. Ophey, "High-quality optical recroding with (Ga, Al)As DH lasers," Appl. Phys. Lett. 34, 15 June 1979, 835.

[3]R. A. Bartolini, A. E. Bell, and F. W. Spong, "Diode laser optical recording using trilayer structures," IEEE J. Quantum. Electron. QE-17, 1 January 1981, 69.

Lasers In Flow Cytometry and Biotechnology. Larry A. Sklar, National Flow Cytometry Resource, Los Alamos National Laboratory, Los Alamos NM 87545 and University of New Mexico School of Medicine, Albuquerque NM 87131.

Lasers are used by the biomedical community in many applications. These include flow cytometry, microscope imaging, solution spectroscopy, and very recently, optical manipulation of cells and subcellular particles. This paper reviews applications of lasers involving fluorescent probes. In most applications, these technologies require ~10 mW of laser power focused to cellular dimension (except for the solution measurements). I estimate that there are several thousand flow cytometers, several hundred laser imaging systems, and several hundred laser spectroscopy instruments distributed between the biomedical, physics and chemistry communities. Optical trapping as a commercial technology is emerging rapidly at the time this paper is being written using IR diode lasers to manipulate the cells.

Flow cytometry involves the use of one or more lasers to excite streams of cells at rates of thousands of cells per second. The cells flow past a focused laser beam (eg., 15 microns) with velocities ~1-10 meter/sec giving rise to a dwell time in the beam ~1.5-15 microseconds. It was recognized but not widely appreciated in the early days of flow cytometry that the photon flux of 10 mW lasers could saturate the excitation of millions of antibody probe molecules bound to cell surfaces. However, because of optical configurations used for cell sorting, commercial cytometers were generally equipped with water-cooled lasers with an output ~1 W at 488 nm. There are at this time two major markets for flow cytometers with fairly distinctive instrumental approaches. By far the largest market is the clinical community which uses cytometers for hematology. This market is served by air-cooled argon ion lasers. This community uses a variety of probes which are illuminated simultaneously at 488 nm. When used in combination, the probes are chosen to exhibit spectrally resolved emission; for example, the emission from fluorescein (green), phycoerythrin (orange), and red dyes are resolved by a combination of dichroic mirrors and bandpass filters and three photomultipliers. These instruments are set up at the factory and provide the users no choice in laser or filters. Up until recently, the research community has been served primarily by argon, krypton, and argon-dye laser systems providing laser lines in the UV and VIS. The research community has, in contrast to the clinical community, taken advantage of multiple excitation wavelengths to resolve multiple probe molecules. One instrument manufacturer (Coulter Electronics, Hialeah, FL) has promoted a new instrument with a flexible optical bench to accomodate up to four lasers. In multilaser cytometers, the excitation beams are spatially resolved and the output signal from individual cells are temporally segregated. Several companies have produced instrumentation using arc lamp excitation which offers versatility in wavelength, but even the best of these instruments has inadequate power for fluorescein immunofluorescence, the benchmark for instrumental sensitivity.

Fluorescence microscopy has traditionally relied on arc lamp sources. Because imaging has involved illumination in the millisec or sec time domain, the power of the source has not generally been the limiting factor in image acquisition. More recent

imaging technology has included laser scanning, confocal imaging, fluorescence recovery after photobleaching of spots or patterns on cell surfaces, and total internal reflection spectroscopy. In the commercial market, the primary demands for lasers are in confocal imaging and 2D scanning. 10 mW of power focused into a 1 um x 1 um area are adequate for photobleaching experiments. Cell obliteration and DNA slicing applications require higher power density than photobleaching. One requirement of the imaging community is to superimpose images obtained from different dyes or ratio images of a single dye without loss of image registration. In the emerging field of diagnostic chromosome imaging, as many as five different dyes are desirable (AMCA and DAPI, excitation ~350 nm; chromomycin ~450 nm, FITC ~490 nm, Texas red ~600 nm, etc.). Tunable or multiline lasers could permit multicolor analysis without loss of registration by bypassing an optical train with moving parts such as multiple optical filters. For dyes with overlapping emission, Fourier transform spectral analysis can be applied to imaging.

The spectroscopy community requires a broad range of applications on both commercial and specialized instruments. Applications in protein spectroscopy use high powered UV lasers pulsed in the nanosecond and subnanosecond time domain to examine molecular dynamics. An emerging use of lasers in the biomedical community is fluorescence lifetime analysis. The excitation is sinusoidally modulated and emission is detected in the frequency domain on the basis of phase shift and amplitude demodulation of the emitted light as compared to the exciting light. Arc lamp sources generally provide barely adequate power density for the widest range of applications. The experiments require excitation spanning the UV and the VIS. ~10 mW is required for most applications; a water-cooled He-Cad laser is needed to obtain adequate power at 325 nm. With the advent of phase sensitive flow cytometry and the possibility of phase sensitive image analysis, lifetime analysis of probes in many other spectral regions will be desirable. The ability to modulate the intensity of the source is likely to be of considerable interest.

Many of us in the biomedical community are beginning to integrate flow cytometry measurements with imaging and/or solution spectroscopy. When we buy instruments or set up laboratories there is a trade-off between the flexibility desired in excitation wavelength, the expense of water-cooled lasers, the inflexibility of the clinical cytometers and a lack of expertise in handling large lasers. Since we may pay up to $10,000 for a high-powered arc lamp, power supply, and monchromator package, $20,000-50,000 for a multiline water-cooled main frame laser and dye head, and comparable amounts for renovating biological facilities to accomodate laser-dependent instruments (i.e., cooling systems and high-voltage lines), the notion of being able to select single line lasers over a wide excitation spectrum at moderate expense (ie, 1,000-5,000 dollars per line) and to freely interchange the lasers to meet the excitation requirements of individual experiments is at.ractive indeed. The versatility permited by such technology would offset the expense of the additional light sources as compared to the expense of extensive renovations of facilities.

The wavelengths of interest for the biomedical community stretch from the UV to the

near IR. A good introduction to fluorescent dyes and their applications is found in the Molecular Probes catalgoue (Eugene, Or). In the UV, we are interested in intrinsic cellular chromophores including aromatic amino acids of proteins and nucleotide bases as well as synthetic probes. As we approach the IR, we use probes which are excited in spectral regions which minimize the fluorescence of cellular constituents, ("autofluorescence"). This has led to a major effort to sythesize probes suitable for excitation with a He-Ne laser such as the new family of cyanine dyes including CY3, CY5, and CY7. Because of the popularity of the air-cooled argon ion laser, there is considerable interest in dyes with large Stokes shifts such as porphyrins or LDS-751 which can be used in combination with fluorescein and phycoerythrin. Another approach involves "tandem" dyes conjugated to the same backbone. For example by using phycoerythrin as donor and a red emittting dye such as Texas Red or CY3 as acceptor for Forster energy transfer, these dye pairs give rise to red emission following exciation at 488 nm which is well separated from the green and orange fluors.

In the wavelength range between 300 and 400, an endogenous molecule of interest is NADP (ex ~340 nm; em ~450 nm) whose presence in the cell can define metabolic compartmentation. Ratio dyes for analysis of intracellular calcium particularly INDO (ex ~340 nm; em ~ 400 nm, 490 nm for Ca^{++} free and bound forms, resp.) have depended largely upon the use of 5W argon ion lasers to obtain the UV capability. In many biological laboratories, ratio calcium measurements are only accomplished with fairly sophisticated technical assistance. There are a number of other dyes in this region which have not been fully exploited such as pyrene (ex ~340 nm) as well as lipophilic dyes such as diphenylhexatriene and parinaric acid (ex ~325 nm) that are useful for studies of membrane fluidity. The DNA staining dyes DAPI or Hoechst also are excited near 350 nm.

In the wavelength range from 400 to 500 nm, the DNA staining dyes chromomycin and mithramycin use the argon ion 457 nm line on the 4 W laser for flow cytometry. A number of popular dyes including fluorescein, NBD, and the bluest of the BODIPY dye family (ex ~ 490 nm, em ~ 520 nm) are derivatized for conjugation to peptides, antibodies, and other proteins and use the 488 nm line. A stain for viability, propidium iodide, and LDS-751 which stains nucleated cells are also excited here.

In the wavelength range beyond 500 nm, rhodamine and its analogues including Texas Red are used as conjugates with many biomolecules. There are a number of pH sensitive fluorescein derivatives which can be used for measurements of intracellular pH as free dyes or conjugated to biomolecules to examine the pH of intracellular compartments. The argon ion lines at 514 and 528 nm, the krypton line at 568 nm, and the R6G dye head are useful for these applications. In addition to the cyanines, a new family of boron containing dyes (BODIPY) conjugates span the region from 500-700 nm.

Compact Visible Lasers in Reprographics

James C. Owens
Imaging Research Laboratories
Eastman Kodak Company
Rochester, New York 14650-1822

Reprography, which originally referred only to printing and duplicating processes for the reproduction of flat originals, today includes a wide variety of technologies for the production of two-dimensional images in applications as diverse as photography, office copying, desktop publishing, graphic arts, medical imaging, and microelectronic fabrication. Although analog processes are still in wide use, the principal area of recent technical development and new application has been in digital electronic imaging systems, and especially in optical methods for non-impact hard copy printing.

We can identify three different types of images: text and line art, as in business graphics; halftone pictorial, as in conventional graphic arts; and continuous-tone pictorial, as in photography. Two of these use one-bit exposure modulation, and the third uses multibit modulation. In addition, recent electrophotographic printers use a hybrid halftoning method in which a multibit gray scale is generated by using both area and exposure modulation.

The characteristics that determine image quality are tone reproduction (dynamic range; bit depth), color reproduction (dimensionality), sharpness (frequency response) and graininess (noise). These can be measured and also predicted quantitatively from the characteristics of the image source, the image processing algorithms, the writer hardware, and the recording material. The avoidance of image artifacts, in particular, places severe requirements on the subsystem specifications.

In designing an imaging system for a particular application, the choice of recording medium is the first consideration. It may be a monochrome or color silver halide film or paper, a photopolymer or diazo material, a photoconductor, or one of a variety of thermal media. These differ in wavelength response, absolute sensitivity, processing requirements, image quality, and stability, to list only the major considerations.

Having chosen an appropriate medium, we next consider the optical writer. Depending on the medium and the throughput required, it may use incoherent or coherent light; may expose one pixel at a time, several pixels, a full line, or even the entire two-dimensional image; and may expose at one wavelength or three simultaneously. Generally speaking, the most useful type of writer for digital hard copy imaging has been the raster-scanning laser/polygon writer. The high

spectral radiance of lasers allows good throughput while exposing each pixel sequentially in synchronism with the digital data stream from an image processor. This approach avoids the exposure uniformity problems of multi-source writers. Although the details of the optical design are complicated, there is a relatively simple and logical procedure for laying out the overall geometry of such a printer, making use of the Lagrange invariant and a simple depth-of-focus calculation. The spot sizes are chosen to give matched resolution in the scan and cross-scan directions.

Having chosen both the recording material and the type of printer, we can determine the requirements for the light source. For example, conventional color photographic films use exposing wavelengths of approximately 430, 550, and 650 nm, while color photographic papers use the slightly different set 470, 550, and 700 nm. A few milliwatts of power gives image throughput adequate for most purposes when writing on silver halide materials, although systems using photoresist or thermal media require several orders of magnitude more power, multiple sources, or lower throughput. Good beam quality is important, and single-mode lasers are needed for most applications. It is an important simplification if the source can be modulated directly to give a dynamic range of 100:1 over a bandwidth from DC to 15 MHz. Depending on the data rate capability of the image source, modulation rates as high as 50 MHz may be required. Noise, stability, and insensitivity to optical feedback are also important concerns. For achromatic systems, the wavelength shifts with drive current and the sudden changes associated with diode laser mode hops are usually unimportant, but the small changes in optical power or noise bursts that sometimes occur at mode hops give visible and objectionable artifacts in continuous-tone images. For systems using holographic deflectors or diffractive optics, these wavelength changes give rise to significant shifts in spot position, and hence conventional diode lasers are unacceptable.

In summary, the most immediate practical advantage of compact blue and green direct-emitting or nonlinear light sources in reprography is that they may allow a wavelength match to existing monochrome or color recording media while retaining the desirable capability for direct modulation and the low intrinsic noise of diode lasers. For high-resolution reprographic applications such as microfilm and microfabrication, the shorter wavelength is, of course, desirable for permitting higher resolution than can be achieved with existing diode lasers. For most other reprographic applications, the required image resolution is low enough that short wavelengths are not required for spot size, but they are advantageous in another way. A shorter wavelength allows the use of a smaller numerical aperture for a given spot size. This not only reduces the size of the optics but also increases the depth of focus at the image and its conjugate planes, which in turn makes the optical and dimensional tolerances of the printer less demanding. The availability of compact coherent sources throughout the visible spectral region having reasonable power, good beam quality, and low noise, would be a significant development for reprography.

IR Pumped Visible Lasers

ThB   10:30am–12:00m
Anasazi South

Jeff Dixon, *Presider*
University of Central Florida/CREOL

Visible Upconversion Fiber Lasers

A C Tropper

Department of Physics & Optoelectronics Research Centre
University of Southampton
Southampton SO9 5NH UK
Tel: 44 703 592103

Summary

Over the past two years several upconversion-pumped visible laser systems based on lanthanide-doped fluorozirconate glass fibre have been reported[1-5], illustrating the great potential of this medium for efficient infrared to visible conversion. Confinement of pump radiation in a small core fiber lead to rapid multiple step pumping of high-lying metastable energy levels for fairly modest levels of pump power. Compared to silica fibers the low vibrational energies of the heavy metal fluoride glass matrix leads to a greatly reduced competition to optical pumping and emission processes from nonradiative decay. A further advantage relative to silica is the narrowness of the absorption and fluorescence bands giving higher peak cross-sections and less likelihood of unwanted excited state absorption(ESA). Fluoride fibre fabrication technology has now reached a point at which small core fibres (i.e. monomode in the visible) with scattering losses down to ~ 0.2dBm^{-1} can be made, so that the remarkable properties of the fluoride glass host can be embodied in efficient compact devices.

Visible laser emission has been generated in fibers of standard ZBLAN composition doped with Tm (455nm, 480nm [1]), Ho (540-553nm [2]) and Er (546nm [5]). In each case pumping is by a 2-step ESA process. The high order pumping schemes reported for some crystal upconversion lasers are not readily applicable to fluoride fiber lasers in which the dopant concentrations are too low to favour efficient cross-relaxation. Tm and Ho were pumped with red krypton laser emission; Er is infrared pumped at the diode-compatible wavelength of 801nm. In Er and Ho a fortunate overlap of the ground and ESA bands allowed operation with a single pump wavelength. Tm required dual wavelength pumping; this is the least efficient of the visible upconversion lasers and the only one to require cooling to 77K to operate.

The trivalent Pr ion is a particularly attractive visible laser activator because there are red, green and blue fluorescence bands originating from the $^3P_0$, $^3P_1$, $^1I_6$ group of metastable levels. Directly pumped by an argon ion laser Pr:ZBLAN fibers have operated [6,7] at 695nm, 635nm, 605nm, 520nm and 491nm with tuning ranges of ~ 10nm reported on the high-gain red transitions. Infrared-pumped upconversion lasing on these transitions has also been achieved via ESA from the 10 000cm^{-1} $^1G_4$ level which in ZBLAN has a 110μs lifetime limited by multiphonon emission. Blue, green and red operation has been reported using a dual wavelength pumping scheme resonant with the $^3H_4$ - $^1G_4$ 1.01μm transition and the $^1G_4$ - $^3P_1$, $^1I_6$ 835nm transition[4]. Absolute infrared to red power conversion efficiencies of ~7% have been achieved. An alternative pumping scheme has been reported [3] in which the $^1G_4$ energy level is populated by energy transfer from Yb ions in a doubly doped fiber, so that only a single pump wavelength in the 0.8μm region is needed. Despite the attractive simplicity of this pumping scheme it appears to make less efficient use of the pump radiation.

Laser action on the lower gain blue and green transitions has not so far been reported in a Pr:Yb fiber.

Infrared-pumped blue and green lasing has been investigated in a fiber of standard ZBLAN composition with a core diameter of 4.6μm, an LP_{11} mode cutoff wavelength of 0.9μm, and a Pr ion concentration of 1.1×10^{-25} m^{-3}. Blue lasing at 491nm occurs on the long wavelength wing of the $^3P_0$ - $^3H_4$ fluorescence band, where ground state reabsorption is weak. Owing to the weak absorption of the $^3H_4$ - $^1G_4$ transition there is negligible depletion of the $^3H_4$ ground state population for available 1.01μm pump powers. The lowest threshold recorded for laser operation, in a cavity formed by butting mirrors with high reflectivity at 491nm at either end of a 1.2m length of fiber, was achieved at *incident* powers of ~ 200mW at 835nm together with ~280mW at 1.01μm power. The launch efficiency was estimated to be approximately 50%. It is interesting to note that the 20 370cm^{-1} laser photon energy is sufficiently large to excite transitions from the 20 000cm^{-1} $^3P_0$ level into the tail of the intrinsic ZBLAN absorption band which extends down to ~35 000cm^{-1}. The extent, if any, to which this affects the blue and green laser performance has yet to be determined.

Green laser operation at 520nm on the $^3P_1$, $^1I_6$ - $^3H_4$ transition was observed when a cavity was formed with the same fiber length between mirrors of >99% reflectivity in the green. A threshold of approximately 160mW incident power at each wavelength was observed. The maximum extracted power at this wavelength was 13mW.

In an optimised fibre, with higher numerical aperture and shorter cutoff wavelength, at least an order of magnitude reduction in threshold is theoretically possible, opening the possibility of diode-pumped operation. With the rapid improvements in ZBLAN fibre fabrication technology, the prospects for developing this system into a compact visible laser source look promising.

[1]   J Y Allain, M Monerie & H Poignant, *Electron Lett* **26** (1990) 166-168
[2]   J Y Allain, M Monerie & H Poignant, *Electron Lett* **26** (1990) 261-263
[3]   J Y Allain, M Monerie & H Poignant, *Electron Lett* **27** (1991) 1156-1157
[4]   R G Smart, D C Hanna, A C Tropper, S T Davey, S F Carter & D Szebesta,
        Electron Lett **27** (1991) 1307-1308
[5]   T J Whitley, C A Millar, R Wyatt, M C Brierley & D Szebesta,
        Electron Lett **27** (1991) 1785-1786
[6]   J Y Allain, M Monerie & H Poignant, *Electron Lett* **27** (1991) 189-191
[7]   R G Smart, J N Carter, A C Tropper, D C Hanna, S F Carter & D Szebesta,
        Optics Comm **86** (1991) 333-341

Bulk Crystal Upconversion Lasers

William F. Krupke

Laser Programs
Lawrence Livermore National Laboratory
P. O. Box 808
Livermore, CA 94550
T(510) 422-5905
F(510) 422-5411

Recent advances in high-power, high-efficiency semiconductor laser diodes and diode arrays has revived interest in the identification and development of practical upconversion lasers (for which the output laser wavelength is shorter than the wavelength(s) of the optical pump(s)). It is hoped that upconversion lasers will compete favorably with alternative approaches, such as wavelength shifting of laser diode radiation using nonlinear processes, to perform commercial applications, such as the production of full color images using laser-based tri-stimulus sources. For upconversion laser action to occur, the energy carried by two or more pump photons must be accumulated in the upper laser level of the gain medium. In most general terms, this accumulation of pump energy occurs by the successive absorption of pump photons via intra-ion radiative transitions, by the summation of absorbed pump photon energy via ion-ion interactions, or by combinations of both. To compete favorably with nonlinear wavelength shifting devices, practical upconversion 'asers will have to operate at room temperature, and with conversion efficiencies of pump energy to laser output that match or exceed those of nonlinear conversion-based devices.

Upconversion lasers take one of two generic geometries: 1) bulk crystal or 2) fiber. In the fiber geometry, pump energy is trapped, guided, and deposited along the relatively long length (~meter) of a glass fiber that is usually lightly doped with rare earth impurity ions. In bulk crystal upconversion lasers, the subject of this talk, pump energy is freely propagated and deposited within a relatively short distance (~centimeter) of a crystal block that it usually more heavily doped with rare earth impurity ions. The output power or energy of such lasers can be scaled to much higher levels than fiber upconversion lasers due to their larger

Table 1
Bulk Crystal Upconversion Lasers Pumped by Two-Step-Absorption (TSA) Processes

Material	Pump (nm)	Pump Type	Laser (nm)	Temp (Max) (K)	Form	Pump Pwr (mW)	Output Pwr (mW)	Opt Eff(%)	Ref.
Er:YALO	792	Dye	550	77	CW	200	1	0.25	1
	848	Dye			CW	200			
Nd:LaF$_3$	790	Dye	380	20 (77)	CW	100	12	3	2
	579	Dye			CW	280			
Nd:YLF	810	Dye	413	12	CW	200	0.01	low	3
	604	Dye			CW	300			
Tm:YLF	781	Dye	450	77 (150)	Puls.	10mJ	0.18mJ	1.3	4
	649	Dye			Puls.	3.5mJ			
Tm:YLF	628	Dye	483	26 (130)	CW	400	30	7	5

Refs: 1. Silversmith, et al., Appl. Phys. Lett., 51, 1977 (1987)
2. Macfarlane, et al., Appl. Phys. Lett., 52, 1300 (1988)
3. Macfarlane, et al., Proc. Laser Matl and Spectroscopy, Shanghai, China, 1988; p24
4. Nguyen, et al., Appl. Opt., 28, 3553 (1989)
5. Macfarlane, et al., CLEO -'90, Anaheim, CA.

Table 2
Bulk Crystal Upconversion Lasers Pumped By Energy-Transfer-Summation (ETS) Processes

Material	Pump (nm)	Pump Type	Laser (nm)	Temp (Max) (K)	Waveform Type	Pump Pwr. (mW)	Output Pwr. (mW)	Opt. Eff. (%)	Ref.
Er:BaY$_2$F$_8$	Broad	Xe-lamp	851	100	Pulsed	--	·	·	
	1530	Er:Glass	1730	208	Pulsed	·	·	·	1
	1530	Er:Glass	2790	300	Pulsed	·	·	·	
Er:YLF	653	Dye		16 (35)	CW	120	6	5	
	796	TIS	470	10 (40)	CW	700	4	0.6	2
	969	TIS		10 (40)	CW	700	2	0.3	
	969	TIS	561	15	CW	200	4	2	3
Er:YLF	797	TIS	551	49	CW	4500	500	13	4
Er:YLF	791	Dye	671	50	CW	300	1	0.3	5
Er:YLF	802	Diode	551	50 (77)	CW	100	2.2	2.2	6

Refs: 1. Pollack, et al., J. Appl. Phys., 67, 648 (1990)
2. Herbert, et al., Appl. Phys. Lett., 57, 1727 (1990)
3. Lenth and Macfarlane, J. Lum., 45, 346 (1990)
4. McFarlane, Opt. Lett., 16, 1397 (1991)
5. McFarlane, Appl. Phys. Lett., 54, 2301 (1989)
6. Herbert, et al., Advanced Solid State Lasers Meeting, Hiltonhead, SC., 1990

transverse apertures, but require the use of pump sources with very high radiances. Because of their differing regimes of impurity doping and physical dimension over which laser gain is produced, non-radiative energy transfer summation (ETS) processes tend to determine the characteristics of bulk crystal upconversion lasers, whereas radiative two step absorption (TSA) processes tend to control the characteristics of fiber upconversion lasers.

Tables 1 and 2 summarize some of the key characteristics of bulk crystal upconversion lasers reported to date. Table 1 lists lasers based on TSA mechanisms and Table 2 lists lasers based on ETS mechanisms. These tables show that: 1) bulk crystal upconversion lasers operate at sub-ambient (mostly cryogenic) temperatures; 2) they have been pumped with relatively inefficient "surrogate" dye or titanium:sapphire pump lasers; and 3) and they have optical-to-optical conversion efficiencies less than 13 percent. Nonetheless, the recent research efforts on upconversion lasers (both bulk crystal and fiber) have contributed new data and insights into the finer aspects of the radiative and nonradiative processes at work in these systems. Additionally, kinetic models that describe the flow of energy among electronic states of rare earth doped crystals, using empirically-derived parameters, are progressively being utilized to help identify and develop practical (room temperature, high pump conversion efficiency) bulk crystal upconversion laser devices.

In this talk, the critical features of known bulk crystal upconversion lasers will be reviewed, and the present barriers to the realization of practical devices will be identified. Trends in research efforts to overcome these barriers will be outlined, including the utilization of more complex sensitization schemes, and the use of host materials in which nonradiative energy transfer rates are substantially increased due to preferential pairing of participating impurity ions.

Tm³⁺ Room Temperature Upconversion Laser

R. J. Thrash
Amoco Technology Company
P. O. Box 3011, Naperville, IL 60566
(708) 420-4695

L. F. Johnson
Laser Consulting
150 Riverwood Ave., Bedminster, NJ 07921

Diode laser pumped, room temperature upconversion lasers are one possible route to all solid-state visible wavelength lasers. The energy level spacing of the thulium ion is such that several visible laser transitions should be possible. Upconversion laser emission from Tm³⁺ at a number of visible wavelengths has been reported in bulk crystal[1,2] and glass fiber[3] hosts.

We report room temperature upconversion laser operation from ytterbium sensitized thulium ions in barium yttrium fluoride. Laser emission at 455, 510, 649, and 799 nm was obtained. The 960 nm chopped output from a cw titanium/sapphire laser was used initially as the pump source. The 649 nm transition has also been pumped by the chopped output of a cw diode laser. In addition, the 649 nm transition could be operated cw when pumped with a titanium/sapphire laser. Room temperature upconversion laser oscillation at 649 nm has been reported by Antipenko et.al. using ytterbium sensitization[1], pumped by a pulsed neodymium laser. However, we believe this is the first report of cw upconversion laser operation in thulium, at room temperature.

For operation at 455, 510, and 649 nm the upconversion laser consisted of a 1 mm thick platelet of $BaY_{1.0}Yb_{0.99}Tm_{0.01}F_8$ in a 1.5 cm radius hemispherical cavity. The 799 nm laser used the same crystal, but in a 5 cm radius hemispherical cavity. Pump radiation at approximately 960 nm was provided either by a titanium/sapphire laser or two laser diodes that were polarization coupled together to form a single pump beam.

Upconversion pumping by energy transfer from the ytterbium ions (excited by the 960 nm radiation) provided the excitation energy necessary to reach the upper laser levels in thulium. The pump light excites only the ytterbium ions present in the sample. It is not energetic enough to reach the upper laser levels of thulium directly, but three successive energy transfers from ytterbium to thulium do populate various thulium excited states (Fig. 1). Thulium-thulium interactions also distribute the accumulated excitation energy among the various higher and lower energy levels. It is through these processes of energy transfer from ytterbium to thulium and thulium-thulium interaction that the energy from the 960 nm pump radiation is used to populate the upper laser levels for the

observed upconversion laser transitions.

The processes described thus far will yield an upconversion laser capable of emitting at 649 nm and 799 nm. A unique feature of this pumping scheme that enables laser emission at shorter wavelengths follows from the observation of the effect of the 649 nm laser action on the population distribution of the thulium excited states. A spectroscopic examination of the blue fluorescence emission from the thulium ions in an operating upconversion laser crystal was made as a function of the presence or absence of the red laser emission. It was noted that the fluorescence emission from the excited state capable of 455 nm and 510 nm emission was significantly enhanced when the red laser was operating (Fig. 2). This indicates that the population of that state is being increased by the presence of the circulating intracavity red laser radiation. One explanation for this observation is that an excited state absorption exists in thulium that absorbs the red laser emission and populates the $^1D_2$ excited state capable of green (510 nm) and blue (455 nm) emission. In effect, the thulium red upconversion laser pumps itself in such a way as to allow higher energy transitions. Often, the existence of an excited state absorption is detrimental to the functioning of a laser. However, in this case the excited state absorption appears to have little negative effect on the red laser operation, but instead offers a significant benefit to the green and blue laser transitions. To accomplish the demonstration of green and blue laser emission from ytterbium sensitized thulium therefore required an optical cavity highly reflecting at all three wavelengths, 649 nm, 510 nm, and 455 nm. With such a cavity, laser emission at all three wavelengths has been obtained. We believe this is the first observation of laser emission on the 799 nm transition from $^1G_4$ and the 510 nm transition from $^1D_2$. Work continues to improve the performance of the green and blue transitions. It is expected that optimization of the thulium concentration and the thulium-ytterbium ratio will lead to diode pumped cw operation at all the upconversion wavelengths.

References

1.   B. M. Antipenko, S. P. Voronin, and T. A. Privalova, Opt. Spectrosc. (USSR) 68, 164 (1990)
2.   D. C. Nguyen, G. E. Faulkner, and M. Dulick, Applied Optics 28, 3553 (1989)
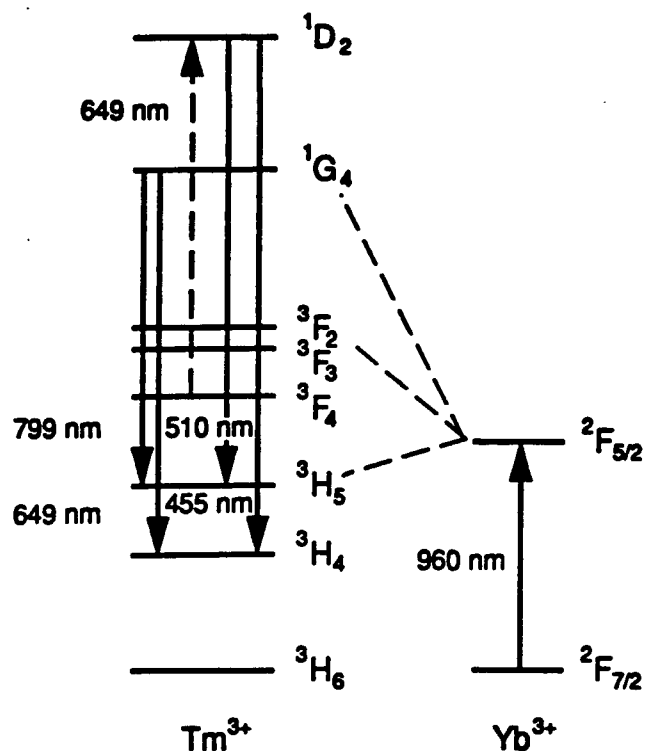3.   J. Y. Allain, M. Monerie, and H. Poignant, Electron. Lett. 26, 166 (1990)

Fig. 1. Energy Level Diagram and Observed
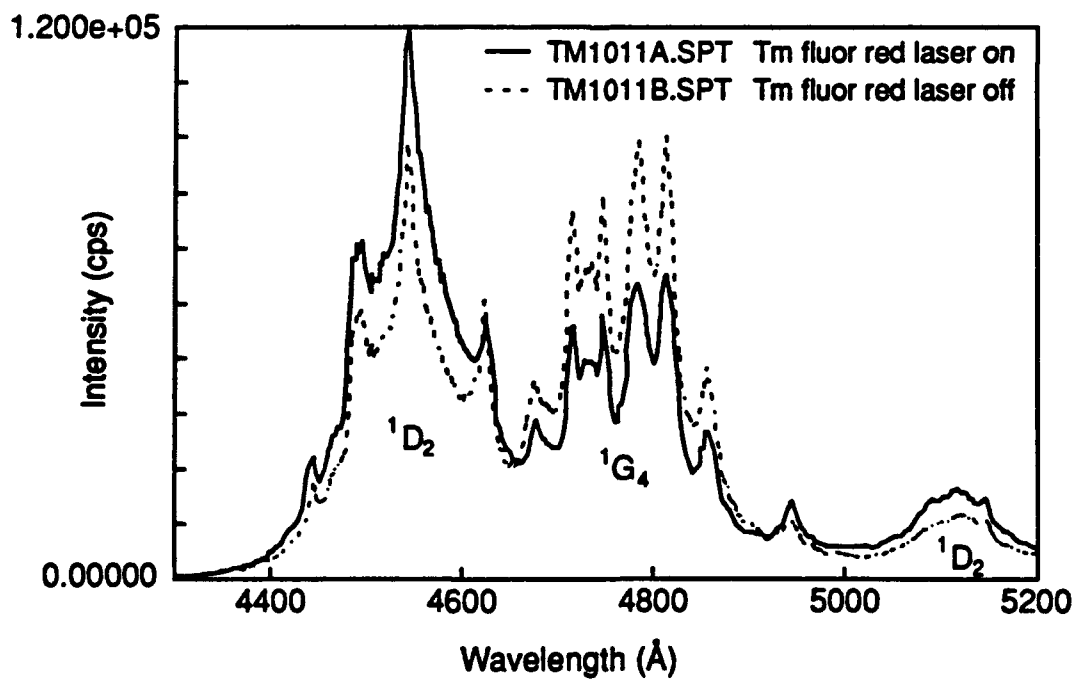Upconversion Laser Transitions in Tm^{3+}

Fig. 2. Fluorescence Emission from $^1D_2$ and $^1G_4$
With and Without 649 nm Laser Operation

Rare-Earth-Doped Waveguide Devices:
The Potential for Compact Blue-Green Lasers

N.A. Sanford
K.J. Malone
D.R. Larson
M.J. McCollum

National Institute of Standards and Technology

Rare-earth-doped channel waveguide devices have demonstrated to lase in the infrared. The possibility for upconversion visible lasing is also being explored.

Blue-Green Diode
Emitters

ThC 1:30pm–3:00pm
Anasazi South

Peter S. Zory, *Presider*
University of Florida

II-VI Blue-Green Diode Lasers

J.M. DePuydt, M.A. Haase, J. Qiu and H. Cheng
3M Company,201-1N-35 3M Center, St. Paul, MN 55144
(612) 736-7247.

Introduction:

Injection lasing in the wide band gap II-VI semiconductors was achieved for the first time in our laboratory in April, 1991.[1] Since then considerable effort has been made toward understanding the properties of these laser diodes and constituent materials as well as making progress toward the development of viable devices. We have demonstrated room temperature, pulsed operation in devices with emission wavelengths from 508-535nm. More recently, we have achieved cw operation at 77K. In this paper we will describe the operating characteristics and fundamental parameters of our blue-green laser diodes.

Laser Construction:

The design of our original II-VI laser diode is illustrated below.
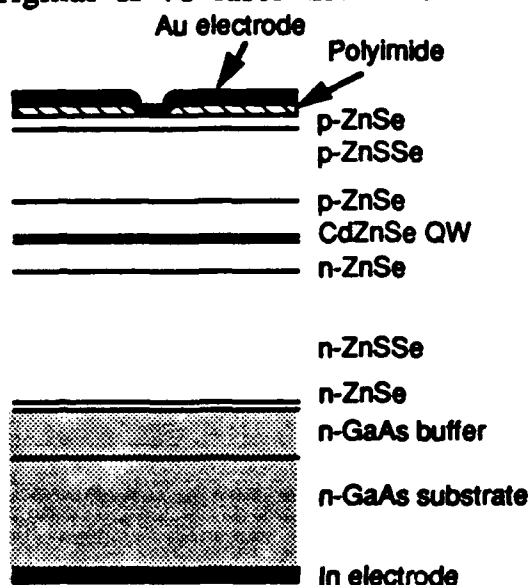
Figure 1. Crossection of the first blue-green laser diodes.

In these devices a ZnSSe cladding is included to confine the optical mode to the ZnSe guiding layer thereby reducing absorption losses by the GaAs substrate and Au contact. Lattice matching to GaAs (at 300 °C) occurs for a sulfur concentration of 7%. Our devices were limited to structures using lattice matched cladding layers. Carrier confinement in these devices is accomplished with a single, strained CdZnSe quantum well. The composition and thicknesses were chosen

to keep the wells pseudomorphic. Chlorine and nitrogen were used as the donor and acceptor impurities, respectively. The net doping densities on both sides of the junction were typically 10^{17} cm^{-3} and the n and p contact layers were doped to approximately 10^{18} cm^{-3}. In devices with 1 μm ZnSe guides and 100Å quantum wells, computer modelling gives an optical confinement factor of $\Gamma=0.013$ and substrate losses less than 1 cm^{-1}.

Although the cladding is lattice matched to the substrate, lattice mismatch exists between the cladding and guiding layers. This lattice mismatch is partially relaxed by the formation of dislocations near the cladding/guiding interfaces. TEM studies show some of these propagate into the CdZnSe quantum well. The presence of dislocations in the well adversely affects the quantum efficiency.

Both gain-guided and index-guided devices have been fabricated. Since their operating characteristics were observed to be similar, most of our studies were done on gain-guided devices. Our most successful heat sinking is achieved bonding the laser p-side up on Cu heat sinks using high purity In.

Operating Characteristics:
Our early devices were operated in the pulsed mode because of problems with heating. Typically 500 ns pulses and 500 μs periods were used. The voltage at threshold for these devices are typically 20 V. The large operating voltages are primarily due to problems with making good ohmic contact to the p-layer.

The emission wavelengths are determined by the composition and width of the CdZnSe quantum well. We have tuned the wavelengths of our devices from 508-535 nm at room temperature (490-512 nm at 77K). It will be difficult to keep the width of the wells below the critical thickness for longer wavelength devices, and significantly shallower wells will not provide adequate carrier capture for room temperature operation. The maximum measured output power is strongly dependent on the pulse length, duty cycle, temperature and collection optics. As an example we have obtained more than 100 mW/facet for devices with uncoated facets operated with 500 ns pulses and 01.% duty cycle at 77K.

Devices with no facet coating have been operated in the pulsed mode up to 250 K. The reflectivity of the cleaved facets is 0.21 which is

significantly smaller than that of cleaved GaAs . Lasing up to room temperature is routinely achieve in devices with 70% reflective coatings on both end facets. The threshold current density for coated devices has been as low as 95 A/cm^2 at 77K and 2200 A/cm^2 at room temperature.

Recently, cw operation has been achieved at 77K. The threshold current for cw operation was unchanged from that obtained in the pulsed mode. The L-I for a 512 nm, cw laser is shown below.
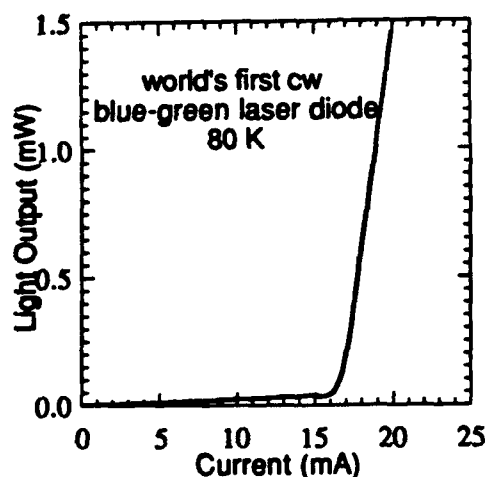

Figure 2 The L-I from a 20 μm wide stripe laser operating cw. The cavity length for this device was 1.2 mm.

Threshold currents have been measured as functions of cavity length and temperature. From these studies we have obtained a differential gain coefficient, β, of 0.046 μm-cm/A . The propagation loss in devices with 1 μm ZnSe guides is 8.1 cm^{-1}. Typical device parameters are J_0=100 A/cm^2 and T_0=80 K.

Summary:
Visible diode lasers have been made from wide band gap II-VI semiconductors. These separate confinement devices have been operated in the pulsed mode up to room temperature and continuously at 77K. Many of the materials properties and current device characteristics suggest that viable devices are likely to evolve in the near future.

[1] M.A. Haase, J. Qiu, J.M. DePuydt and H. Cheng, Appl. Phys. Lett. 59, p. 1272-1274 (1991).

Overview - Blue-Green Semiconductor LED/Laser Work in Japan

Hiroshi Kukimoto

Imaging Science and Engineering Laboratory

Tokyo Institute of Technology

4259 Nagatsuda, Midori-ku, Yokohama 227, Japan

+81-45-922-1111 Ext. 2084

Summary

The research in Japan on the wide-bandgap materials for short-wavelength light emitting devices based on modern growth techniques of MOVPE and MBE started in early 1980s. The first attempt to organize a cooperative research system for wide-gap semiconductors in Japan can be traced back to the year 1984, when about 20 university research groups which had already been engaged in research on wide-gap II-VI materials gathered and started to make plans for joint research. This was followed by a three-year period research project on the property control of compound semiconductors, especially of II-VI, wide-gap III-V and I-III-VI$_2$ materials, within a priority area research program for "New Functionality Materials - Design, Preparation and Control", which started in 1987 under support of the Ministry of Education, Science and Culture. It was renewed in 1990 as an advanced project for additional three years, and since then it has been running with emphasis on atomic-scale control of crystal growth, control of localized electronic states, creation of new optical functionality, quantum structures and new properties, and control of material properties for new optical devices. Under the project, the growth of wide-gap II-VIs, especially of ZnSe and related alloys and superlattices has been very actively studied in many university laboratories.

It seems that the activity at university laboratories under the project stimulated research in this field at industrial laboratories, resulting in recent increasing activities at many organizations in Japan of the epitaxial growth of wide-gap materials by metalorganic vapor phase epitaxy (MOVPE), molecular beam epitaxy (MBE) and MOMBE and their characterization. The first domestic workshop on II-VI compounds was held in 1989 with many participants who were actively engaged in research in this field in industry as well as universities, followed by the second and third ones in 1990 and 1991, respectively. Discussion at these workshops was focused on the fundamental subjects such as p-type conductivity control, photoassisted growth and quantum structures.

A remarkable progress in epitaxial growth of ZnSe and related alloys of high quality, in terms of purity, surface morphology and crystallinity, on GaAs and GaP substrates has been

made by MOVPE and MBE. Important keys for the progress include the purification of source materials [1], lattice matching to the substarate [2,3], insertion of a strained superlattice buffer layer between epilayer and substrate [4] and sulfur treatment of substrate surface [5]. N-type conductivity control of ZnSe, ZnS and their alloys has been well established by doping with a variety of impurities which include Al, Ga, Cl, Br and I [2]. Many efforts have been made to achieve the p-type doping of these materials with Li, N or O [2]. An effective p-type doping utilizing plasma excited N_2 gas during MBE growth has been found recently [6]. The effectiveness of this unique doping technique, which has also been used for the recent success in US of blue-green lasers of ZnSe based materials, raises a question whether p-type control can also be achieved by using different growth techniques, e.g., MOVPE and MOMBE, and N and other impurities. I would like to make a brief comment on that based on our recent results. Anyhow, on the basis of these studies, blue emitting LEDs of ZnSe with p-n junction, where N, Li and N, or O are used as p-type dopants, have already been reported from several research groups although further improvements of efficiency and reproducibility must be made toward a goal of practical devices [7-10].

Extensive studies have been performed on a variety of strained-layer superlattices and quantum well structures of widegap II-VIs grown by various methods. The materials systems studied include ZnSe/ZnTe by MBE, MOMBE and hot-wall epitaxy (HWE), CdS/ZnS by HWE, ZnSSe/ZnSe by MOVPE and ZnCdSe/ZnSSe by MOMBE [2]. Structural and optical characterization has been actively carried out to optimize the growth conditions. Some of them have shown photopumped blue stimulated emission. However, the blue-green injection lasers of these structures have not yet, to the best of my knowledge, been demonstrated in Japan.

Another candidate as a blue emitting material is GaN with a direct bandgap of 3.4 eV. A remarkable improvement of crystallinity of GaN epitaxial layers has been demonstrated by the prior deposition of AlN as a buffer layer on sapphire substrates before the growth of GaN by MOVPE [11]. Another notable progress in this material is an achievement of p-type conduction by the low energy electron beam irradiation of Mg-doped MOVPE-grown layers [12]. On the basis of these results GaN p-n junction LEDs have been fabricated for the first time. Details of these works together with more recent results will be presented by Amano et al. at this meeting.

A major advantage of SiC over other materials for blue emitting devices is that it can be easily made of both n and p types by using a well-established technique of liquid phase epitaxy (LPE), although it is suited only for LEDs and not at all for lasers since it is an indirect bandgap material. A main problem for SiC LEDs has been the difficulty of fabricating large area substrate of SiC of a specific crystal structure, 6H-SiC, on which epilayers of the same structure, which is capable for blue emission, are to be grown. The growth of substrate crystals of 1-1.3 inch diameter have been demonstrated [13], but the size semms to be still small. Recently, blue LEDs with a high brightness of 12 mcd at 20 mA have been developed on the basis of an improvement of crystallinity by LPE growth on off-oriented substrates and an optimization of

the Al concentration in an n-type layer. A major problem with mass production capability would still be related to a fact that large-area substrate wafers are not commercially available.

In view of the research history and main activities described above, the works in this field performed up to date in Japan could be regarded as rather oriented to the establishment of the epitaxial growth of high quality materials and their conductivity control as a necessary step toward future development of optical devices utilizing these materials. I guess that the activities in Japan have stimulated to some extent the research on wide-bandgap materials in US. The recent success achieved in US of making blue-green lasers based on ZnSe and related alloys has given us a good shock in its turn. I believe that the research in Japan, especially in industry, will dramatically change, making a step forward to the development of practical devices. Finally, I hope that the research in this field will bloom up beautifully over the world.

References

[1] H. Kukimoto, *J. Cryst. Growth*, **101**, 953 (1990).

[2] H. Kukimoto, *Mater. Res. Soc. Symp. Proc.*, **161**, 953 (1990): *J. Cryst. Growth*, **107**, 637 (1990); *Semicond. Sci. Technol.*, **6**, A14 (1991); and references therein.

[3] N. Matsumura, M. Tsubokura, J. Saraie and Y. Yodogawa, *J. Cryst. Growth*, **86**, 311 (1988).

[4] S. Hayashi, T. Sakamoto, Sz. Fujita and Sg. Fujita, *Appl. Surf. Sci.*, **41/42**, 534 (1989).

[5] Y. Wu, T. Toyoda, Sz. Fujita and Sg. Fujita, *Japan. J. Appl. Phys.*, **29**, L144 (1990).

[6] K. Ohkawa, T. Karasawa and T. Mitsuyu, *Japan. J. Appl. Phys.*, **30**, L152 (1991).

[7] T. Yasuda, I. Mitsuishi and H. Kukimoto, *Appl. Phys. Lett.*, **52**, 57 (1988).

[8] M. Migita, A. Taike, M. Shiiki and H. Yamamoto, *J. Cryst. Growth*, **101**, 835 (1990).

[9] K. Akimoto, T. Miyajima and Y. Mori, *Japan. J. Appl. Phys.*, **28**, L532 (1989).

[10] K. Ohkawa, A. Ueno and T. Mitsuyu, *Japan. J. Appl. Phys.*, **30**, (1991) (in press).

[11] H. Amano, N. Sawaki, I. Akasaki and Y. Toyoda, *Appl. Phys. Lett.*, **48**, 353 (1986).

[12] H. Amano, M. Kito, K. Hiramatsu and I. Akasaki, *Japan. J. Appl. Phys.*, **28**, L2112 (1989).

[13] Y. Matsushita, Y. Nakata, T. Ueda, T. Uetani, Y. Fukikawa, K. Koga and T. Niina, *Proc. 5th Inern. Display Research Conf.*, p.696.

Versatile Blue-Green Laser Diodes and LEDs in ZnSe-based Quantum Wells

H. Jeon, J. Ding, and A.V. Nurmikko

Division of Engineering and Department of Physics

Brown University, Providence, RI 02912

(401)863-2869

W. Xie, D. Grillo, M. Kobayashi, and R.L. Gunshor

School of Electrical Engineering

Purdue University, West Lafayette, IN 47907

Summary

The culmination in the development of wide bandgap II-VI compound semiconductors towards light emitting applications in the blue-green has been the recent demonstration of diode laser action by the 3M group [1] and the Brown-Purdue team [2]. In this paper we show different variations in the heterostructure design to produce high power, high efficiency laser action, which is especially clear at low temperatures. Our system is based on the (Zn,Cd)Se/ZnSe or (Zn,Cd)Se/Zn(S,Se) QWs the former of which had earlier been shown by us to show good electronic confinement [3], enhanced excitonic effects [4], and good optically pumped laser action, including cw operation at T=77K [5].

Figure 1 shows the principal heterostructures, including the two "growth polarities" (on lattice amtched p-type and n-type InGaAs or GaAs epilayers, respectively). In both cases diode laser action has been achieved at comparable performance levels. We find, however, that with structures grown on p-GaAs (hence terminating with n^+-ZnSe), the built-in heterojunction barriers lead also to lateral current flow. We have made use of this to demonstrate a LED display 'device', shown in Figure 2 [6]. The area defined by the letters though lithography and wet etching emits brightly (especially when cooled) in the LED mode over the entire area of the letters eventhough these are point contacted only in a few locations at the top surface.

The option of varying the polarity of the structure may be important in designing low loss electrical contacts to the wide gap II-VI portion, an issue which is central to further improvement of the laser diode devices. While both the 3M group and ourselves initially incorporated Zn(Se,S) epilayers to aid in the device operation, we have now operated dozens of devices without extra cladding layers. This lasing is partly facilitated by the good waveguiding action which we have

shown to exist in these structures in a separate study [7]. Most of our laser structures incorporate mesas of 20-40 μm in width in devices of about 1mm in optical resonator length. **Figure 3** shows the output from a (Zn,Cd)Se/Zn(S,Se) MQW device (L_w=75 Å) with uncoated facets from T=77K to T=273K. The corresponding threshold current density I_{th} is about 350 A/cm^2 and considerable further lowering is possible with coating of the cleaved resonator facets. The I_{th} has been found to increase by about a factor of five to room temperature conditions. Our best devices have shown η_{ext} to 60% at T=77K to date.

Since the blue-green diode lasers exhibit strong stimulated emission cross-section, the possibility of rapid gain switching exists. In preliminary transient experiments, we have employed subnanosecond electrical pulses to generate optical pulses of less than 100 psec in duration. Finally, a novel aspect of the gain and stimulated emission in the (Zn,Cd)Se/ZnSe quantum well system are the strong excitonic contributions which have been recently shown by us to be of key importance in optical pumping studies [8]. An important piece of evidence is the ability to obtain laser action by direct resonant optical pumping to the n=1 heavy-hole exciton state over a wide temperature range. **Figure 4** shows the comparison between the exciton absorption of a (Zn,Cd)Se quantum well sample and the corresponding stimulated emission from a laser diode at T=77K. When allowing for a small heating in the laser (hence thermal shrinkage of the bandgap), we find that the laser emission actually occurs in the low energy tail of the QW exciton absorption resonance as in the optically pumped case. A model detailing the excitonic gain in these quantum wells has been put forth by us recently [9].

[1]   M. Haase et al, *Appl. Phys. Lett.* **59**, 1272 (1991).

[2]   H. Jeon et al, *Appl. Phys. Lett.* **59**, 1945 (1991)

[3]   W. Walecki et al,   *Appl. Phys. Lett.* **57**, 466 (1990)

[4]   J. Ding et al, *Appl. Phys. Lett.* **57**, 2885 (1990)

[5]   H. Jeon et al, *Appl. Phys. Lett.* **57**, 2413 (1990); 2756 (1990); **59**, 1293 (1991).

[6]   H. Jeon et al, *Appl. Phys. Lett.* **60** (Jan 13, 1992)

[7]   W. Walecki et al, *J. Opt. Soc. Am.* **B8**, 1799 (1991)

[8]   J. Ding et al, QELS'91 Baltimore, (1991); Proc. of Conference on Modulated Semiconductor Structures, Nara, Japan (1991), *Surface   Science* (in press)
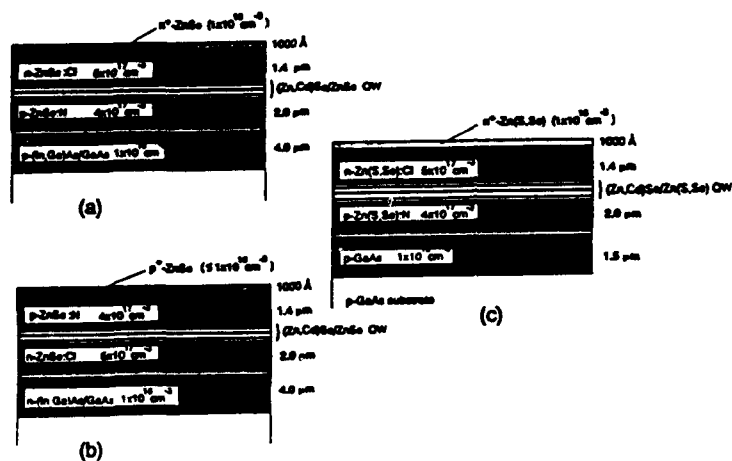
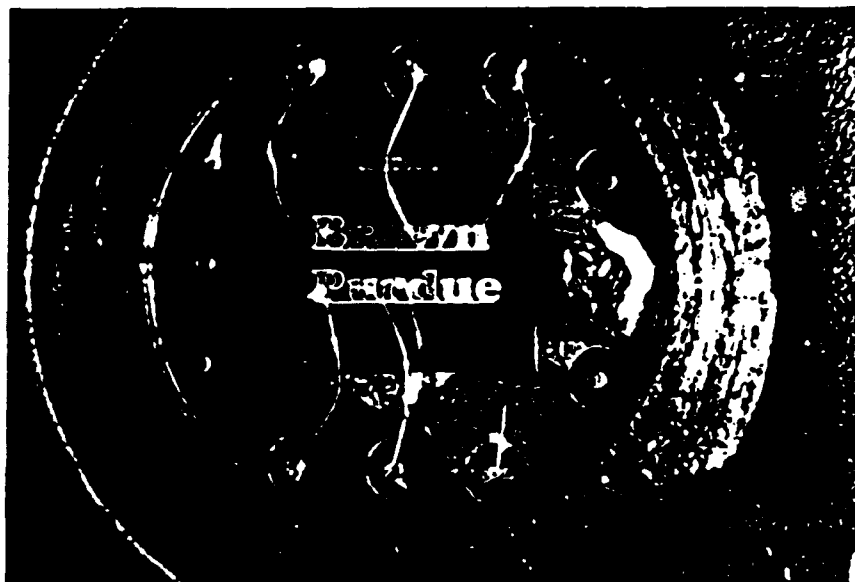Figure 1: Schematic of the principal QW LD and LED structures including opposite p-n heterostructure "polarity".

Figure 2: A display demonstration of a patterned and etched structure at $T = 77K$, with the MQW emission transmitted through the top layers of the sample. Note that the electrical contacting is made only at a few locations on the sample.
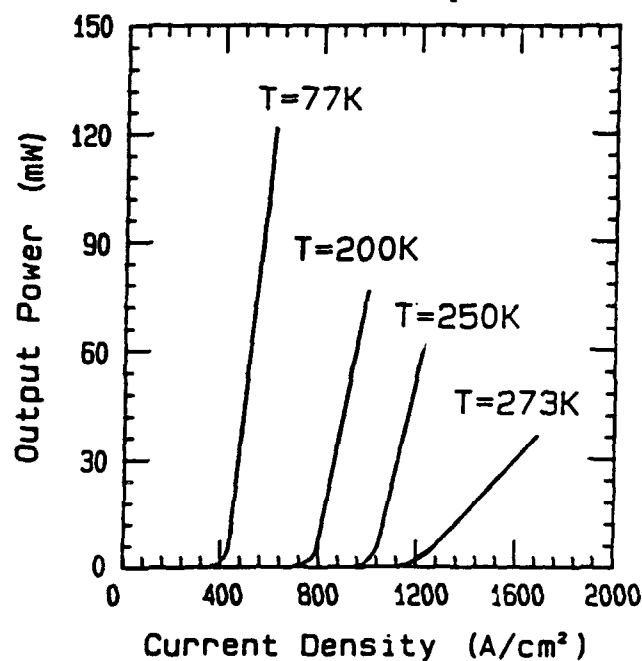
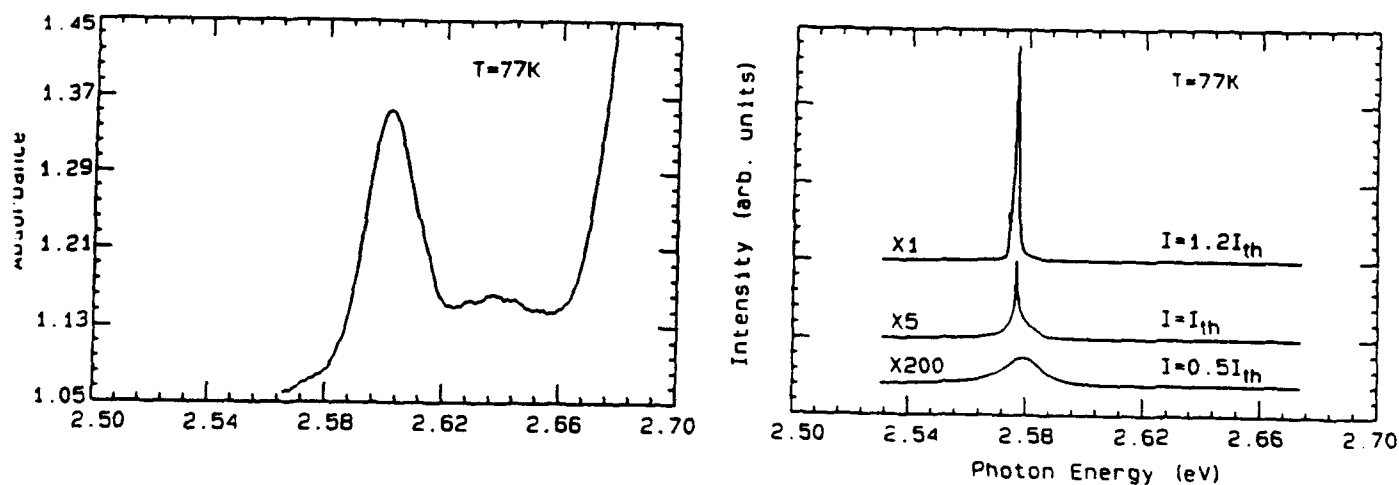**Figure 3:** Laser power per facet vs. current density for a (Zn,Cd)Se/Zn(S,Se) diode laser from T=77K to T=273K (uncoated facets).

Figure 4: Comparison between the stimulated emission and absorption spectra at T=77K showing the spectral correlation between the two.

Perspective of GaN/GaAlN based ultra-violet/blue lasers

H. Amano, I. Akasaki, K.Itoh and H.Murakami

Department of Electronics, Nagoya University
Furo-cho, Chikusa-ku, Nagoya 464-01, Japan
81-52-781-5111

Summary:

In order to realize compact and high density optical and electro-optical storage system, the demand for the fabrication of compact short wavelength light emitting devices such as light emitting diode(LED) or laser diode(LD), especially compact ultra-violet(UV)-LD or blue-LD is increasing.

Gallium nitride (GaN) and gallium aluminum nitride $(Ga_{1-x}Al_xN:x>0)$ alloy system have attracted much attention as a candidate for the realization of such a short wavelength LD, because they have wide and direct transition type band structure with their band gap ranging from 3.4eV to 6.2eV at room temperature (RT). However, difficulty in growing high quality thin film of single crystal and difficulty in controlling electrical properties, especially in obtaining low resistive p-type films have prevented the realization of UV/blue-LD.

Recently, we have succeeded in growing high quality GaN[1,2] and $Ga_{1-x}Al_xN(0<x\leq0.4)$[3,4] films and their multiple heterostructure[5] on the sapphire (0001) substrate by metalorganic vapor phase epitaxy using thin aluminum nitride (AlN) 50nm thick deposited at low temperature as the buffer layer. The GaN film thus grown shows best figure up to date in this material in various characterization, such as double crystal X-ray diffraction measurement, photoluminescence measurement and the Hall effect measurement. Moreover, optically pumped stimulated emission can be observed even at RT from the "bulk" GaN film with AlN buffer layer[6].

As concerns the electrical properties, GaN films usually show n-type conduction. By doping with acceptor impurity such as zinc or magnesium (Mg), GaN film shows high resis-

tivity. Until recently, low-resistive p-type GaN film has been hardly obtainable. In 1989, we found that low-resistive p-type GaN can be obtained by treating Mg-doped GaN(GaN:Mg) film with low energy electron beam irradiation (LEEBI)[7]. The typical hole concentration and the resistivity of the GaN:Mg treated with LEEBI are $2*10^{17}cm^{-3}$, and $12\Omega \cdot cm$, respectively. These results[1~7] show the possibility for the realization of current injection type UV/blue-LD.

In this work, various GaN/GaAlN heterostructures have been fabricated such as $P-Ga_{0.9}Al_{0.1}N/n-GaN/N-Ga_{0.9}Al_{0.1}N$ double heterostructures (DH's) or $P-Ga_{0.9}Al_{0.1}N/n-GaN/N-Ga_{0.92}Al_{0.08}N/N-Ga_{0.9}Al_{0.1}N/n^{+}-GaN$ separate confinement heterostructures(SCH's). The stacked structure of the DH is schematically depicted in fig. 1. Figure 2 shows the I-V characteristics measured at RT of the DH's with 10μm stripe and 0.6mm cavity. Figure 3 is the photograph taken at one side end of the cavity of this DH's operated at RT with a forward current of 18mA. Blue emission from the 10μm stripe is clearly observed, and more intense UV emission is detected by the EL spectrum measurement.

Results on the high pulsed current density operation at both low and room temperatures will be presented.
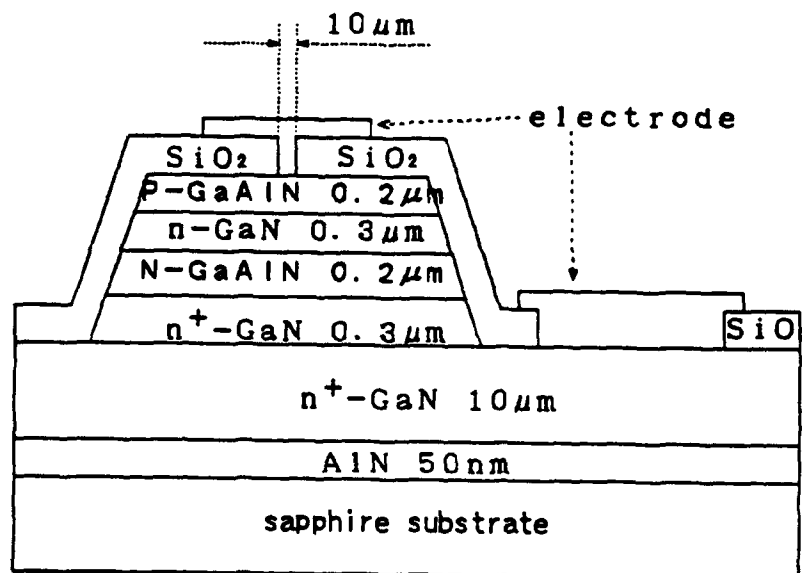
Figure 1 Schematic drawing of the stacked structure of the fabricated DH's.

1V/div.
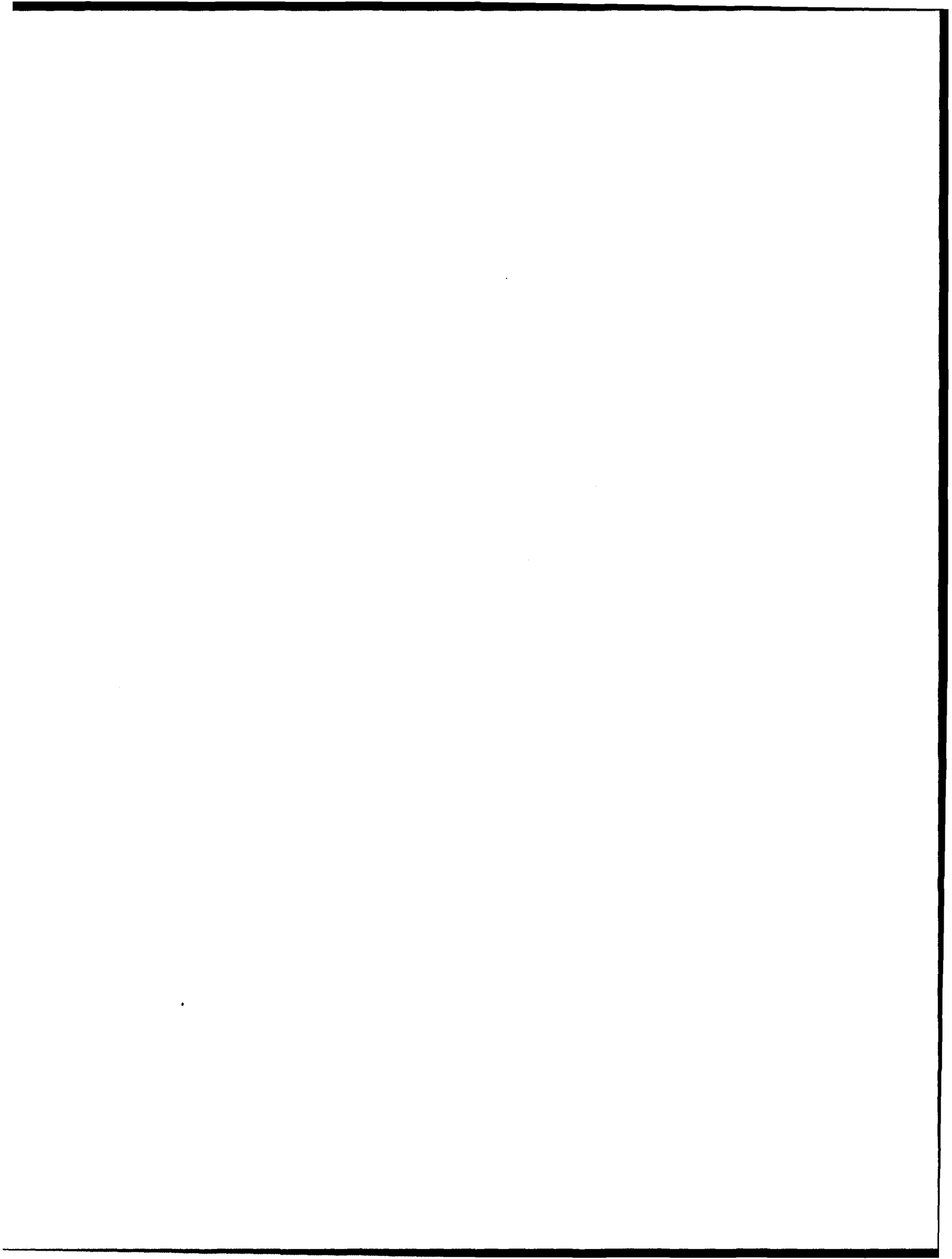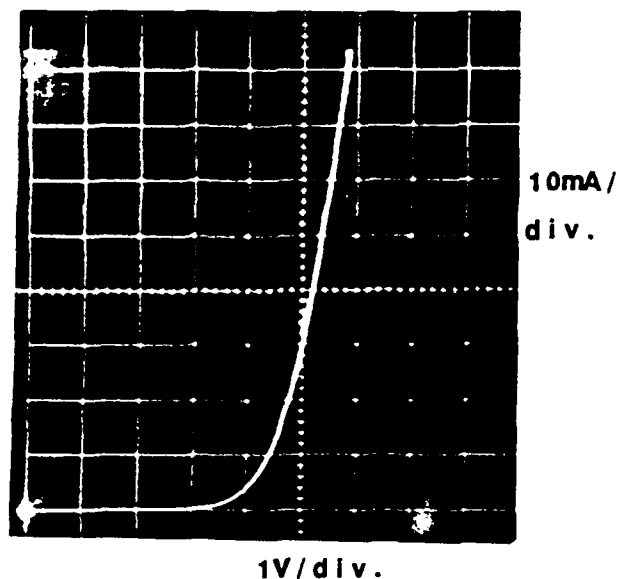
Figure 2 I-V characteristic of the DH's.

Figure 3 Photograph taken at one side end of the DH's operated at RT with a forward current of 18mA.

References

[1]H.Amano,N.Sawaki,I.Akasaki and Y.Toyoda;Appl.Phys.Lett. 48(1986)353.

[2]H.Amano,I.Akasaki,K.Hiramatsu,N.Koide and N.Sawaki;Thin Solid Films 163(1988)415.

[3]I.Akasaki,H.Amano,Y.Koide,K.Hiramatsu and N.Sawaki; J.Cryst.Growth 98(1989)209.

[4]Y.Koide,N.Itoh,K.Itoh, N.Sawaki and I.Akasaki; Jpn.J.Appl.Phys. 27(1988)1156.

[5]K.Itoh,T.Kawamoto,H.Amano,K.Hiramatsu and I.Akasaki; Jpn.J.Appl.Phys. 30(1991) To be published.

[6]H.Amano, T.Asahi and I.Akasaki; Jpn.J.Appl. Phys. 29(1990)L205.

[7]H.Amano,M.Kito,K.Hiramatsu and I.Akasaki; Jpn.J.Appl. Phys. 28(0989)L2112.

Materials

ThD   3:30pm–5:30pm
Anasazi South

John D. Bierlein, *Presider*
E. I. du Pont de Nemours & Company

Inorganic Crystals for Frequency Conversion

Peter Bordui

Crystal Technology, Incorporated

Bulk organic crystals, including KTP, $KNbO_3$, $Mg:LiNbO_3$, and periodically poled $LiNbO_3$, are known to offer attractive potential for frequency conversion devices. Although problems remain, significant progress has been made in developing these materials for practical application.

Organic Nonlinear Materials for Frequency Conversion:
Property Trade-off and Recent Applications.

L.-T. Cheng

Central Research and Development Department, E. I. Du Pont De Nemours & Co., Inc.,
Experimental Station,
P.O. Box 80356, Wilmington, Delaware 19880-0356

Frequency doubling of short wavelength diode lasers has significant technological applications in imaging and optical recording. One of the major hurdles towards achieving efficient doubling remains to develop highly nonlinear materials with appropriate linear optical properties such as birefringence and transparency. One approach is to engineer materials by doping or grafting nonlinear organic molecules into transparent polymeric matrixes. Second-order nonlinearity is obtained by the acentric alignment of these molecules along their dipole moments under an external electric field. With this approach, several molecular properties are important, including large molecular dipole moment and hyperpolarizability inner product ($\mu\beta_\mu$) as well as very low absorption at the first and second harmonic wavelengths of diode lasers (near 800 and 400 nm). An established guideline in identifying organic molecules with large hyperpolarizabilities is by the presence of low-lying strong charge-transfer (CT) electronic transitions. However, such an approach is in conflict with the requirement of transparency.

One objective is to investigate the extent of such a nonlinearity-transparency trade-off and to identify suitable classes of organic molecules for efficient frequency doubling in the blue spectral region. We review results obtained by solution phase DC electric-field induced second-harmonic generation (EFISH) measurements on benzene, styrene, biphenyl, fluorene and stilbene derivatives. A systematic study of charge transfer (CT) molecules with donor and acceptor substituents of varying strengths is conducted to investigate their impacts on the CT band positions, hyperpolarizabilities, as well as their trade-off. we examine the relationship between the β_μ values and the λ_{max} of CT bands for a series of conjugated CT molecules. The β_μ and λ_{max} for a given π system are varied with combinations of donor and acceptor groups of varying strengths. 1.91 μm measurement results obtained for these molecules in weakly polar solvents are presented in logarithmic plots in Figure 1. Data points include *para* or 4-4'

Figure 1. Logarithmic plots of β_μ (1.91 μm) and the λ_{max} for CT molecules.
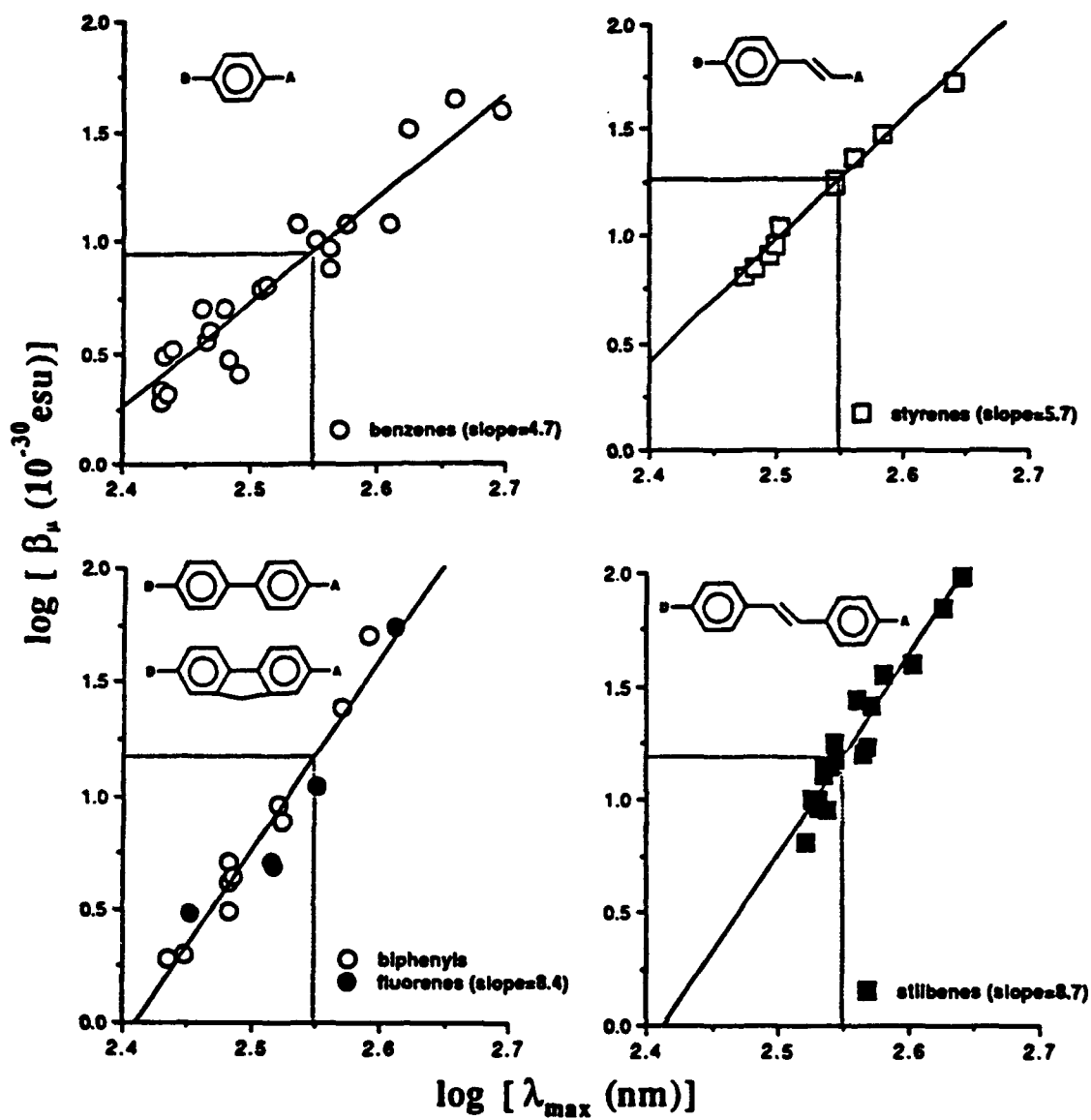
disubstituted derivatives of donor-acceptor combinations of donor, such as CH_3, Br, OH, SH, OR, SR, $NHNH_2$, primary, secondary, tertiary, or julolidine amines, and acceptor, such as SO_2R, CN, CO_2R, COR, COH, NO, NO_2, $CHC(CN)_2$, or $CCNC(CN)_2$, in increasing effectiveness. Evidently, strong correlations between β_μ and λ_{max} exist for all five molecular classes with nonlinearities and CT band wavelengths increasing with the combined strengths of donor and acceptor groups. Within the uncertainty of some dispersion enhancement for the high λ_{max} data, strong power law dependence between quadratic nonlinearity and CT band position are found, with exponents ranging from 4.7 to 8.7. This dependence is considerably stronger for the extended biphenyl, fluorene, and stilbene π systems. Therefore, for a given λ_{max}, better trade-off can be realized by extending the π system which probably affords higher $f\Delta\mu$ products. Within a certain transparency requirement, as indicated by the dash boxes in Figure 1, materials are confined to derivatives with weak donors and acceptors. In particular, cyano and aldehyde substituted benzenes and styrenes are found to yield mostly white materials with usable nonlinearities. For single crystals where molecular alignment can be high, investigation of these molecular classes should yield materials suitable for harmonic generation applications.

Aromatic CT derivatives of accepting groups with strong inductive contributions, such as the fluoromethyl carbonyl, perfluoroalkylsulfonyl, and perfluoroalkyl sulfonylsulfimide groups, are identified as promising candidates for the application at hand. Inductive effect is considered to be an interaction through space in the form of an effective internal field which should result in an electronic biasing effect for all states with different electronic distributions. Nonlinearity arising from substituents with strong inductive contributions should have better transparency trade-off since low lying transitions are not required. In addition to a high nonlinearity and a large dipole moment, colinearity of the molecular dipole and the CT axis is necessary in order to achieve high macroscopic nonlinearity through electric poling. Due to the pyramidal sulfur center, the carbon oxygen bonds are tilted off the aromatic plane in sulfonyl substituted CT derivatives. For methyl sulfonyl derivatives, the molecular dipole is tilted about 63° off the aryl carbon sulfur bond, leading to a cosine projection loss of more than 50%. However, as a result of the polar trifluoromethyl group, the dipole moments of fluoromethylsulfonyl derivatives are less than 13° off the CT axes, which is less than 3% off optimum projection. The total dipole moments are also found to be about one Debye higher than the unfluorinated derivatives. Therefore perfluoroalkyl sulfonyl derivatives should give a factor of 2 enhancement in properties over those of the unfluorinated materials.

Organizational approaches for establishing a macroscopic nonlinear optical response re diverse for organic materials; including single crystals, Langmuir-Blodgett (LB) and

self-assembling films, as well as polymeric and sol-gel matrices. Single crystals offer maximum chromophore number density and a high degree of permanent alignment. Given the transparency requirement for short wavelength frequency conversions, the modest molecular hyperpolarizability should be optimally organized via an efficient single crystal structures. However, difficulties such as unpredictable crystalline structures, crystal growths, and waveguide fabrications have discouraged efforts in this important direction. LB and poled polymeric approaches offer considerable flexibility for material engineering and waveguide formation, but rely on a dynamically frozen and inherently "temporary" polar alignment of nonlinear optical chromophores. Dilution of number density due to bulky end-groups in the case of LB films and polymeric backbone in the case of poled polymers represents addition difficulties with these approaches. For poled polymers, alignment is also limited by the dielectric breakdown potential of a poling field. Nevertheless, phase-matched harmonic generations via Cherenkov, modal dispersion, quasi-phase-match, and anomalous dispersion have all been recently demonstrated with crystalline or amorphous organic materials.

Large Second-Order Nonlinearity in Poled Fused Silica*

R. A. Myers, N. Mukherjee and S. R. J. Brueck

Center for High Technology Materials, University of New Mexico

Albuquerque, NM 87131;   Telephone: (505) 277-3317

Fused silica is ubiquitous in modern technology, playing an essential enabling role in both optoelectronics and microelectronics. Fused silica is amorphous with a macroscopic inversion symmetry that forbids second harmonic generation (SHG). Thus the discovery by Österberg et. al. [1] of efficient SHG in glass fibers upon "training" with optical fields has generated considerable interest.

Here, we report the first observation of a permanent second-order nonlinearity in the near surface region of bulk fused SiO_2 induced by a combined temperature / static electric field poling process. The observed $\chi^{(2)}$ is three to four orders of magnitude larger than found in the fiber experiments and approaches that of $LiNbO_3$.

The preparation process for generating the $\chi^{(2)}$ nonlinearity involves heating to 250-325°C, in laboratory ambient, while applying a DC bias of 3-5 kV across the nominally 1.6-mm thick samples. For most experiments, the electrodes (typically stainless steel and Si) were simply lightly physically contacted to the sample rather than deposited. After ~15 minutes at temperature, the sample is allowed to cool to room temperature. Once cooled, the voltage (and electrodes) are removed and a stable $\chi^{(2)}$ nonlinearity is observed by SHG in transmission using 10-ns pulses at 1.06 μm from a 10-Hz Q-Switched Nd-Yag laser weakly focused to an intensity of 10 MW/cm². The SHG signals were recorded with a photomultiplier (signal/noise > 1000:1). No observable SHG signal was obtained for poling temperatures below ~210°C.

Poled samples kept at room temperature for several months without any special precautions show no noticeable degradation of the nonlinearity. Application of heat alone, above ~250°C, erases the nonlinearity. In contrast to the fiber results, irradiation at 257 nm at a cw power level of 100 mW/cm² from a frequency doubled Ar-ion laser for over an hour does not effect the nonlinearity.

The necessary poling voltage did not simply scale with the sample thickness. Attempts to pole commercial fused silica coverslips (180-μm thick) with a linearly scaled voltage were unsuccessful. However, large nonlinearities were observed when the same samples were placed atop a 1.6-mm thick sample and the 3-5 kV was applied across both samples in series.

SHG experiments were carried out at fundamental wavelengths of 1.06 μm, 740 nm (YAG-pumped dye laser) and 533 nm (second harmonic of YAG laser). In addition, sum frequency generation was observed using the 1.06 μm and 740 nm sources. As shown in Fig. 1, no signal was observed at normal incidence and there was a symmetric increase in the signal as the normal to the sample was rotated away from the incident beam direction. As expected, the poling electric field direction is the symmetry axis. A model fit to the data gives a best fit for a $\chi^{(2)}_{33}/\chi^{(2)}_{31}$ ratio of 2:1.

No fringes were observed at any wavelength. This indicates that the nonlinearity is confined to a layer thickness less than or comparable to the coherence length, which is 3 μm at 532 nm [2]. The absence of fringes also indicates that the nonlinearity is generated only on one side of the sample. From the periodicity of the interference fringes observed from two adjacent samples, it was determined that the nonlinearity was always on the side of the sample that had been positively biased. The nonlinearity could be switched from one side to the other of a sample by repoling with reversed polarity.

The depth profile of the nonlinearity was probed by chemical etching using 49% HF acid solution. Etch depths were measured by surface profilometer scans at each step. Fig. 2 shows the variation of the SHG signal for samples poled for a duration of 15 minutes, and for a duration of two hours. While the initial SHG signal was approximately the same for both samples, the increase of the layer thickness on longer poling time is significant.

The $\chi^{(2)}$ coefficient was measured by comparing with the SHG power generated in crystal quartz and LiNbO$_3$ reference samples at four different wavelengths. Using the coherence lengths for quartz, LiNbO$_3$, and fused silica and the characteristic decay length of the nonlinearity α^{-1}, measured from the etching experiments, a maximum value of $\chi^{(2)}_{33} \sim 1 \times 10^{-12}$ m/V for the poled fused silica was obtained. The measured $\chi^{(2)}_{33}$ value is almost 20% of the $\chi^{(2)}_{22}$ value of LiNbO$_3$. Within experimental error, no dispersion of the value of $\chi^{(2)}_{33}$ was observed at the four wavelengths used.

Comparable nonlinearities were observed in a number of commercial fused silica grades including optosil, homosil, infrasil and commercial TO-8. Supersil was an exception with a significantly smaller (< 0.1x) nonlinearity. This suggests that impurities might play a significant role in the nonlinearity. One possibility for the macroscopic mechanism of this nonlinearity involves the creation and orientation of AlO$_{3/2}^-$-Na$^+$ or other nonlinear complexes during the poling process [3]. However, for nominal impurity concentrations this model leads to questionably large values for the molecular nonlinearity or hyperpolarizability. Another possibility is the generation of a large DC field ($\sim 10^6$ - 10^7 V/cm) by charge transport and screening under the poling conditions. This large field then interacts with the third-order susceptibility of the fused silica to produce an effective second-order nonlinearity much as is postulated for the fiber experiments [4] and for nonlinearites in paraelectric compositions of PLZT and related materials [5]. At the temperatures used in these experiments, Na$^+$ is known to exhibit a significant mobility.

Because of the ready manufacturability of silica optical materials and their established integration with semiconductor optoelectronics, this nonlinearity will have important applications in waveguide and other optoelectronic devices. A novel waveguide architecture designed to utilize this large, near surface nonlinearity of both the bulk and the thin film SiO$_2$ is presented.

References:
1.   U. Österberg and W. Margulis, Opt. Lett. 11,516 (1986).
2.   I. H. Malitson, J. Opt. Soc. Amer. 55,1205 (1965).
3.   K. L. Brower, Phys. Rev. B 20, 1799 (1979).
4.   R. H. Stolen and H. W. K. Tom, Opt. Lett. 12, 587 (1987)
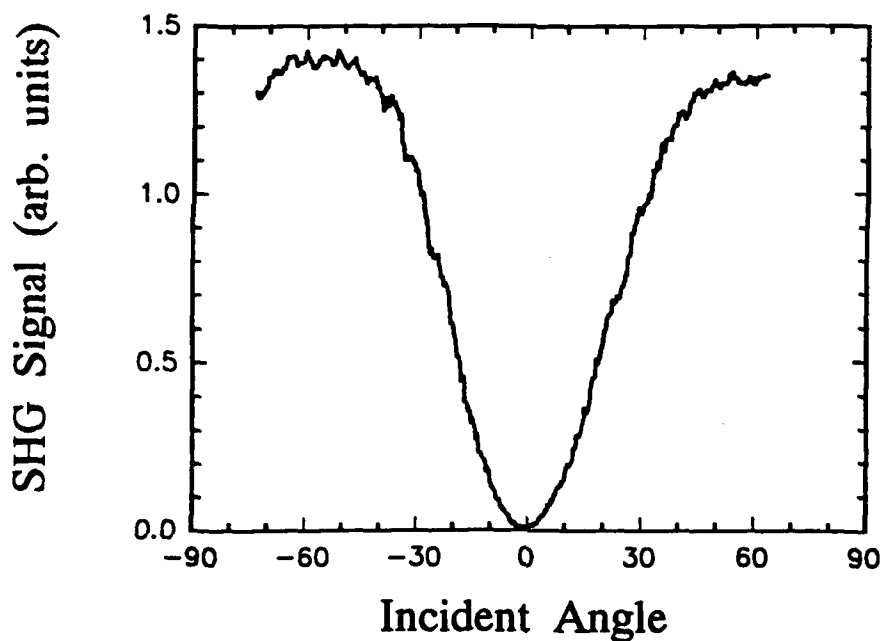5.   A. Mukherjee, S. R. J. Brueck and A. Y. Wu, Opt. Commun. 76, 220 (1990)

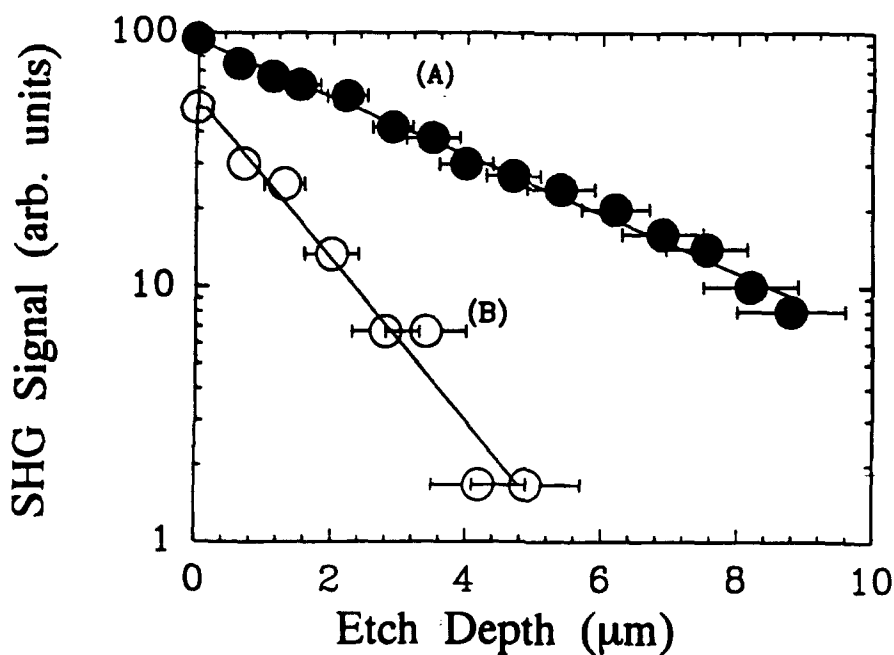Fig. 1: Angular variation of the SHG signal from an optosil sample for a TM polarized incident beam at 1.06 μm.

Fig. 2: SHG signal as material is successively etched away. Poling voltage 5 kV, poling temperature 280°C. Sample (A) was poled for two hours, sample (B) for 15 min.

Self-frequency-doubled high δn Proton Exchange Nd:LiNbO₃ waveguide lasers

Q. He, M.P. De Micheli, D.B. Ostrowsky
Laboratoire Physique de la Matière Condensée
Université de Nice, Parc Valrose, O6034 Nice Cedex, France
Tel: (33) 93 52 98 92
E. Lallier, J.P. Pocholle, M. Papuchon, F. Armani, D. Delacourt
Thomson-CSF, Laboratoire Centrale de recherches
Domaine de Corbeville 91404, Orsay, France
Tel: (33 1) 60 19 70 00
C. Grezes-Besset, E. Pelletier
Laboratoire d'Optique des Surfaces et des Couches Minces
Domaine Universitaire Saint Jerôme, 13397 Marseille, France
Tel.: (33) 91 28 83 28

Neodymium doped lithium niobate offers the possibility of combining laser action and non-linear effects in the same structure[1,2]. Low threshold, efficient, CW, proton-exchange (PE)[3] waveguide lasers and amplifers at 1.085 microns have been fabricated [4] and, recently, the integration of such a waveguide laser and an FM mode locker was demonstrated[5]. In view of the high nonlinear coefficients of lithium niobate, it would be interesting to combine parametric interactions, such as second harmonic generation (SHG), with the laser action. The "Cerenkov" doubling configuration appears to be the most interesting for this application since it provides automatic phase matching and the possibility of high efficiency, when realized with high δn step index guides[6]. Here we report on what is, to our knowledge, the first high δn waveguide lasers in lithium niobate and the observation of SHG and sum-frequency mixing with these devices. Depending on the pumping level, the high δn devices typically lase simultaneously at several wavelengths, and while the conversion efficiencies of these first devices are rather low, essentially due to strains induced propagation losses which we shall describe, we outline the way to overcome this.

High δn proton exchanged stripe waveguides were fabricated on a Z-cut Nd:MgO:LiNbO₃ crystal doped with 0.13 at.% Nd³⁺ and 5 mole% MgO[7] and highly reflecting mirrors around the expected wavelength were deposited on the polished end-faces. In figure 1 we show the results of microguide prism coupling measurements made at 1.06 μm indicating the effective indices for guides having different widths. An important point to note, is that constraints induced in this kind of PE waveguide gives rise to modifications of the optical axes in the guiding layer leading to a strong coupling of the ordinary and extraordinary polarized fields[8]. The modes of these guides are no longer quasi TM or quasi TE extraordinary modes, but hybrid modes[9] formed by two orthogonally polarized fields. Then, due to the negative birefringence of LiNbO₃, two families of hybrid modes are to be distinguished :

- pure guided modes characterized by $n_e + \delta n_e > n_{eff} > n_o$
- semi-leaky modes characterized by $n_o > n_{eff} > n_e$ whose ordinary polarized component radiaties in the substrate, resulting in important losses. This is the case for the guides having 1 and 2 microns widths on figure 1.

Laser action has been observed for each of the seven guides of different widths, indicated on figure 1, but with very different behaviours. As we have seen, the two narrowest guides have waveguide modes whose effective indices are lower than the ordinary index of the substrate, leading to laser action in the form of semi-leaky modes. The radiated wave contains approximately half the power, confirming the prediction of high loss. The laser regime is very unstable and the threshold high, on the order of 50 mW of absorbed pump power. The guides with a width higher than 3 μm were more interesting, because they fulfill the condition $n_{eff} > n_o$. A stable laser regime was then achievable, and the experimental results which follow concern a laser fabricated using a 6 μm width mask. In figure 2 we show the laser output power as a function of pump power for this device. Spectral analysis of the output revealed three lines at 1.0903, 1.0917, and 1.0923 microns (Fig. 3).

The high δn PE technique used provides two possibilities for SHG phase matching. In the first one, low order guided infrared modes are phase matched with high order guided modes in the visible[10]. This configuration has been observed previously[11], but has the disadvantage of coupling guided modes of very different field distributions (low order harmonic modes and high order pump modes), and thus presents only discrete phase matching possibilities with very poor overlap integrals severely limiting the conversion efficiency. It was observed using the guides having widths between 3 and 7 microns, the doubling interaction taking place between the TEM_{00} mode of the fundamental and the TEM_{50} mode of the harmonic The total harmonic power, consisting of the three doubled laser lines, emerging from one extremity of the laser, as a function of laser power, is shown on figure 2. In addition to the guided harmonic frequencies, we observed Cerenkov radiation generated by addition of the three laser frequencies with pump photons (Fig. 3).

In the second configuration, the "Cerenkov" configuration[12], $((n_{eff}(\omega) < n_e(2\omega))$ the guided infrared modes radiates into the substrate at an angle that assures automatically phase-matching. Furthermore, this configuration has been shown to be very efficient for optimized PE waveguides[13]. To be able to realize a self doubled waveguide laser one has then to fulfill two conditions which are a low loss completely guided mode at the fundamental laser frequency and "Cerenkov" condition.

The only lasers which allow satisfying the Cerenkov condition are the two narrowest. Unfortunately, due to their semi-leaky character they present high thresholds, unstable laser action, and generate only some weak Cerenkov SHG radiation. Due to the instability of the lasers, no reliable conversion efficiency measurement was possible. To improve this behavior one must optimize the guide structure. The Cerenkov efficiency will be greatly improved by a reduction of the guide depth to the 0.5 to 0.6 micron range. The use of guides, with widths between 3 and 4 microns, should, furthermore, lead to low-loss, fundamental laser modes. We are currently fabricating such structures and will report results at the conference.

We have demonstrated the operation of a CW-self-frequency-doubled waveguide laser in neodyium doped lithium niobate. The laser and harmonic production behavior were in agreement with theoretical predictions. An increase of several orders of magnitude in the conversion efficiency should be possible through the realization of a laser having an effective index permitting a nearly fully guided fundamental to generate Cerenkov configuration harmonic and we will report the results of ongoing efforts to fabricate such structures.

References

[1] V.G. DMITRIEV, et al.. "Simultaneous emission at the fondamental frequency and the second harmonic in an active nonlinear medium : Neodimium doped lithium niobate", Sov. Tech. Phys. Lett. vol. 5, pp. 590-591

[2] T.Y. FAN, et al. "Nd:MgO:LiNbO3 spectroscopy and laser devices" J. Opt. Soc. Am. B/Vol. 3,n°1, pp.140-147, (1986).

[3] J. L. JACKEL, et al. "Proton exchange for high-index waveguides in LiNbO3", Topical Meeting on Guides Wave Optics, Asilomar, CA, January 1982; and Appl. Phys. Letters, vol. 41, 607,1982.

[4] LALLIER E., et al. "Nd:MgO:LiNbO3 chanel waveguide laser devices", IEEE J. Quant. Elect. "Special issue on Photonics devices" Mars 1991

[5] LALLIER E., et al. "Integrated Nd:MgO:LiNbO3 FM mode-locked waveguide laser ", El. Lett.,. 27, n°11, 23 May 1991

[6] M.J. LI,, et al. " SHG in Cerenkov configuration ", J.Q.E. Vol. 26, n°8 pp.1384-1393.

[7] Supplied by SUMITOMO, Mitsui Mining Co., Japan

[8] S. CHEN, et al. "Constraints and modes propagation in PE waveguides", to be published.

[9] A. KNOESEN,, et al. "Hybrid Guided Modes in Uniaxial Dielectric Planar Waveguides", J. Light. Tech., vol. 6, n°6, pp. 1083-1103 (1988)

[10] J.P. BARETY "Génération du second harmonique dans des guides d'ondes réalisés par échange protonique" Thèse soutenue à Nice (France) 1986

[11] S. NEVEU, et al. "Phase matched SHG using d33 coefficient in proton exchanged LiNbO3 waveguides", IGWO 84, post deadline paper, 24-26 April 1984, Kisimmee Florida.

[12] M.J. LI, , et al. "Cerenkov configuration Second Harmonic Generation"

[13] T. TANIUCHI and K. YAMAMOTO, "Second harmonic generation by Cerenkov radiation in proton-exchanged optical LiNbO3 waveguide", CLEO' 86,WR3.
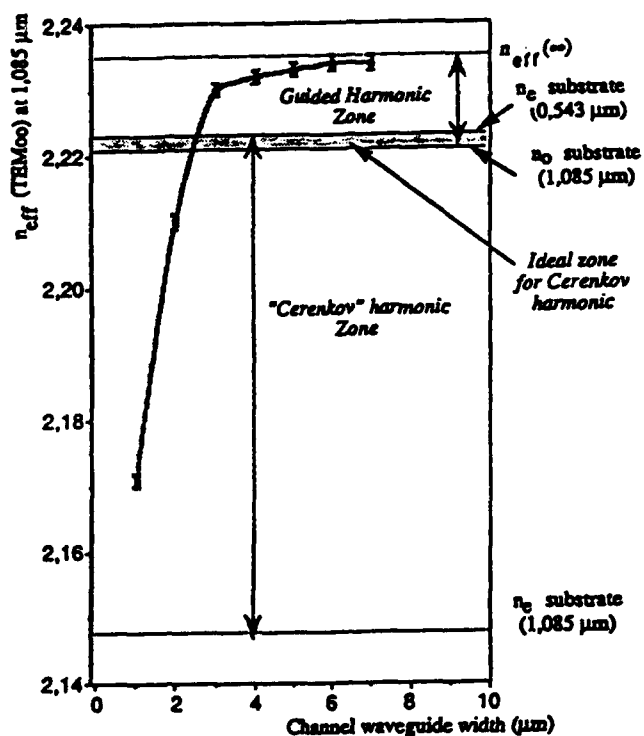
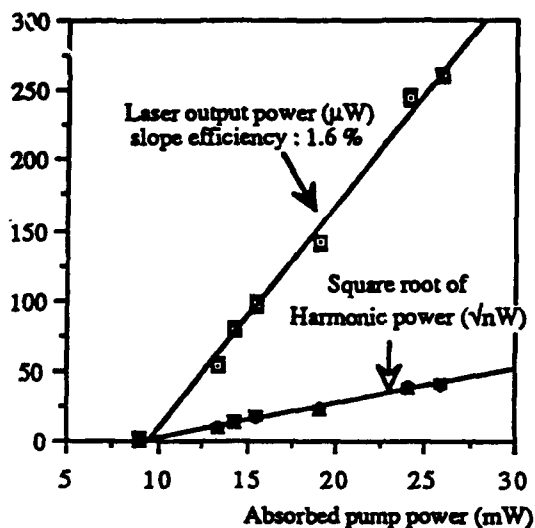Fig. 1 . Effective indices, at 1.06 μm, as a function of mask width

Fig. 2 .Laser and guided harmonic power (extraordinary polarization component) as a function of absorbed pump power. The ordinate scale refers to microwatts for laser output power and to the square root of nanowatts for the square root of harmonic power.
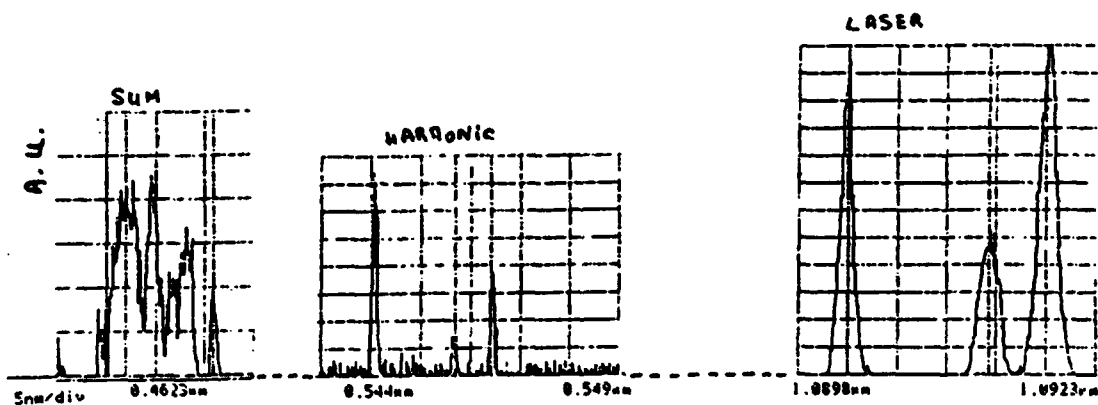

Fig. 3 .Spectrum of the CW-self-frequency-doubled waveguide laser in neodymium doped lithium niobate

Periodically-poled Lithium Niobate Crystals for Efficient Frequency-Doubling

D. H. Jundt, M. M. Fejer and R. L. Byer
Applied Physics Department, Stanford University, Stanford, CA 94305
(415) 725-2160

In periodically poled LiNbO3, first order quasi-phase-matching (QPM) allows nonlinear interactions between waves polarized along the z-axis, for which the largest nonlinear coefficient $d_{eff} = 2d_{33} / \pi = 20.9$ pm / V can be used, leading to 15 times larger conversion SHG efficiency per unit length compared to birefringent phase-matched interactions. The periodicity of the inverted ferroelectric domains must equal twice the coherence length of the nonlinear interaction. Fig. 1 shows the required period vs wavelength for SHG using d_{33}.
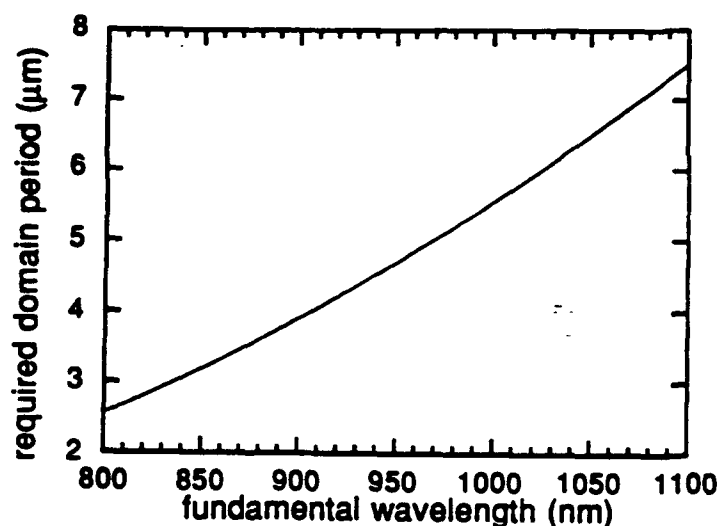
Fig. 1 Required period of the inverted domain pattern in LiNbO3 vs the wavelength of the fundamental.

In practice, the creation of the required, finely spaced domains with sufficiently accurate periodicity is a challenging task. We used the laser heated pedestal growth method to grow 5% MgO-doped LiNbO3 miniature crystal rods with good control of the average growth speed and thus the domain period. To start the growth, a CO_2 laser was focused on the tip of a source rod to make a small molten droplet into which a a-axis seed crystal was dipped. Domain reversal was achieved by periodically interrupting the heating power for a duration of 20 – 40 ms, leading to a periodic variation in the magnesium dopant concentration. Crystals with domain periods ranging from 2.6 to 13 μm could easily be grown. These crystals phase-match second harmonic generation (SHG)

using d_{33} to generate radiation covering a wide spectral range from 400 nm to 660 nm. Typical average growth speeds were 2 mm/min. Due to the crystal symmetry, the domains are discontinuous along a plane bisecting the rod at its center.

To demonstrate high average power QPM SHG, a 800 µm-diam 1.24 mm long sample with domain period of 6.94 µm was placed at the center of a bow-tie ring cavity. 75% of the single frequency Nd:YAG laser power was mode matched to the cavity mode with a beam waist of $w_0 = 15$ µm in the sample. The sample endfaces were AR-coated at 1064 nm with a single SiO_2 layer, and had a second harmonic transmission of 86%. Fig. 2 shows the overall performance of the doubler. To compensate for a slight periodicity error, the sample was heated to 140°C. The experimental data is well described for an effective length of 0.56 mm and a cavity round-trip loss of 1.7%.[1] The resulting SHG power for a perfect sample where the full 1.24 mm length is used is also shown in the graph. By using dielectric coatings AR coatings for the sample, the performance of the doubler could be improved by 14%.

Very slight variations in domain period along the crystal length lead to phase-errors in the second harmonic wave. An effective sample length can be defined as the length of a crystal with perfect domain structure that would yield the same second harmonic power. Typical effective lengths for periodically-poled $LiNbO_3$ samples range from 0.32 to 0.68 mm. [1,2,3,4] These position errors are probably caused by variations in growth speed due to thermal fluctuations during the crystal growth.

The wavelength acceptance of a 1.4 mm long sample with domain period of 4.6 µm was investigated with a Ti:sapphire laser in a single-pass room-temperature doubling experiment. The observed width of the tuning curve was twice what one would expect for a crystal with perfect domain spacing.[1] A slow drift in freezing interface position during growth on the order of 10 µm can account for this observation as well as for the observed effective sample length.
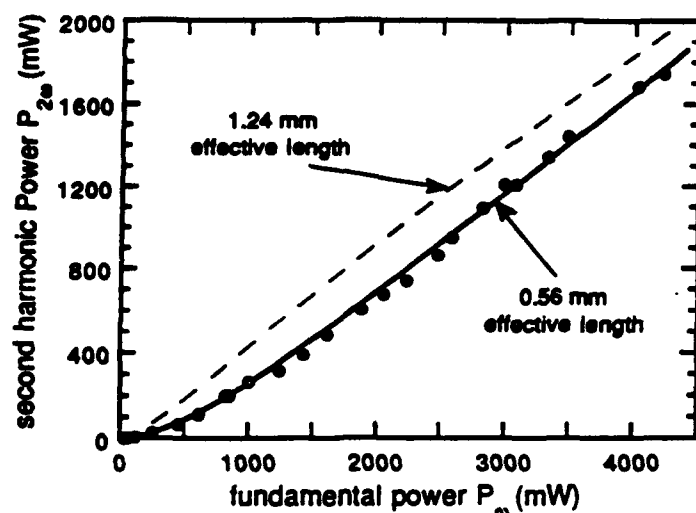
Fig. 2   Overall performance of the 1.064 μm external doubler for a sample 1.24 mm long. The calculated performance for a perfect sample 1.24 mm long is also shown.

Periodically-poled LiNbO₃ is well suited for SHG of diode lasers. Efficient coherent sources should be obtainable at 415 nm by locking a diode laser to the SHG cavity resonating the fundamental field. The domain period for this interaction has to be on the order of 3 μm which can easily be produced with the laser heated pedestal growth technique.

By growing a crystal with a varying domain period, the wavelength and temperature acceptance bandwidth of the crystal can be expanded.[5] Tuning data for a crystal grown with intentionally modulated domain periodicity will be presented, as will a comparison of the properties of KTP, KNbO₃ and periodically-poled LiNbO₃ (PPLN) for SHG in the visible, and data on the photorefractive behavior of PPLN.

References

1. D. H. Jundt, G. A. Magel, M. M. Fejer and R. L. Byer, Appl. Phys. Lett. Nov. 15, (1991).
2. G. A. Magel, M. M. Fejer and R. L. Byer, Appl. Phys. Lett. 56, 108 (1990).
3. D. Feng, N. B. Ming, J. F. Hong, Y. S. Yang, J. S. Zhu, Z. Yang and Y. N. Wang, Appl. Phys. Lett. 37, 607 (1980).
4. Y.-L. Lu, L. Mao, S.-D. Cheng, N.-B. Ming and Y.-T. Lu, Appl. Phys. Lett. 59, 516 (1991).
5. M. M. Fejer, G. A. Magel, D. H. Jundt and R. L. Byer, submitted to IEEE J. Quantum Electron.

High efficiency frequency doubling around 430nm

E. S. Polzik and H. J. Kimble

Norman Bridge Laboratory of Physics 12-33

California Institute of Technology

Pasadena, California 91125

(818) 356-8342

Potassium niobate ($KNbO_3$) is known for its high nonlinear coefficient which together with the increasing quality of crystals available makes it a very attractive candidate for frequency doubling into the blue. Previous work has demonstrated that frequency doubling in an external cavity is a good alternative to doubling within the laser cavity since it allows for independent optimization of the laser and doubling cavities. With reference to $KNbO_3$ in an external cavity, 40mW of blue output was obtained by doubling a diode laser,[1] while 154mW was achieved by nonlinear mixing of diode and Nd:YAG emission.[2]

For our high-power doubling experiment,[3] fundamental radiation from a titanium-sapphire laser ($Ti:Al_2O_3$) was mode-matched into a ring cavity consisting of four flat mirrors and two lenses. In spite of the quality of the coatings ((0.15%)/surface at 860nm) passive losses from the lenses reduced the cavity buildup relative to astigmatically compensated cavities with curved mirrors. However, the setup employed facilitated the exploration of a range of focussing geometries which is of special importance since this arrangement allows fine tuning of the cavity mode to compensate for effects of thermal lensing at high power. Our best result to date is 0.65W of single-frequency blue light around 430nm generated for an input of 1.35W of infrared light. Though a simple theory predicts an increase of the nonlinear conversion efficiency for higher input power such is in general not the case in our experiment due to the combined effects of thermal lensing and of blue-light induced infrared absorption in the $KNbO_3$ crystal.

In order to obtain higher conversion efficiencies for reduced values of infrared pump

power, we have built a doubling cavity with total passive losses (0.4-0.5)%. This ring folded cavity consisted of two curved mirrors and two flat mirrors. The folding angle was chosen to be 3°. Such a small angle allowed us to employ a normal cut crystal without special concern about astigmatism. For this second cavity, a 10mm long a-cut $KNbO_3$ crystal[4] was placed between curved mirrors with radius of curvature =50mm; the beam waist for the cavity was $w = 22\mu$. This beam size is close to the optimum size for doubling and provided a measured single pass nonlinear coefficient $E_{NL} = 0.018W^{-1}$. Based upon the formalism of Ref. [3], we calculated the optimum transmission of the input coupler for the infrared pump to be close to 5% in the range of infrared pump from 20mW to 60mW and close to 10% for pump power $\gtrsim$ 100mW. Mirrors with these transmission coefficients were actually used in the experiment over the appropriate ranges.

The results of our doubling experiments with Cavity 2 are as follows. Conversion efficiencies of about 70% are achieved for input power between 50mW and 500mW. For higher infrared pump powers thermal lensing in the folded cavity leads to unstable behavior. The simple theory without thermal effects predicts conversion efficiencies greater than 80% for input powers above about 50mW. Apart from thermal lensing, the principal cause for the decrease in efficiency has been found to be increased absorption of the infrared in $KNbO_3$ which is induced by the presence of the blue light. Direct measurements of this effect have been made by injecting an external blue beam into the doubling cavity and measuring the effect on a circulating infrared beam. We will describe observations including laser calorimetry that quantify the role of light-induced absorption.

1. W. T. Kozlovsky, W. Leuth, E. E. Latta, A. Moser and G. L. Bona, Appl. Phys. Lett. **56**, 2291 (1990).

2. M. K. Chun, L. Goldberg, I. N. Duling III, T. F. Carruthers, CLEO (Anaheim, CA 1990), Paper CWE2.

3. E. S. Polzik and H. J. Kimble, Optics Lett. **16**, 731(1991); CLEO (Blatimore, MD 1991), paper CWA1.

4. The crystal was fabricated by G. Mizelle, Virgo Optics, FL.

Poster Session

ThE 6:00pm–7:30pm
Anasazi North

Narrow Band Iso-Index Filters
for Blue-Green Laser Communications

Roger F. Belt, Mark Randles, and John Creamer

Airtron Division Litton Systems Inc.
200 E. Hanover Ave, Morris Plains, NJ 07950

Oscar M. Stafsudd
Department of Electrical Engineering
University of California, Los Angeles, CA 90024

Summary

Communications through the 440-470nm water transmission
window requires a laser, a narrow band high field of view
filter, and an appropriate detector. Polarization interference
filters offer very narrow transmission bands, wide angular field
of view, and tuning capability. The Lyot-Ohman, Solc, various
hybrids, and recent designs are powerful examples of
technologies employing common single crystals of quartz,
calcite, or ADP. The superior iso-index filter ($n_o = n_e$ at a
particular λ) is potentially the most useful. Materials for
iso-index filters are not common since they must be stable
single crystals, high quality, and usually involve mixed ions in
an isomorphous structure. The research group at UCLA has shown
that $\beta"-Al_2O_3$ fulfills these conditions within the Na-Ag system[1].
However, $\beta"-Al_2O_3$ does not melt congruently and large single
crystals are not attainable readily. An alternate superionic
conductor, $\beta -Al_2O_3$, behaves similarly and can be grown as
sizeable (1 x 6 inch) boules.

Single crystals of $\beta -Al_2O_3$ with a nominal composition of
$Na_2O.11 Al_2O_3$ were grown from stoichiometric melts using an
iridium crucible. Seeding was achieved from an Al_2O_3 single
crystal. The growth axis was along a and X-ray data confirmed

the unit cell parameters of a = 5.595 A and c = 22.531 A. The top and bottom lattice constants of the boules were equal to $\pm$ 0.002 A and indicated a fairly uniform composition. The measured density was 3.25 g/cm^3. The boules remained physically intact with no major cracks. However some cleavage progressed on the basal planes as determined by the appearance of interference fringes. Water vapor and CO_2 did not enhance the cracking. Crystals were stored in a desiccator but continued to cleave. Figure 1 shows an example of a grown crystal.
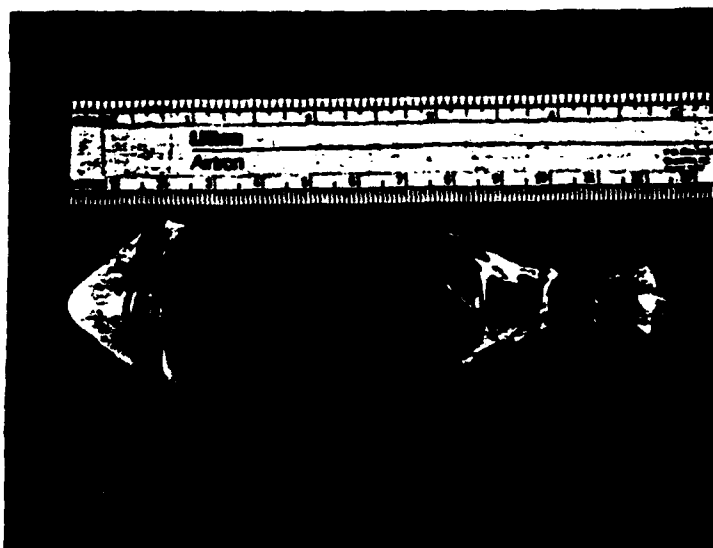
Figure 1. Single crystal of a-axis β -Al$_2$O$_3$ grown by Czochralski method.

Ionic diffusions of Na^{1+}, Ag^{1+}, Pb^{2+}, Rb^{1+}, Ca^{2+}, Cd^{2+}, Tl^{1+} were performed by immersion of β-Al$_2$O$_3$ into nitrate or hloride melts at temperatures of 360-740°C. The amount of exchange was measured by weight increase. The X-ray lattice constants were also measured for the exchanged crystals. The g^{1+} exchanged material was light stable when tested with 10^4 hots of a 308nm excimer laser. All of the divalent ions gave xchanged crystals which cracked more easily than the original -Al$_2$O$_3$. These appeared to be tension related since attice constants increased markedly. To achieve iso-index atching in the visible, the diffusing ions should possess high

electronic polarizability. Pb^{2+}, Cd^{2+}, and Tl^{1+} satisfy this requirement. The Tl^{1+} works best because of charge, size, and index change.

Single crystals of the exchanged materials were cut and fabricated into prisms. Their refractive indices were measured by the method of minimum deviation. The Na^{1+}, Rb^{1+}, Ag^{1+} crystals were all uniaxial negative ($n_e < n_o$). Measurements were not obtained on Ca^{2+}, Cd^{2+}, Pb^{2+}, and Ba^{2+} because of cracking. The Tl^{1+} ion exchanged material is uniaxial positive and when combined with Rb^{1+} or Ag^{1+} offers the best hope for an iso-index material in the visible.

We discuss the theory for an iso-index filter and calculate the bandpass, angular variation of bandpass, and field of view characteristics of a Lyot-Ohman filter (Figure 2). The construction of such a filter is explained with the use of exchanged $\beta -Al_2O_3$.
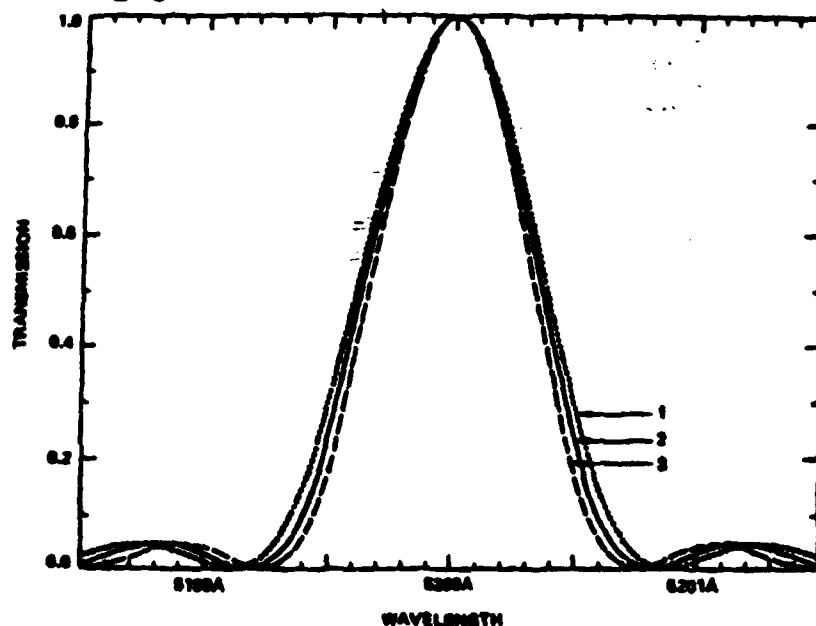
Fig. 2 Field of view characteristics of a Lyot-Ohman iso-index filter. Curve 2, normal incident light; curve 1 is for extreme angle of incidence ($\theta = 90°$) with plane of incidence parallel to the c axis of plates ($\phi = 90°$); curve 3 is for the same extreme angle of incidence ($\theta = 90°$) with plane of incidence perpendicular to the c axis of plates ($\phi = 0°$).

1. S.C. Adams, B. Dunn and O.M. Stafsudd, Optics Letters 13, 1072 (1988).

2. Crystal growth was performed under contract N00014-90-C-0006.

Application of Blue-green Lasers to High Data Rate Underwater Communications

Judith B. Snow and Jacob R. Longacre
Naval Underwater Systems Center, Code 3422, New London, CT 06320
(203) 440-6487

High data rate underwater laser communications are highly constrained by laser propagation characteristics in the marine environment. Many of these limitations are mitigated by using an optimally designed laser for seawater transmission, namely a compact blue-green laser. Digital data can be transmitted through seawater by an amplitude modulated laser beam that is detected by a remote optical receiver. The primary technical issue for this application is the distance over which error-free optical communication is possible. Maximum range for a laser beam propagating through seawater is in the hundreds of meters. Achievable distances are limited because optical signals transmitted through seawater are exponentially attenuated according to

$$I = I_0 e^{-cr}, \tag{1}$$

where I is the received optical signal strength, I_0 is the initial optical signal strength, r is the transmission range, and c is the beam attenuation coefficient. The attenuation coefficient has absorption and scattering components,

$$c = a + b, \tag{2}$$

where a is the absorption coefficient and b is the scattering coefficient. For a given water type, the inverse of the beam attenuation coefficient, $1/c$, defines the attenuation length (i.e., the length over which the signal is reduced by $1/e$).

Absorption of light in ocean water is strongly wavelength dependent. Pure water preferentially absorbs short wavelength light via electron excitation and long wavelength light via molecular excitation, with a transmission window in the blue-green portion of the spectrum. In clear open ocean water, optimum transmission is obtained with blue light of approximately 480 nm. But even for the clearest seawater, the attenuation coefficient at 480 nm is approximately 0.02 m^{-1}, corresponding to an attenuation length of only 50 m.[1] Absorption of light by contaminants in the water is also highly wavelength dependent. "Yellow substance", found in coastal waters, is a common contaminant that preferentially absorbs in the blue. The presence of yellow substance causes a shift in the transmission spectrum toward the red, in which longer wavelength light in the green (at approximately 530 nm) has the best transmission characteristics.[2] Therefore, absorption by seawater and contaminants limits transmission range and determines optimum optical transmission wavelength.

Scattering limits transmission range by deflecting energy out of the signal beam. A small fraction of scattering is from water molecules, but organic and inorganic suspended particulates account for the majority of the scattered light in ocean water. Scattering produces spatial beam spreading, decreasing the intensity of the signal beam impinging upon the detector surface. We have conducted a series of experiments to measure these characteristics and limitations in coastal ocean water. Fig. 1 shows the spatial profile of a cw 532 nm Nd:YAG laser beam for different propagation ranges in coastal seawater. The normalized experimental measurements indicate that at longer ranges there is increased signal intensity at large lateral distances from the laser beam axis. The increase in spreading at longer ranges is due to the cumulative effect of scattering from suspended particulates. Although light multiply scattered from particulates makes up the majority of the light field at larger lateral distances from the beam axis, Fig. 1 indicates that the divergence of the laser determines the diameter of the central, intense portion of the beam.
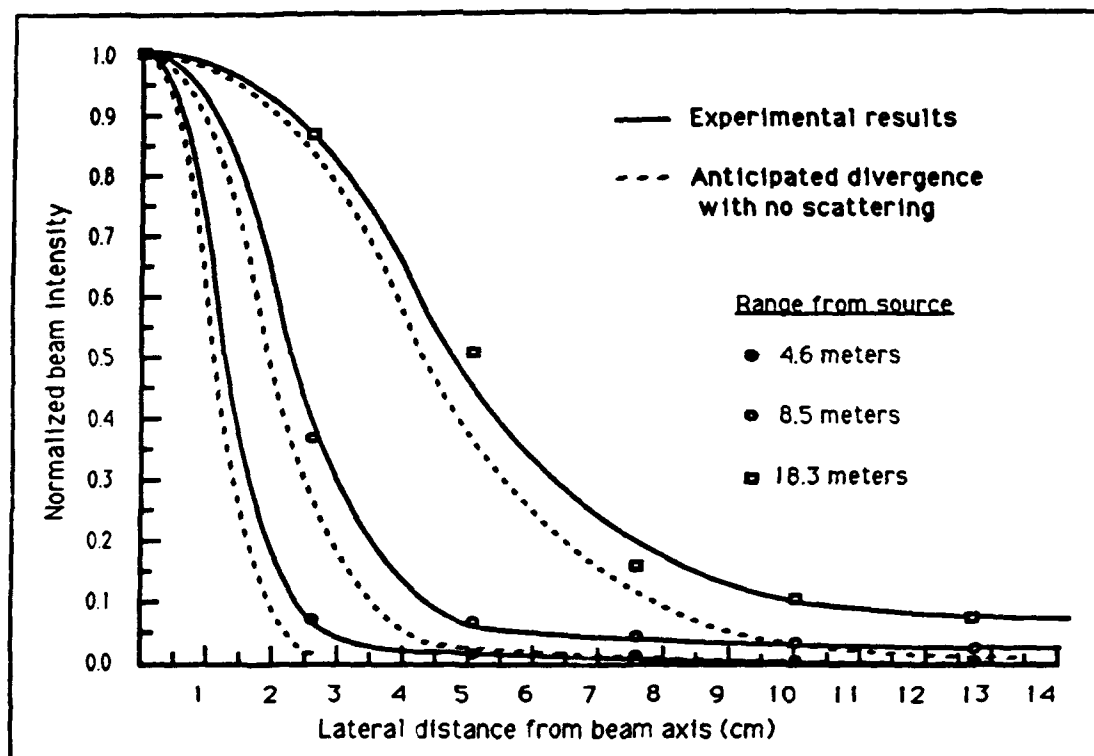
Fig. 1. Normalized intensity profile of cw 532 nm laser beam in 2.5 m coastal ocean water at 4.6 m (1.8 attenuation lengths), at 8.5 m (3.4 attenuation lengths), and at 18.3 m (7.3 attenuation lengths),

Scattering also generates "multipath" noise by deflecting some of the transmitted light out of and then back into the signal beam. The longer pathlength of this multiply scattered light delays photon time of arrival at the detector, producing temporal stretching of the optical signal pulses. Temporal pulse stretching limits maximum attainable data rate. However, scattering functions for oceanic water show that the vast majority of the scattered light is forward scattered

through a small angle. Our theoretical analysis of multiple scattering in different marine environments predicts that temporal pulse stretching becomes an issue only under the following conditions:

(1) at high data rates (> tens of MHz),
(2) at long attenuation lengths (>10 m), and
(3) at long ranges (>100 m).

These predictions are supported by our experimental results in coastal seawater. We have investigated temporal propagation characteristics using a pulsed, diode-pumped 532 nm Nd:YAG laser. An 18 ns laser pulse showed no stretching over a distance of 15 attenuation lengths.

Since absorption and scattering cause exponential losses in the optical signal, an order of magnitude increase in laser power will only increase transmission range by 2.3 attenuation lengths. For a system designed to transmit over 20 attenuation lengths, this represents a minimal improvement in range (12%). However for open ocean water, achievable propagation range could be increased dramatically by shifting the laser wavelength from green to blue. For example, the attenuation coefficient for a 532 nm laser beam transmitted through extremely clear seawater is 0.05 m-1 (corresponding to a 20 m attenuation length), while the attenuation coefficient at 480 nm is 0.02 m-1 (corresponding to a 50 m attenuation length).[1] In this case, changing the laser wavelength from 532 nm to 480 nm would result in a 150% increase in range.

An ideal laser for underwater laser communications would be a compact, solid state, tunable, pulsed, low divergence laser. Since beam diameter depends on laser divergence, low divergence increases the amount of light incident on the detector, leading to increased signal-to-noise ratios. A pulsed laser, as opposed to a modulated cw laser, would maximize peak optical power available at the detector. A high pulse repetition rate is required in order to obtain reasonably high data rates (ideally on the order of tens of MHz). A tunable laser would permit the selection of the laser wavelength having optimum propagation for a given water type. Size and power requirements are also critical issues, particularly for expendable and short duration system applications. Compactness is critical for underwater applications because complexity of pressure housings and delivery systems increases dramatically with size. Laser efficiency is critical since available power is limited in many applications. Additionally, increased laser efficiency minimizes heat dissipation problems.

Initial experimental results indicate that high data rate underwater laser communications are feasible. The overall utility of this application will depend on the availability of suitable compact blue-green lasers.

1. R. C. Smith and K. S. Baker, Appl. Opt. 20, 177 (1981).
2. J. Y. Simonot and H. Le Truet, J. Geophys. Res. 91, 6642 (1986).

Characteristics of ZnSe Light Emitting Diodes as a Function of Temperature

Y. Guan, L. Calhoun, R. M. Park and P. S. Zory

University of Florida, Gainesville, FL 32611, Phone: 904-392-0950

Blue light emitting devices are of special value in optical recording, information processing, display and undersea applications. Recently, ZnSe has been shown to be a promising material for making such devices with reports of pulsed ZnSe based diode lasers at low temperature [1] and light emitting diodes (LEDs) at room temperature (RT) [2][3]. However, efficient and reliable operation of these device types at RT has yet to be demonstrated. In this work, we study the temperature dependence of the output spectral features and current-voltage (I-V) relations of ZnSe LEDs. The results may prove useful for developing efficient/reliable blue LEDs and lasers.

The structure of the LEDs employed in this study is shown in Fig. 1, the structures being grown by molecular beam epitaxy and shaped into 200 μm square chips. A gold contact stripe, 100 μm wide, was made on each chip. Since the output light is emitted from the edges of the chip at both ends of the stripe, the device is an edge LED or ELED. The n-type and p-type ZnSe layers were doped with chlorine and nitrogen, respectively, both to the level of 5×10^{17} cm^{-3} (see Fig. 1). The n$^+$-layer was doped to 10^{18} cm^{-3}. For below room temperature measurements, the device was mounted in a liquid nitrogen cooled dewar having a precision temperature control unit. Current pulses of 10 KHz repetition rate and 10% duty factor were used to generate the light.

Two readily distinguishable peaks in the emission spectrum are observed at 80 K (Fig. 2), a phenomenon reported previously for ZnSe electroluminescent devices involving nitrogen as the p-type dopant [3][4]. Since peak 1 (the sharper peak) shifts with temperature at the same rate as the energy bandgap, it is identified as due to band-to-band recombination [5]. The broader peak (peak 2), whose wavelength does not have a strong temperature dependence, is believed to be associated with band to acceptor recombination. It was also found that the magnitude of both peaks decreases exponentially with increasing temperature in the range shown in Fig. 4. The decay rate for peak 1 is less than that for peak 2. At RT, only peak 1 is observed and its wavelength is 475 nm. A similar peak is observed at RT from n-side up ZnSe ELEDs made using similar doping techniques [6].

The stability of output light was also found to depend strongly on temperature. At 80 K, the output light and the I-V characteristic curves are stable with a turn-on of about

7 V (see Fig. 5). As temperature is increased, the turn-on voltage gradually increases and the I-V curve and output light become unstable. At RT, the turn-on occurs at about 15V. The cause for this instability is believed to be associated with the nature of the contact between the metal and the p-type ZnSe layer.

References:

[1] M. Hasse et al., Appl. Phys. Lett., vol. 59, pp. 1272-1274, 1991

[2] J. Ren et al., Appl. Phys. Lett., vol. 57, pp. 1901-1903, 1990

[3] R. M. Park et al., Appl. Phys. Lett., vol. 57, pp. 2127-2129, 1990.

[4] K. Akimoto et al., Jpn. J. Appl. Phys., vol. 28, pp. L528-L530, 1989.

[5] B. R. Nag, *Electron Transport in Compound Semiconductors*, Springer-Verlag, 1980.

[6] Y. Guan et al., IEEE/LEOS Annual Conf., Conf. Digest, p. 52, 1991.
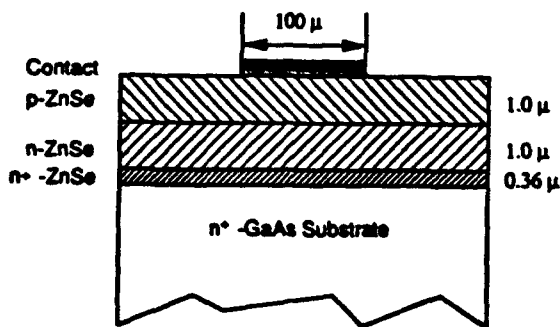
Fig. 1. ZnSe edge light emitting diode structure used in this work
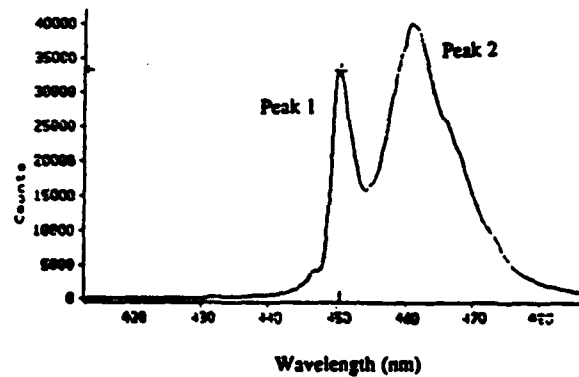
Fig. 2. Typical electroluminescence recorded at 80 K.
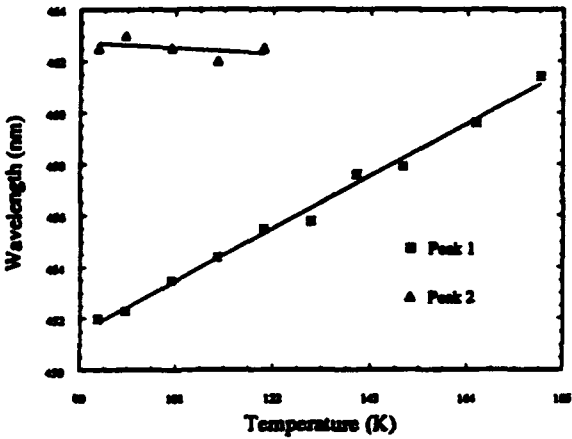
Fig. 3. Temperature dependence of the wavelengths of principal emission peaks
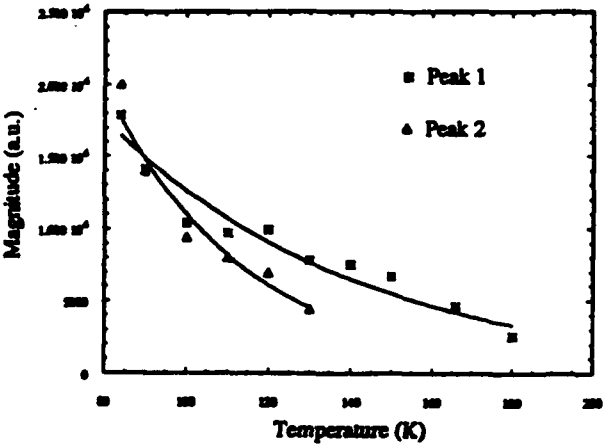
Fig. 4. Temperature dependence of the intensities of principal emission peaks
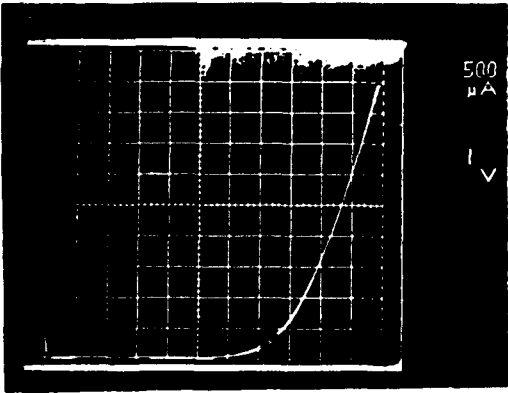
Fig. 5. Current vs. voltage characteristic at 80 K.

Two-dimensional modal analysis of blue-green lasers using ZnSe based p-n and metal-insulator-semiconductor (MIS) heterostructures

C. Chung and F. Jain[1]

Department of Electrical and System Engineering and Institute of Materials Science
University of Connecticut, Storrs, CT 06269-3157 (203-486-4816)
[1]Sabbatical address: United Technologies Research Center,
East Hartford, Connecticut 06108

The wide energy gap II-VI compounds semiconductors, such as ZnSe, ZnS, MnSe, CdSe, and their ternary and quaternary alloys, are particularly suitable for the realization of short wavelength optoelectronic devices. These materials have been found to exhibit excellent luminescent properties as demonstrated by photoluminescent spectra [1] and the successful operation of photopumped lasers [2]. Recently, Haase et al[3] reported p-n heterojunction injection laser operating at cryogenic temperatures. Currently, several research groups are investigating p-type doping of ZnSe using MBE, MOCVD and CBE growth techniques. However, compensation at high nitrogen level ($>10^{18}$ cm^{-3}) still remains a problem[4]. While the effort in optimizing p-n heterojunctions to obtain room temperature lasers is being pursued intensely, an alternate approach is the use of MIS structures to obtain injection luminescence[5,6]. This paper discusses modal analysis of p-n double heterojunction and MIS laser heterostructures. In particular, ZnSe-ZnSSe, ZnSe-ZnCdSe structures are analyzed. Numerical computations of field intensities, confinement factors Γ and the threshold current densities J_{TH} are presented. Experimental data of luminescence spectra in Au-SiO$_2$-ZnSe MIS devices is also presented.

The injection luminescence and photon confinement in p-n double heterostructures (DH) blue-green lasers is similar to those in conventional GaAs-AlGaAs DH lasers [7]. Injection luminescence and photon confinement are obtained in a different manner in the MIS laser structures [5,6]. The fabrication of super current gain ($\beta = 25,000$) bipolar transistors having MIS emitters[8], and high efficiency MIS solar cells are examples of the attainment of very high minority carrier injection efficiencies in these structures. The photon confinement is achieved by the reflecting barrier metal on one side and the heterostructure dielectric discontinuity (e.g. ZnCdSe-ZnSe or ZnSe-ZnSSe) on the other [5,9].

The modal analysis of the two-dimensional stripe geometry lasers presented here follows the work of Bulter and Delaney[10] and Buus[11] on double p-n heterostructures, and formulation by Jain and Kazi[12] on asymmetric MIS lasers. Figs. 1 and 2 show the transverse light intensity profile for a ZnSe-Zn$_{0.8}$Cd$_{0.2}$Se-ZnSe and a Au-SiO$_2$-ZnSe-ZnS$_{0.2}$Se$_{0.8}$ laser structures obtained using the numerical technique. The lateral field distributions are shown in fig. 3, and are similar to those of diode lasers [7]. The numerical computation is done by solving the 2-D wave equation for an active layer thickness d($= 0.2~\mu$m) and a stripe of width 2S($=10\mu$m). Equations 1-4 define the field inside and outside of the cavity [10,11] for double heterostructures. The transverse and lateral field distributions are expressed by ϕ and ψ, respectively, in terms of eigenvalue q_m, propagation constant p, and wavevector k.

$$\phi(y) = A_m \cos(q_m y) \quad , \qquad for~|y| \leq d/2$$
$$= A_m \cos(q_m d/2)~e^{[-p(y-d/2)]} \quad , \quad for~|y| > d/2 . \tag{1}$$

$$\psi_m(x) = H_m(\sqrt{a}k)~e^{-\frac{ak^2}{2}x^2} \quad , \qquad for~|y| \leq d/2 \tag{2}$$
$$= R(\zeta) \cos(\zeta x) \quad , \qquad for~|y| > d/2 .$$

$$\Psi(x,y,z) = \sum A_m \cos(q_m y)~H_m(\sqrt{a}kx)~e^{-\frac{ak^2}{2}x^2}~e^{-j\gamma z} \quad , \quad for~|x| \leq S, \quad and~|y| \leq \frac{d}{2} , \tag{3}$$

$$\Psi(x,y,z) = \int_0^\infty R(\zeta)\ \cos(\zeta x) e^{(\frac{d}{2}-y)\sqrt{\zeta^2-k^2-\gamma^2}}\ d\zeta\ e^{-j\gamma z}\ ,\quad for\ |x| < S,\ \ and\ \ |y| > \frac{d}{2}\ . \tag{4}$$

For a MIS laser, the total field distributions inside and outside the active region are equations 5-6,

$$\Psi(x,y,z) = \sum A_m\ \sin(q_m y)\ H_m(\sqrt{a}\,kx)\ e^{-\frac{ak^2}{2}x^2}\ e^{-j\gamma z}\ ,\quad for\ |x| \leq S,\ \ and\ \ 0 \leq y \leq d\ , \tag{5}$$

$$\Psi(x,y,z) = \int_0^\infty R(\zeta)\ \cos(\zeta x)\ e^{(d-y)\sqrt{\zeta^2-k^2-\gamma^2}}\ d\zeta\ e^{-j\gamma z}\ ,\quad for\ |x| \leq S\ ,\ \ and\ \ |y| > d. \tag{6}$$

The solution of wave equation for the MIS case is different due to boundary conditions along the transverse (y) axis. In addition, the $y=0$ is chosen at the metal/oxide boundary. The coefficients A_m are obtained numerically solving a 4x4 matrix. Here, $k_a = k \cdot \sqrt{\epsilon_{cladding}}$, and γ is the propagation constant in the z-direction and is determined by the matrix Ω[11]. The threshold current density J_{TH} for the pZnSe-nZn$_{0.8}$Cd$_{0.2}$Se-nZnSe system comes out[7] to be 1045 A/cm^2 at room temperature using quantum efficiency $\eta = 0.9$, index change $\Delta n = 0.25$, $R_1 = R_2 = 0.7$, $d = 0.2\mu m$, $W = 2S = 10\mu m$, $L = 300\mu m$, confinement factor $\Gamma = 0.637$ and $J_{nom} = 3\times10^4$ A/cm^2-μm. The J_{TH} value is expected to be smaller for strained layer single quantum well lasers.

Figure 4 shows the luminescent spectra of a Au-SiO$_2$-ZnSe MIS stripe geometry device at 77°K with the forward current ramped up to 2.7 KA/cm^2. The ZnSe was annealed in molten zinc and was processed to grow a thin SiO$_2$ layer using the low-temperature CVD reactor. A 12.5μm gold stripe was deposited by photolithographic techniques. An indium/gold based multilayered ohmic contact was formed. The growth of SiO$_2$(at ~400°C) and ohmic contact formation was done in a compatible manner to obtain a relatively low resistance contact. The processing sequence was found to be crucial in order to obtain an ohmic contact.

The computed threshold current density value for an active layer of 0.2 μm thickness appear to be reasonable. However, the J_{nom} and index difference (between active and cladding layers) used are somewhat ad hoc as published experimental data is not precisely available. It is believed that ZnSe-ZnCdSe-ZnSe structure grown on ZnSe substrate would yield better performance than on GaAs. In the case of homojunction MIS structures, it is our belief that high current density pulsing at around 4.2 °K will yield injection lasing. An optimization of SiO$_2$ thickness, reduction of room temperature ohmic contact resistance, and implementation of a quantum well active region (ZnCdSe) with ZnSSe or ZnSe cladding would result in room temperature lasing in MIS devices such as shown in fig. 2.

References

[1] X.W. Fan and Woods, Phys. Stat. Sol. (a)70, K27, 1982.

[2] C.A. Zmudzinski, Y. Guan and P.S. Zory, IEEE Photonics Tech. Lett., 2 (1990) 94.

[3] M.A. Haase, J. Qiu, J.M. DePuydt and H. Cheng, Appl. Phys. Lett.59 (1991) 1272.

[4] J. DePuydt, Fifth Int. Conf. on II-VI Compounds, September 8-13, 1991 (Tamamo, Japan).

[5] F.C. Jain, J. Crystal Growth, 86 (1988) 929.

[6] C. Chung, F. Jain and G. Drake, Fifth Int. Conf. II-VI Compounds, Sept. 8-13, 1991 (Tamamo, Japan).

[7] H.C. Casey, Jr. and M.B. Panish, Heterostructure Lasers, Academic Press, New York, 1978.

[8] M.A. Green and R.B. Godfrey, IEEE EDL-4 (1983) 225.

[9] F.C. Jain, and J.W. Marciniec, IEEE J. Quantum Electron, QE-14 (1978) 358.

[10] J.K. Bulter and J.B. Delaney, IEEE J. of Quantum Electronics, QE-14 (1978) 507.

[11] J. Buus, IEEE J. of Quantum Electronics, QE-18 (1982) 1083.
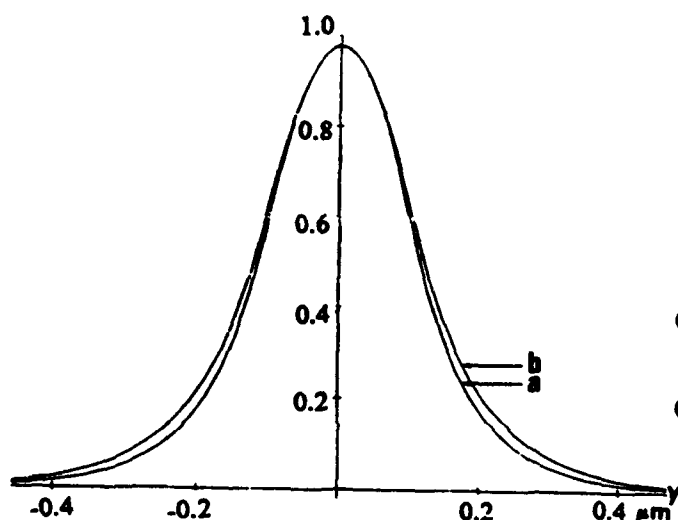
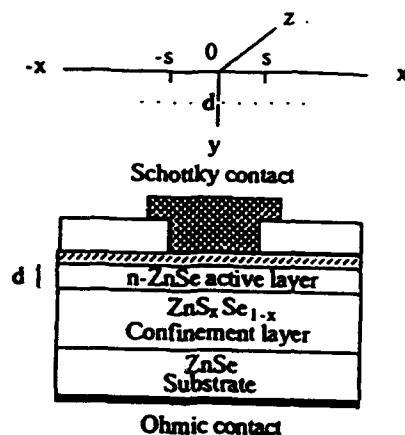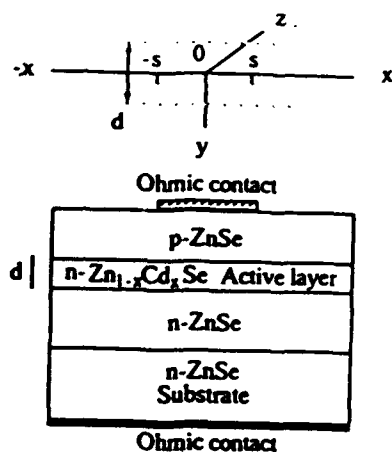[12] F.C. Jain and K. Kazi, SPIE Proc. 723 (1986) 109.

Fig 1. The transverse field distributions of DH lasers for (a) ZnCdSe-ZnSe, and (b) ZnSe-ZnSSe systems.
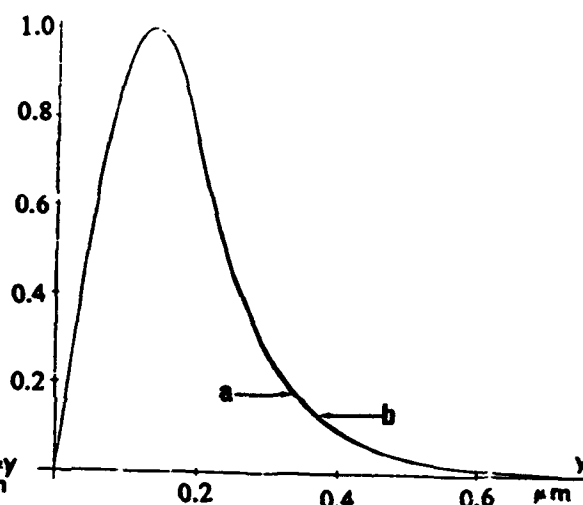
Fig 2. The transverse field distributions of MIS lasers for (a) Metal-SiO_2-ZnSe-ZnSSe, and (b) Metal-SiO_2-ZnCdSe-ZnSe systems.
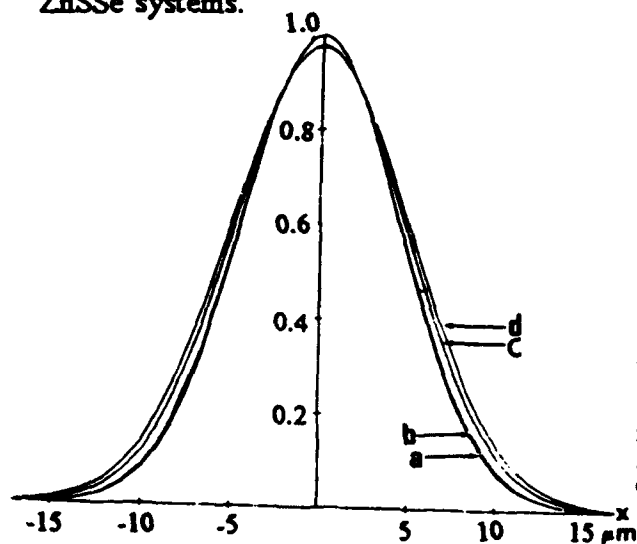
Fig 3. The lateral field distributions for (a) MIS ZnCdSe/ZnSe (b). MIS ZnSe/ZnSSe (c) DH ZnCdSe/ZnSe and (d) DH ZnSe/ZnSSe.

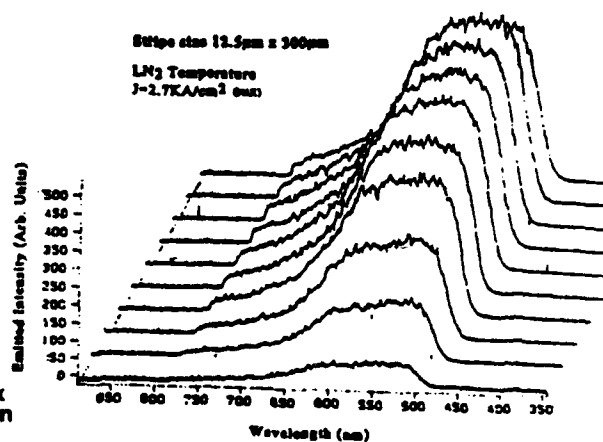Fig 4. The luminescent spectra for a homojunction MIS ZnSe structure.

High peak and average power diode-pumped NYAB green laser

R. E. Stone and S. C. Wang
Lockheed Palo Alto Research Laboratory
97-30, B 202
3251 Hanover Street, Palo Alto, California 94304
(415) 424 - 2800

The self-frequency-doubling crystal Neodymium Yttrium Aluminum Borate (NYAB) is an ideal candidate for diode-pumped compact green laser system. Because it has several unique features including broad and strong absorption at the diode laser wavelengths, high nonlinear optical coefficient, high damage threshold, and low luminescence quenching effects. Besides it has shorter fluorescence lifetime than Nd: YAG crystal that allows the laser to operate at relatively higher repetition rate. The operation of diode-pumped NYAB at green wavelength 531 nm has been reported by us and several groups recently. [1-3] However, the reported green laser output powers are relatively low due partly to the poor quality of the quality of the crystal which is still under development. Besides the relatively strong absorption at green wavelength is also considered to be a contributing factor. We report here the achievement of the high power output obtained from a NYAB crystal under both cw and Q-switched operation at room temperature.

We use a 2 mm long NYAB crystal with 3 x 3 mm cross section in this experiment to reduce the internal green absorption. The absorption coefficient of the NYAB crystal at diode laser pumping wavelength of 804 ~ 808 nm is about 9 cm^{-1}. and at the green wavelength is about 0.9 cm^{-1}. [4] Therefore nearly all of the diode pump power is absorbed within 2 mm crystal length, while the green absorption is substantially reduced compared to a typical crystal length of 5 ~ 6 mm used by many researchers. The crystal was cut at 32.9 ° for type 1 phase matching condition. The front

facet of the crystal is coated with a dielectric material with high reflectivity at 1.06 μm and high transmission at the pumping wavelength of 804-808 nm. The back facet of the crystal is antireflection coated at 532 nm and 1.06 μm for an end-pumped and external cavity configuration.

For cw operation, an output coupling mirror with a curvature of 7.5 cm and reflectivities of about 99 % at 1.06 μm and 20 % at 532 nm is used. For Q-switched operation, a 10 cm curvature output mirror is used to allow the insertion of an acoustooptic Q-switch in the cavity between the crystal and the output mirror.

Two high-power GaAlAs laser diode arrays were used as pumping source. One with an output power of 1 W and another with a rated output of 3 W. When both pump sources are used in cw operation, a polarizing beam splitter cube is used to combine the two sources. The laser beam is collimated by a microscope and and a cylindrical lens combination and focused on to the crystal facet by another microscope objective. The emission wavelength of each laser diode is centered around 808 nm by a temperature controller. The output power of the laser diode was varied by controlling the driving current. The cw green laser output power was measured by a laser precision radiometer (Model 5710). The green output power increases quadratically with the diode laser pumping power as expected. We obtained cw power as high as 30 mW under the current experimental conditions. For Q-switched operation, a laser precision energy meter (Model 7200) is used to measure the output energy and a Si p-i-n photodetector is used for accurate pulse shape measurements. We obtained peak green output power as high as 55 W and an average power of near 30 mW. A typical Q-switched green peak power versus diode pump power is shown in Fig. 1.

References

1. S. C. Wang, R. E. Stone, and J. T. Lin, "Characteristics of NYAB as a diode pumped laser material," Proc. Advanced Solid State Lasers, Vol. 6, 23, March 1990.

2. I. Schultz and R. Wallenstein, " Self-frequency doubling of Nd:YAB laser pumped by a diode laser," Technical Digest, Conf. Laser and Electro-Opt. paper CWC4, 1990.

3. R. E. Stone, R. C. Spitzer, and S. C. Wang, " A Q-switched diode-pumped Neodymium Yttrium Aluminum Borate laser," Photonics Tech. Lett. Vol. 2, 769, Nov. 1990.

4. R. E. Stone and S. C. Wang, " Spectroscopy and laser properties of self-doubling Neodymium-doped Yttrium Aluminum Borate crystals," Technical Digest, Advanced Solid State Lasers, paper WD5, March 1991.
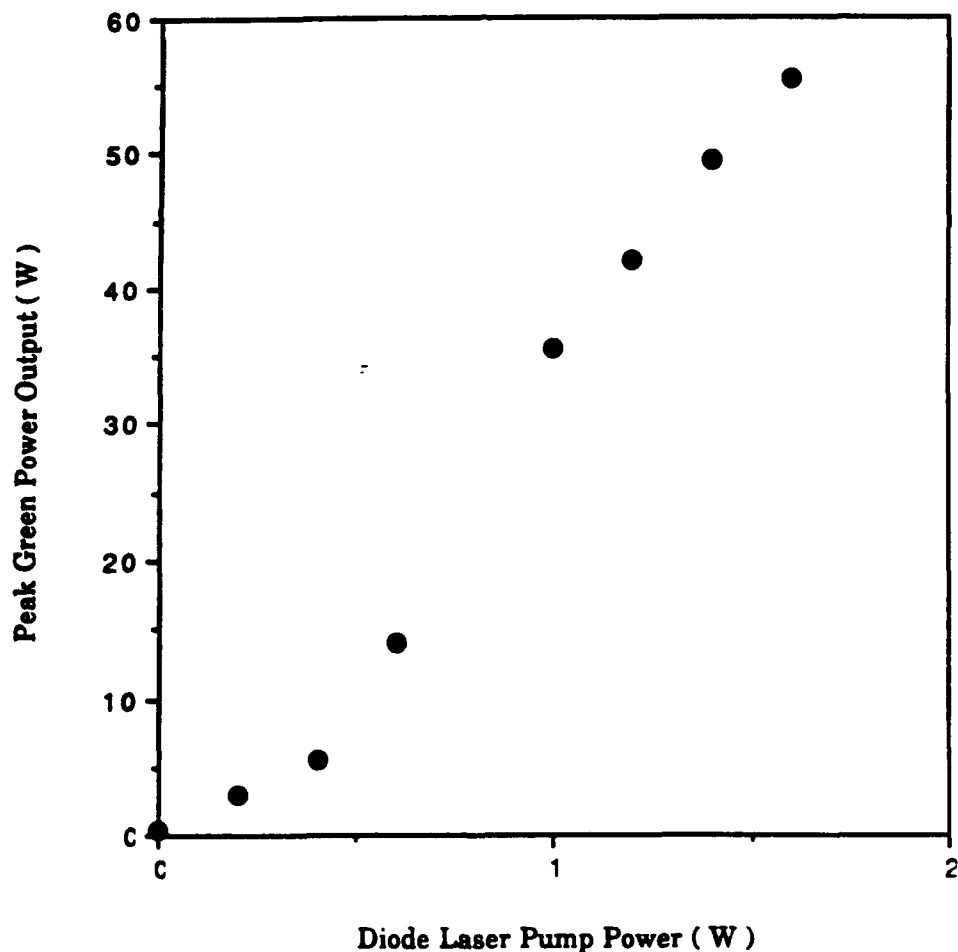
Fig. 1 Peak green laser output power versus diode pump power

A Diode Pumped Self—Doubling Laser of

Modified Neodymium Yttrium Aluminum Borate Crystal

Yujing Huo*   Pu Wang**   Jinxing Cai*   Hengfu Pan**

Qinqing Zhang*   Jing Xue**   Bingkun Zhou*   Baosheng Lu**

*: Dept. of Electronic Engeneering, Tsinghua Univ., Beijing, 100084, China

**: Institude of Crystal Material, Shandong Univ., Jinan, Shandong Province, 250100, China

INTRODUCTION: The blue—green lasers have great application in optical disk technology, image processing, color projection, printing and underwater optical communication. A good scheme for diode pumped frequecy doubling laser is diode pumpedself doublinglaser. In this kind of lasers, a single block of a compound—functionmaterial material was used both as the laser material to generate the fundmental laser and as the frequency doubling material to dou the fundmental laser to the second harmonic light. This kind of lasers have the advantages of compactness, high doubling efficiency, narrow breadth of spectrum line of second harmonic light, lower costs, and easy to adjust[1,2,3,4].

The compound—fuction materials reported up to now are single crystals of Neodymium— and Magnesium—Oxide—doped Lithium Niobate (NMLN), Chronium—doped Potassium Titanyl Phosphate (Cr:KTP) and Neodymium—doped Yttrium Aluminium Borate (NYAB). The Chronium—doped Potassium Titanyl crystal can generates a fundmental laser at 800—850nm and self—doubles it into the second harmonic blue light at 400—425nm, but its upconversion efficiency is still smaller because of its higher absorption in the blue and lower nonlinear coefficient in the type I phase—matching. The Neodymium— and Magnesium—Oxide—doped Lithium Niobate crystal is the first compound—fuction material used as the self—doubling laser material, but its threshold pumping power is higher and it must be heated to relative high temperature to achieve the phase matching condition. It is very difficult to realize a diode pumped self doubling laser of Neodymium— and Magnesium—Oxide—doped Lithium Niobate crystal. So as a compound—fuction material, the applications of the Neodymium— and Magnesium—Oxide—doped Lithium Niobate crystal are limited. As a compound—fuction material for diode pumped self—doubling laser material the Neodymium—doped Yttrium Aluminium Borate (NYAB) crystal is the best crystal reported up to now. The Neodymium—doped Yttrium Aluminium Borate crystal has some advantages, such as a larger nonlinear coeffecient, broader spectral, angular and temprature acceptance widths and operation at room temperature, etc.. But it has some disadvantages. For example, its threshold pumping power is still higher and it is difficult for most of the diode pumped Neodymium—doped Yttrium Aluminium Borate self—doubling laser to operate at

the fundmental transversal mode. So we have made much efferts to growth Modified Neodymium—doped Yttrium Aluminium Borate (M—NYAB) crystal of better quarlity and developed a new sort of diode pumped self—doubling lasers with this new crystals. The crystal properties of the Modified Neodymium—doped Yttrium Aluminium Borate crystal is similar to that of the Neodymium—doped Yttrium Aluminium Borate crystal. The details about this crystal will be given at the meeting. Here we report the experiment results of the lasers.

EXPERIMENTS AND RESULTS: In June, 1991, we developed the the first diode pumped M—NYAB SFD laser. For comparison, we conducted some experiments with the M—NYAB and NYAB crystal samples. The M—NYAB and NYAB crystal samples were cut for type I phase matching. They are $3 \times 3mm$ square rod, 3mm long in phase matching direction. The two end—face of the samples through which the laser beam passed were optically polished and coated with antireflective films for both the fundmental laser and the second harmonic light. The diode end—pumped direct—coupled external cavity SFD laser experimants and the diode—pumped optical—fiber—coupled external cavety SFD laser expetimants were conducted.
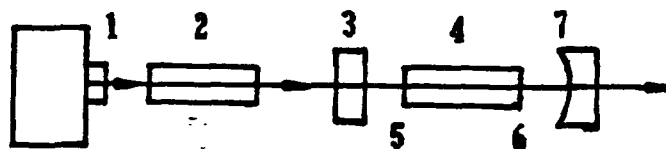
Fig.1. Experimental setup for diode end—pumped direct—coupled external cavety SFD laser

The scheme of the experimental setup of Diode end—pumped direct—coupled external cavety SFD laser of M—NYABis shown in Fig.1. It is composed of LD (Laser Diode) (1), focus system (2), input reflective mirror (3), SFD crystal rod (4), antireflective films (5) and (6), output coupler mirror (7). The LD radiation is collimated and focused longitudinally on the laser rod. The laser resonant cavity consists of the input plane mirror (3) and the output spherical mirror which is used as the output coupler. The input plane mirror is coated for high reflectivity at both the fundamental laser (1.062μ m) and the second harmonic light (0.531μ m) and high transmitivity($\sim 75\%$) for diode pumping light(0.804μ m). The antireflective films (5) and (6) for both the fundamental laser radiation and the second harmonic light were coated on the faces of laser rods. The output spherical reflector (7) (the radius of curvature is 100mm) is highly reflective at the fundamental laser (1.062μ m) and transmits 80% of second harmonical light (0.531μ m).
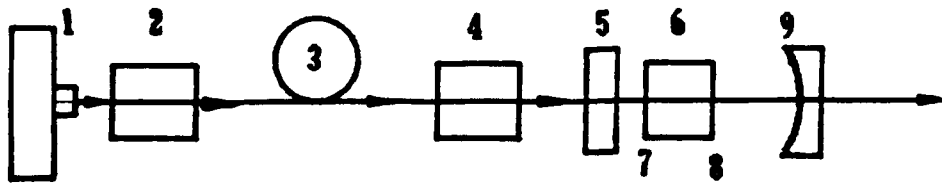
Fig.2. Experimental setup for LD end—pumped OF—coupled external cavety SFD laser

The scheme of the experimental setup for LD end—pumped optical—fiber—coupled external cavety SFD laseris shown in Fig.2. This device consists of LD (1), two focus systems (2) and (4), coupling fiber (3), input reflective mirror (5), SFD laser crystal rod (6), antireflective films (7) and (8), and output coupler mirror (9). Two end facets of the fiber are antireflecting coated for pump light (0.804 μ m) in order to decrease the loss of pump light. The other elements are the same as that in the LD end—pumped direct—coupled SFD laser.

The output power of 0.531 μ m green light is measured after dispersion prism which separated the fundamental beam and the second harmonic beam in space. The center wavelength is measured by optical spectrum analyzer. The Polarization degree is measured with polarizer and powermeter. The experiments of both the M—NYAB SFD lasers and the NYAB SFD lasers were conducted under the same conditions. The experimental results show:

The threshold pump power of the LD pumped M—NYAB SFD lasers is 65~70 percent of that of the NYAB SFD lasers, and it is easy for the LD pumped M—NYAB SFD lasers used up to now to operate at the fundametal transverse mode, while few of the the LD pumped NYAB SFD lasers can operate at the fundametal transverse mode.

CONCLUSION: M—NYAB crystal is a compound—function crystal which has greater non—linear coefficient and high laser quality. We have developed LD pumped direct—coupled M—NYAB SFD laser and LD pumped OF—coupled M—NYAB SFD laser. Its threshold pump power is much lower than that of the NYAB SFD lasers and it easily operates at the fundamental transverse mode. It will be broadely used in various application.

REFRENCES

(1) L. M. Dorozh'in, I. I. Kuratev, N, I, Leonyuk, T. I. Timchenko, and A. V. Shestakov, Sov. Tech. Phys. Lett.,vol.7, pp.555—556, 1981.

(2) S.Amano, S.Yokooama, H.Koyomo, S.Amano, and T.Mochizuki, Rev, Laser Eng.,vol.17,pp.555—556,1981.

(3) S.C.Wang, R.E.Stone, and J.T.Lin, Advanced Solid State Lasers Techn. Dig., Salt lake City UT, paper TuB4,1990.

(4) J.T.Lin, Lasers & Optronics, P34, December,1990.

SECOND HARMONIC GENERATION AND DEGRADATION
IN CRITICALLY PHASE MATCHED KNbO$_3$ USING
DIODE PUMPED, Q-SWITCHED ND:LASERS

W. Seelert, P. Kortz

ADLAS GmbH, Seelandstrasse 67, D-2400 Lübeck 14, Germany

D. Rytz, B. Zysset, D. Ellgehausen and G. Mizell

Centre de Recherche en Optolectronique,
SANDOZ S.A., F-68330 Huningue, France

Efficient requency doubling of low power diode pumped Q-switched Nd lasers requires frequency doubling crystals with high nonlinear coefficients, such as KTiOPO$_4$ (KTP) (1), MgO:LiNbO$_3$ (2,3), and KNbO$_3$ (4,5).

While KTP and MgO:LiNbO$_3$ have been studied extensively, KNbO$_3$ crystals have not yet received the same attention in the case of second harmonic generation (SHG) of one micron lasers.

KNbO$_3$ is a useful nonlinear optical material because of its high nonlinear optical coefficients d$_{31}$ = - 15.8 and d$_{32}$ = - 18.3 pm/V and because it is phase matchable over a wide spectral range (6). At room temperature, KNbO$_3$ is in its orthorhombic phase, which is stable between 233 and 493 K. The orthorhombic axes a, b, and c are defined in such a way that the indices of refraction follow the relationship n$_b$ > n$_a$ > n$_c$.

Temperature tuning of the birefringence allows noncritical type I phase matching for SHG of 1064 and 1047 nm light propagating along the b-axis when the KNbO$_3$ crystal is heated to 461 (6-9) or 435 K, respectively.

Angle tuned phase matching is also achievable at room temperature, although it has not been extensively described in the literature. For a propagation direction in the (b,c) plane, the effective nonlinear coefficient d$_{eff}$ is

$$d_{eff} = d_{31} \sin \phi$$

where ϕ is the phase matching angle measured from the c-axis. This angle is near 71° for Nd:YAG or Nd:YLF laser radiation. For angle tuning in the (a,c) plane, the effective nonlinear coefficient is

$$d_{eff} = d_{32} \sin \theta$$

where the angle θ is again measured from the c-axis. For Nd:YAG or Nd:YLF, this angle is equal to 46 and 48.5°, respectively.

Taking advantage of the higher d$_{eff}$, the larger acceptance angle and the more favorable orientation for repoling in the (b,c) geometry, we have prepared KNbO$_3$ samples for room temperature angle tuned SHG of ND:YLF radiation. The samples were uncoated.

For the measurements of the intensity dependent conversion efficiency, we used an ADLAS model 321 Q diode pumped Q-switched Nd:YLF laser with 170 µJ pulse energy and a temporal pulse width of 11 ns at 1 kHz repetition rate. The laser output was pure TEM_{00} i.e. circular and diffraction limited. Fig. 1 is a schematic of the experimental setup.
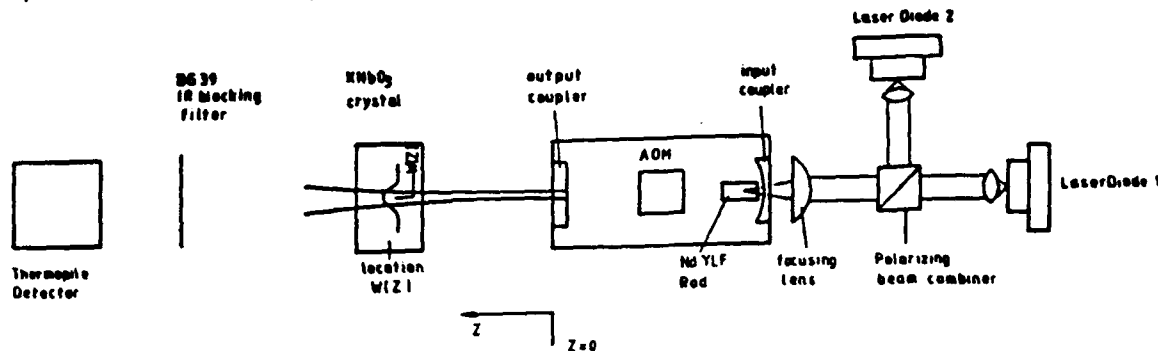

Fig.1   Schematic of the experiment

To avoid high experimental tolerances for the excitation intensity due to imaging optics we used the pure geometrical laser parameters i.e. the well known beam waist w_0, and the laws for gaussian beams. The beam waist w_0 was 130 um (radius) at the location z = 0 in front of the output coupler. For a gaussian beam, w_0 increases as a function of distance z as

$$w(z) = w_0 \sqrt{1 + (z/z_R)^2}$$

where z_R is the Rayleigh length given by

$$z_R = \pi w_0^2 / \lambda$$

with λ equal to 1047 nm.

The fundamental intensity was determined at a position corresponding to the center of the SHG crystal. Taking into account the reflection losses (14 %) of the $KNbO_3$ sample at the uncoated entrance face, the maximum intensity inside the crystal was 29 MW/cm^2. With the crystal positioned as discribed in Fig. 1, the intensity could only be lowered when increasing the distance between the output coupler and the crytal. Because no focussing optics were used, errors caused by the imaging lenses could be excluded for intensities below 29 MW/cm^2. When higher intensities were required for degradation experiments, we had nevertheless to use a focusing lens.

The green SHG pulse energy was measured by means of an infrared (IR) blocking filter and a calibrated thermopile. The conversion efficiency measurements were based on a measured IR fundamental energy of 170 µJ corrected for reflection losses (i.e., the energy was reduced to 86 % of 170 µJ) and a corrected SHG output energy (i.e., divided by 0.86). The maximum conversion efficiency including refelectivity corrections was 27.4 % and corresponded to measured 34.5 µJ of green light available with no focussing optics. With a focusing lens, we achieved a conversion efficiency of 40 % with 58 µJ of 523 nm light. The intensity dependence of the conversion efficiency is depicted in Fig. 2.
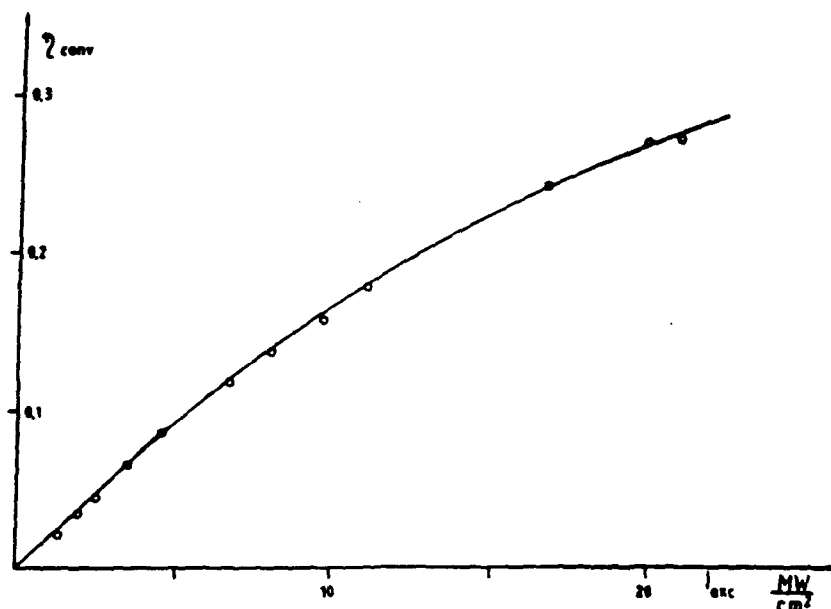
Fig.2
Conversion effi-
ciency as a func-
tion of excitation
intensity

When operating with 90 MW/cm^2 and observing a conversion efficiency of 40 %, no degradation of the SHG output was observed after $2 \cdot 10^8$ pulses or 55 hours of operation. Neither gray tracking (10) nor photorefractive damage were observed in $KNbO_3$ at this intensity level. Under similar experimental conditions, we observed gray tracking damage in flux grown KTP after 10^7 pulses. In hydrothermally grown KTP, we found an irreversible distortion of the initial circular SHG beam shape after 10^8 pulses indicating the beginning of gray tracking. In $MgO:LiNbO_3$, we observed photorefractive effects after 10^7 pulses at 40 MW/cm^2.

Although a much more detailed comparison study of various nonlinear materials is needed before damage thresholds can be asserted, our experiments show at $KNbO_3$ is a very attractive candidate for SHG of 1 μm lasers from the point of view of efficiency, damage resistance and long term reliability.

References

1) J.D. Bierlein and H. Vanherzeele, J. Opt. Soc. Am. B 6, 622 (1988)
2) W.J. Kozlovsky, E.K. Gustafson, R.C. Eckhardt and R.L. Byer, Opt. Lett. 13, 1102 (1988)
3) W.J. Kozlovsky, C.D. Nabors and R.L. Byer, IEEE J. Quant. El. 24, 913 (1988)
4) W.P. Risk, R. Pon, and W. Lenth, Appl. Phys. Lett. 54, 1625 (1989)
5) J.C. Baumert and P. Günter, Appl. Phys. Lett. 50, 554 (1987)
6) J.C. Baumert, J. Hoffnagle and P. Günter, Proc. SPIE 492, 374 (1984)
7) Y. Uematsu and T. Fukuda, Jap. J. Appl. Phys. 4, 507 (1971)
8) Y. Uematsu, Jap. J. Appl. Phys. 13, 1362 (1974)
9) Y. Uematsu and T. Fukuda, Jap. J. Appl. Phys. 12, 841 (1973)
10) M.G. Roelofs, J. Appl. Phys., 65, 12, 4976 ff (1989)

A Novel Thermal Poling Technique for Fabricating QPM SHG Structures in X-cut Lithium Tantalate

R.A. Rubino, D.E. Bossi, and J.D. Farina

United Technologies Research Center
M.S. 81, Silver Lane East Hartford, CT 06108
(203) 727-7051

We report a novel laser-assisted thermal poling technique for producing quasi-phase-matched (QPM) structures in planar x-cut Lithium Tantalate. As a proof of concept, low loss annealed proton exchanged (APE) waveguides were subsequently fabricated in these structures in order to demonstrate efficient second-harmonic generation (SHG) of blue light. Though others [1,2], have demonstrated higher QPM SHG conversion efficiencies in z-cut LiNbO$_3$ and LiTaO$_3$, we believe this process for x-cut material shows great promise for achieving higher SHG efficiencies. Furthermore, this process is compatible with the preferred crystallographic orientation for on-chip integration of IO (integrated-optic) devices such as high quality intensity modulators.

For optically non-linear materials which lack adequate birefringence for classical phase-matched SHG, such as LiNbO$_3$ and LiTaO$_3$, the QPM technique allows for the fundamental and second-harmonic waves to co-propagate in a quasi-synchronous manner in a material which is otherwise dispersive at these wavelengths [3]. Quasi-phase-matching is achieved by producing a repetitive sign reversal of the non-linear coefficient of the material, which acts to periodically "reset" the phase to ensure the proper phase relationship is maintained for a continuous growth of the second harmonic wave. For first order QPM structures designed for frequency doubled components in the blue/green region, this amounts to reversing the non-linear coefficient approximately every 1.5 microns. To ease the fabrication tolerances, higher order QPM structures may be employed. However, the conversion efficiency will be reduced by the square of the order number.

In order to "write" the sign-reversed domains in x-cut LiTaO$_3$, we have developed a laser-assisted thermal poling technique. In particular, a wafer of x-cut LiTaO$_3$ is patterned with two electrodes, separated by 200 microns, in the y-direction along the entire length of the desired QPM grating. By appropriately adjusting the intensity and spot size of an infrared beam having a wavelength which is absorbed by LiTaO$_3$, such as 10.6 μm, the material surface temperature in the illuminated region can be raised above the Curie temperature (610°C). A bias voltage of 200 volts is applied to one of the electrodes while the other is grounded, thereby producing an electric field which is either parallel or anti-parallel to the z-axis. The applied electric field orients the spontaneous ferroelectric polarization within region which exceeds the Curie temperature (T_c). Once cooled below the T_c, the realignment is permanent.

The QPM grating "writing" process continues by moving the substrate along the y-direction corresponding to one pole width (half the grating period) and repeating the heating/cooling process with the exception of reversing the bias field in order to reverse direction of the polarization axis. As illustrated in Fig. 1a, the QPM structure is produced by sequentially "freezing" out the desired domain orientation along the trailing edge of the heating beam. In this way, pole dimensions appreciably smaller than the T_c diameter of the impinging beam can be produced without sacrificing pole

profile. As shown in Fig. 1b, the resulting domain profiles appear crescent shaped, however, when compared to the dimensions of the waveguide, the profile is nearly the desired rectangular profile. Achieving lowest order gratings with near optimum profile, ensures a strong overlap between the guided-mode profile and the domain inverted regions which in turn allows for maximum SHG conversion efficiency.
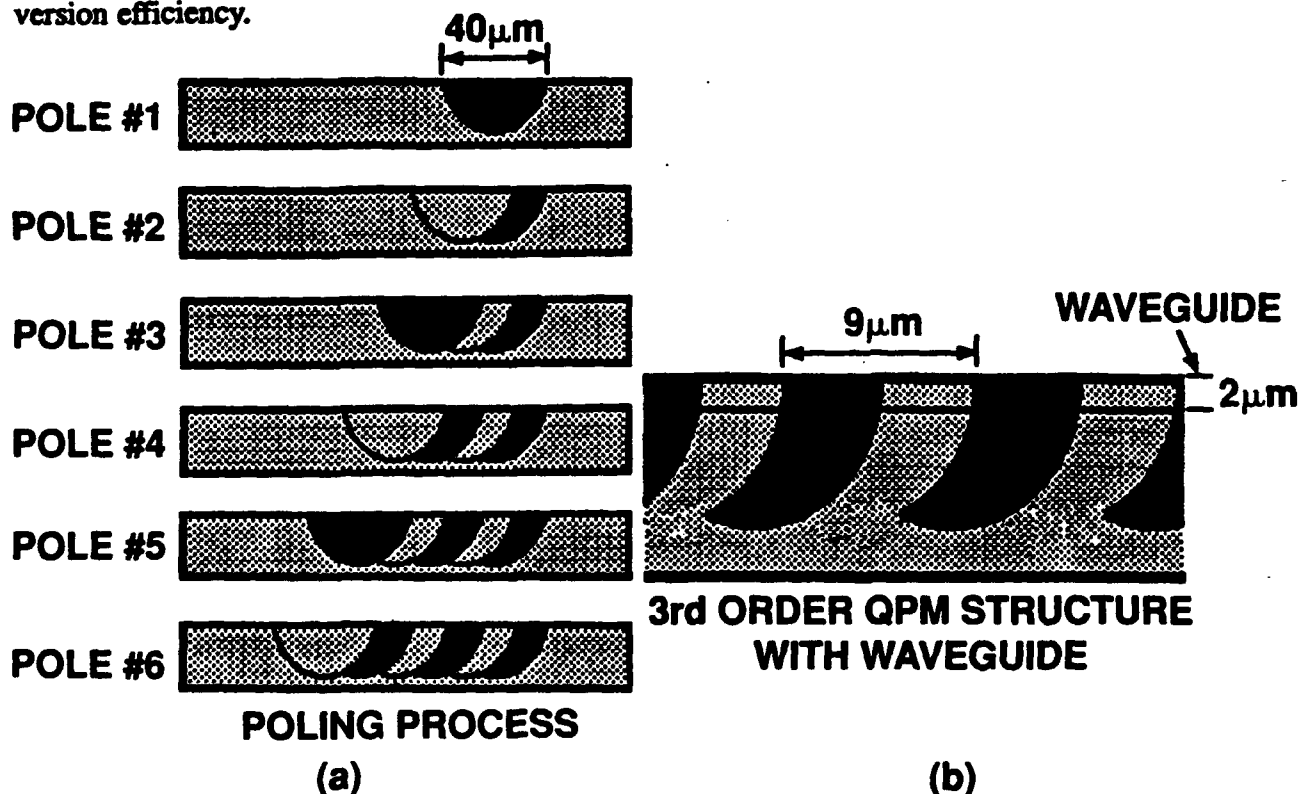

POLING PROCESS

(a)

3rd ORDER QPM STRUCTURE WITH WAVEGUIDE

(b)

Figure 1 (a) The UTRC thermo-electric process involves iteratively "writing" an inverted domain, moving the substrate a distance corresponding to half the period and re-inverting a portion of the domain to its original orientation. (b) The resulting domain profile appears crescent shaped, however, when compared to dimensions of the waveguide, the profile is nearly the desired rectangular profile.

The photograph in Fig. 2 is of a cross section of a substrate in which a 40 micron period QPM structure has been diced, polished and then processed with a preferential etch which reveals the -c face and leaves the +c face untouched. The most striking feature of the QPM grating cross section is the sharpness and definition of the individual poles. Closer inspection of the material between the etched poles reveals an extremely uniform and featureless profile indicating the thermal poling process is 100% complete. This finding is even more surprising when one considers the poling technique to produce these structures may "write" and "rewrite" any given domain four or five times as the substrate moves under the heating beam.

50μm
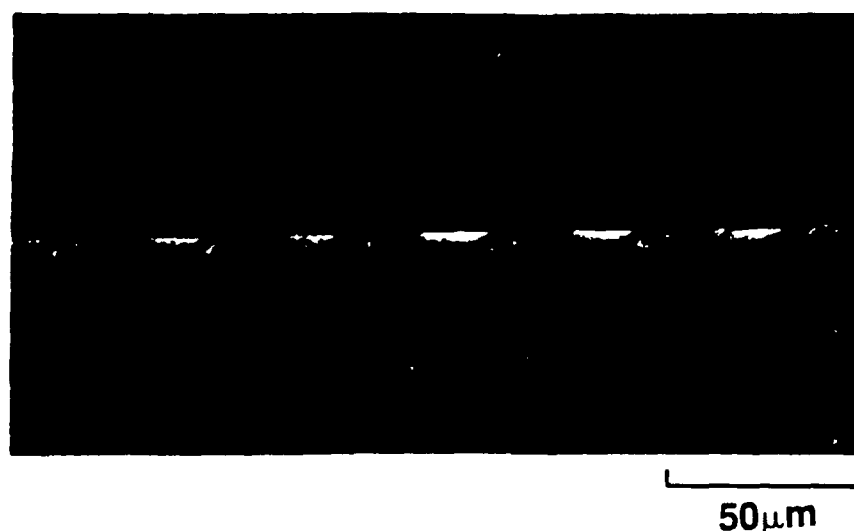
Figure 2 Preferential etching of cross sections of QPM gratings fabricated with the UTRC thermo–electric poling process reveals sharp and well defined domain boundaries indicating 100% complete domain inversion. The 40 μm period structure shows extremely good uniformity and depth.

As a preliminary demonstration of the applicability of this technique in the manufacture of high efficiency QPM SHG devices, a 3rd order, 3 mm long QPM waveguide frequency doubler was fabricated in LiTaO3. Coupling 25 milliwatts of 880 nm into the device produced nearly 2 microwatts of 440 nm light. Using this number, we calculate a normalized conversion efficiency of 3.6% $1/(W*cm^2)$. The full width wavelength acceptance bandwidth of this structure is several nanometers, indicating significant random errors in domain positions of the device. These errors can also explain the relatively low SHG conversion efficiency. Relatively minor improvements to our process control should yield significantly higher efficiencies for these devices, including first and second order structures. Process technique, fabrication tolerances and SHG results for devices manufactured using the thermal poling technique will be presented.

REFERENCES

1. E. J. Lim, M. M. Fejer, R. L. Byer and W. J. Kozlovsky, "Blue Light Generation by Frequency Doubling in Periodically Poled Lithium Niobate Channel Waveguides," **Electron. Lett.**, Vol. 25, pp. 731–732, 1989.

2. K. Yamamoto, K. Mizuuchi, "High Power 12 mW Blue Light Generation In Periodically Domain–Inverted LiTaO3," **CLEO–91**.

3. S. Somekh and A. Yariv, "Phase Matching by Periodic Modulation of hte Nonlinear Optical Properties," **Opt. Commun.**, Vol. 6, pp. 301–304, 1972.

Simultaneous Blue and Green Second Harmonic Generation

in Quasi-Phase Matched LiNbO$_3$ Waveguide

Xiaofan Cao, Ramakant Srivastava, and Ramu V. Ramaswamy

Photonics Research Laboratory

Department of Electrical Engineering

University of Florida

Gainesville, Fl 32611

We report the first simultaneous quasi-phase matched (QPM) generation of blue (433 nm) and green (532nm) light by second harmonic generation in LiNbO$_3$ channel waveguides.

Quasi-phase matched (QPM) guided wave frequency conversion is rapidly emerging as a viable technology to obtain light at visible wavelengths. Using this method, efficient blue light generation was recently obtained in annealed proton exchanged (APE) LiNbO$_3$[1] and LiTaO$_3$[2] waveguides. A compact light source which would generate red, green, and blue simultaneously is of particular interest for applications in high resolution color laser printers and displays. However, due to the narrow phase matching bandwidth in QPM, simultaneous phase matching for SHG into blue and green wavelength has not been demonstrated as yet.

In this paper, we report for the first time efficient simultaneous generation of two of the fundamental colors need for display, namely blue and green, by QPM frequency doubling in APE waveguides. This approach holds a distinct advantage over the Cerenkov phasematching method for generation of blue green coherent radiation[3] due the high conversion efficiency and diffraction-limited output mode profile from a single channel waveguide. This approach is possible because the required periodic domain inversion grating period for second order QPM at 865 nm coincides with that of first order QPM at 1064 nm in LiNbO$_3$ waveguide. From the phase matching curves shown in Fig. 1, this scheme is possible for both LiNbO$_3$ and LiTaO$_3$.

The periodically domain-inverted structure was fabricated by diffusing titanium stripes on LiNbO$_3$ substrate at 1050 $^\circ$C with the grating period of 6.8 μm. The channel waveguides were fabricated by annealed proton exchange (APE) technique as described elsewhere.[4] SHG experiment was performed using a Ti-Sapphire laser and a Nd:YAG laser. As illustrated in Fig. 2, the output of both lasers were first combined by a wavelength selective 45° mirror (HR at 1064 nm), and endfire coupling into the LiNbO$_3$ channel waveguide with a 40x (N.A.=0.65) microscope objective lens. Using such a coupling setup the laser output power can be coupled into the waveguide with a throughput efficiency of about 20%. First, the QPM SHG condition for 1064 nm was achieved by fine tuning the phasematching wavelength to 1064 nm by the waveguide temperature tuning. The temperature variation of the LiNbO$_3$ substrate was implemented by wrapping the heating wire and thermal coupler around the copper sample mount. The temperature was controlled within 0.1°C by a programmable voltage supplies with a temperature feedback servo loop. Using the Ti-Sapphire laser, the QPM waveguide phase matching bandwidth was found to be 0.11 nm (indicating an effective phase matching length of 6 mm). Keeping the waveguide at the first order QPM temperature for 1064 nm (36 $^\circ$C), the Ti:Sapphire was tuned to the second order QPM wavelength for efficient blue generation. The highest generated blue power at 433 nm is 0.45 mW with SHG conversion efficiency of 22%/W. Up to 0.15 mW of green light was generated for 23 mW transmitted ᵀR (1064nm) power with

THIS
PAGE
IS
MISSING
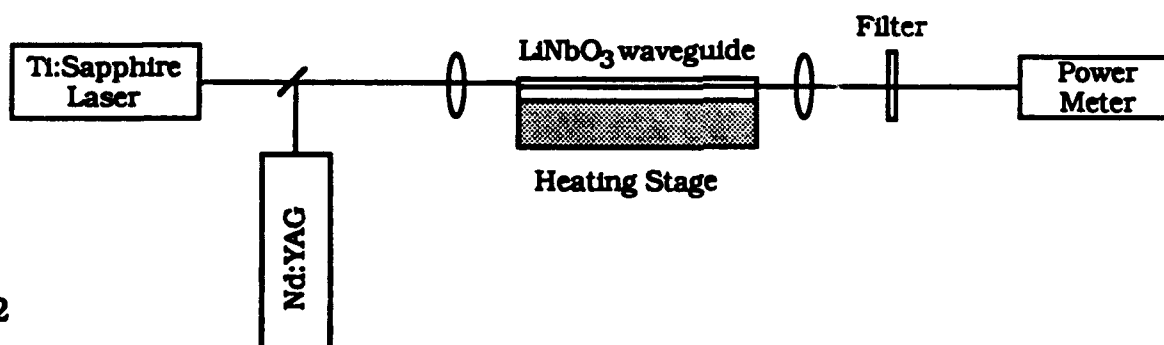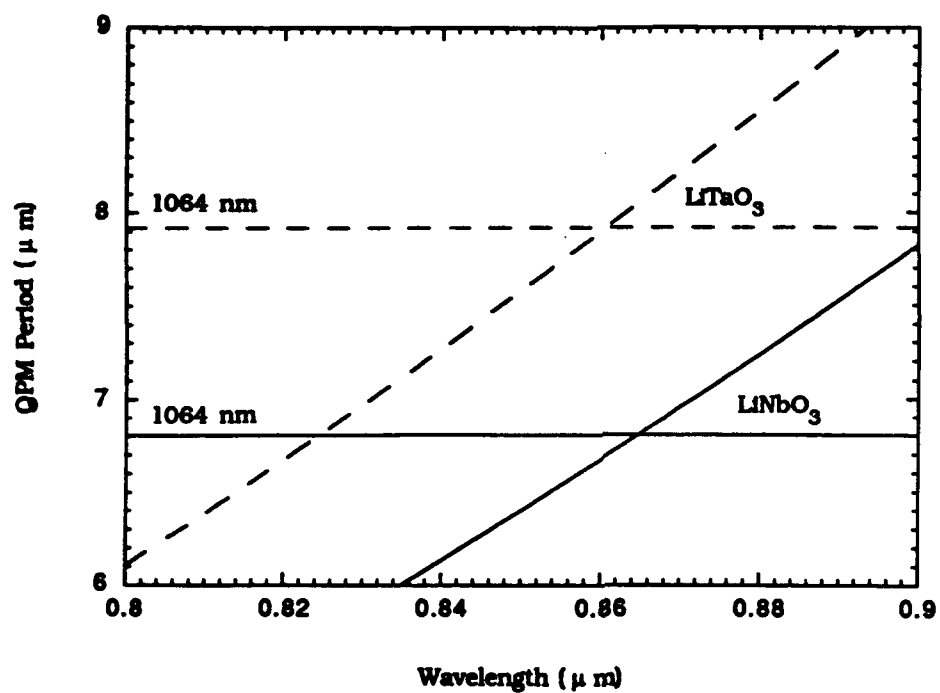IN
ORIGINAL
DOCUMENT

Fig. 1

Fig. 2

Novel Organic Nonlinear Optical Materials for SHG Devices of Semiconductor Lasers.

Yuzo Itoh, Yasuo Imanishi, Masakazu Sagawa, Hiroyuki Kagawa, Tomoyuki Hamada, and Atsushi Kakuta

Hitachi Research Laboratory Hitachi Ltd.

4026 Kuji-cho, Hitachi, Ibaraki 319-12, Japan

Tel: 294-52-5111 ex. 3471

Fax: 294-52-7610

In order to apply organic nonlinear optical materials to the SHG devices for semiconductor lasers, cut-off wavelength of the materials should be shorter than around 400 nm since the wavelength of commonly used semiconductor lasers is about 800 nm. Unfortunately, in the case of organic materials, enlargement of nonlinearity(hyperpolarizability) and shortening of the cut-off wavelength are the tradeoff relations. To develop novel organic nonlinear optical materials both with large nonlinearity and short cut-off wavelength, we used a molecular design method and chose heteroconjugate molecules as target materials.

Semi-empirical and *ab initio* molecular orbital methods were used for estimation of hyperpolarizabilities and absorption wavelength. Crystal energy calculations were used for estimation of crystal structures. In Fig. 1, calculated hyperpolarizabilities and absorption wavelength of several excellent molecules selected from a large number of calculated molecules, are shown. A semi-empirical molecular orbital method (CNDOS3-CI) was used in these calculations. These materials (Fig. 1) have two superior properties: large nonlinearity and short cut-off wavelength. Among those materials, xanthone derivatives are shown to be of good quality. For example, measured absorption spectrum of 2,7-dinitroxanthone crystal is shown in Fig. 2.

Among these materials 3-aminoxanthone showed very good nonlinear optical properties for application to SHG device of semiconductor lasers. Powder efficiency of this material is 13 times of urea and cut-off wavelength is 420 nm at the solid state. The latter is short enough to be applied to SHG devices for semiconductor lasers. The crystal structure was determined by x-ray crystallographic analysis. The space group is $P2_1$(monoclinic) and the cell dimensions are a=13.394, b=4.718, c=8.084 Å, β=103.12°.

Using the oriented gas model approximation, nonlinear susceptibility of this material was calculated: the largest component of the susceptibility tensor, d_{112}=30pm/V. Experimental results of Cherenkov type SHG application will be presented at the meeting.
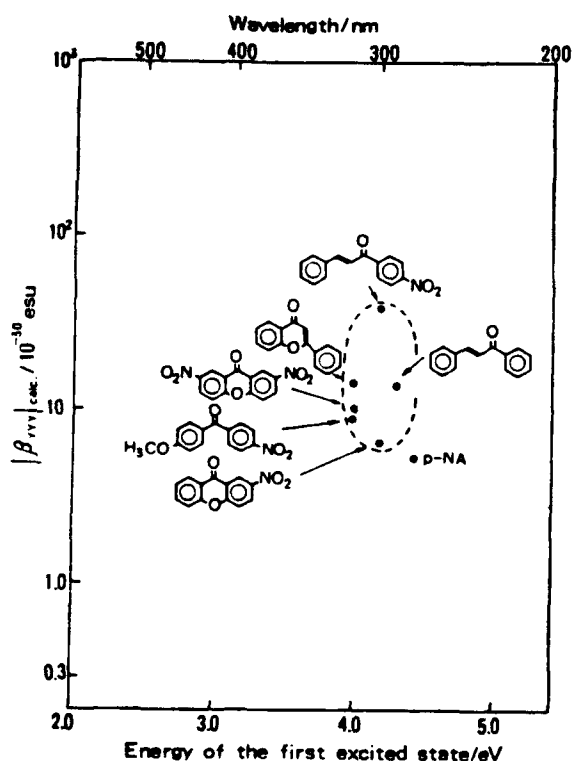
Fig. 1 Calculated hyperpolarizabilities and absorption wavelength of several materials considered.
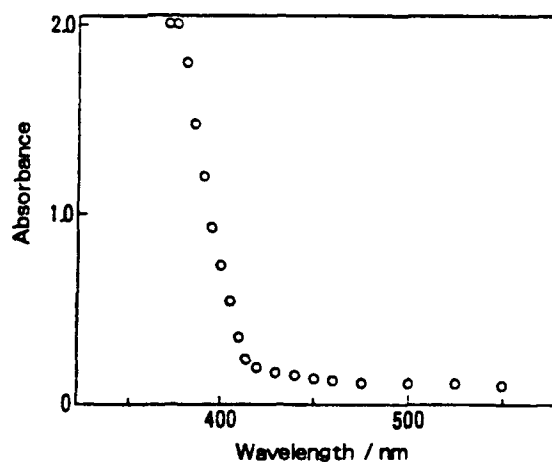
Fig. 2 Absorption spectra of 2,7-dinitroxanthone.

Blue Green Injection Laser
Made of Nitride Semiconductors

Jacques I. Pankove
Center for Optoelectronic Computing and
Department of Electrical & Computer Engineering
University of Colorado at Boulder
Boulder, Colorado 80309-0425
(303) 492-5470

An injection laser is proposed that is capable of emitting coherent radiation in the spectral range from green to ultraviolet. This will be achieved by injecting holes from a p-type substrate through an asymmetric barrier into InN quantum wells, while the electrons will be provided by the host GaN. The electrons will be retained in the region of the quantum wells by the asymmetric barrier. Radiative recombination will occur inside the quantum wells at a wavelength determined by the thickness of the InN layer. The shortest wavelength obtainable in this system is 360 nm, corresponding to recombination across the GaN bandgap. The blue-green spectral region will be readily obtained with InN strained layers.

The source of holes is a wide bandgap p-type semiconductor such as SiC or GaP. SiC is preferred since its lattice constant is closely matched to that of GaN. Either basal plane hexagonal SiC or (100) β-SiC are suitable substrates.

The asymmetric barrier that blocks GaN electrons but allows the injection of holes from the substrate is shown in Figure 1. This barrier is made of acceptor-compensated insulating GaN having a thickness of at least 300 Å to block electron tunneling.

Upon the application of a forward bias, holes are injected into the valence band of GaN and from there into the quantum wells.

To make this device into a laser, one can cut and polish the edges to form a Fabry-Perot cavity. A preferred version will be to make a super-lattice of quantum wells forming a distributed feedback (DFB) grating when the active regions are spaced $\lambda/2n$ apart. (λ = wavelength in vacuum, n = refractive index of GaN.) Such a DFB structure can be operated as a surface-emitting laser. Note that, with a DFB surface-emitting

structure, one does not need a reflector at the exit end facet. Hence an antireflection coating may be deposited on the exit facet to maximize the laser output.
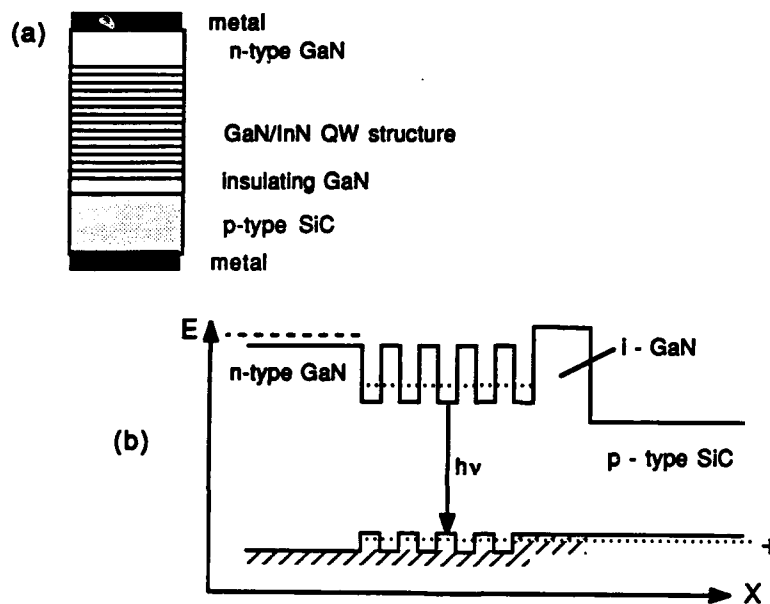
Figure 1. (a) Structure of the short wavelength injection luminescent device. (b) Energy band diagram of device with forward bias applied.

Investigation of the Compact S_2 Vapor
Blue-Green Laser

Yu Jun-hua,Zhang Zhong hua,Zhang hua

Zhu Zhong wei,Ma Zu guang

Institute of Opto-Electronics,Harbin Institute of

Technology,P. R. China

The properties of diatomic sulfur and the characteristics of S_2 potential curves $B^3\Sigma_u^- - X^3\Sigma_g^-$ make it possible to lase in S_2 vapor by laser pumping or electric discharge pumping[1]. The S_2 laser is efficient, of low pumping threshold and near continuously tunable over a wide spectral range.

In 1987, the S_2 laser oscillations from near ultraviolet to blue-green spectral region were obtained by optical pumping and dissociating S_{3-8} into S_2 by heating in our laboratory[2][3]. 11 spectral bands were observed in the wavelength region of 420-540nm for the first time.

In order to study the compact tunable S_2 laser further, a design of S_2 laser with transverse double-pulsed fast discharge excitation was put forward in 1989 and the kinetics for sulfur discharge was first investigated.

Under the condition of 2 torr He-buffer in sulfur cell, the following results were observed.

①Stable self-sustained glow discharge was first achieved with sulfur temperature $180^0 - 250^0C$ (the vapor pressure 1-10torr)and pulse-discharged voltage 2. 9-4. 8KV. The S_2 fluorescence spectra in 350-520nm range were measured with Optical Multichannel Analyzer(EGFG PAR) as shown in Fig1

②Holding the temperature of S_2 vapor at a fixed value. the S_2 fluorescence intensity is increased linearly with the pulse-discharged voltage.

③When the time interval of These two discharge pulses was kept at about 200 μs the second discharge current pulse profile (corresponding to S_2 discharge), measured by a current monitor transformer, is better than the first discharge current(corresponding to He discharge). As is shown in Fig 2.

When 2 torr Ne-buffer is added into S_2 cell, there were following results.

①Under the same condition as He-buffer, the stable self-sustained glow discharge appeared, but the discharge voltages decreased to 1500-3500V.

②The fluorescence with Ne-buffer was more intense than with He-buffer in blue-green range.

It can be realized,

①Under the same condition, the smaller discharge voltage in Ne-buffer than that in He-buffer is due to the lowes ionigation potential of Neon.

②In gas discharge, the efficiency for generating excited states has close relation with the distibution of the election energy of the discharge. The excitation energy for $S_2B^3\Sigma_u^-$ is approximately larger than 4eV. The energy distribution function of electrons in dischange $V^{1/2}F(v)_{Ne} > U^{1/2}F(U)_{He}$.

So, under the same E/N (E; the electcic field intensity, N_1 the density of S_2 molecule), the excitation efficiency of S_2 with Ne-buffer is higher than that with He-buffer.

③The intersity of each spectral band increases synchronously with the discharge veltage. This corresponds to the derived theoretical resulte form Born approximation that S_2-election collision crocs section has a property of resonance in a wide band.

④The experimental results showed that the current pulse profile of the second disoharge is better than the first. This expressed that the dynamic resistance Z_s, and inductance L_s, of S_2 vaper are lower than the Z_{He} and the L_{He} respectively. It shows that stable self-sustained discharge is easy realized in S_2 vapor.

Since the specific resistance of the plasma in Ar-buffer is larger than that of He and Ne($k_{Ar} > k_{Ne} > k_{He}$), the discharge stability in Ar will be worse, So we didn't take Ar as buffer gas.

The kinetics of S_2 discharge is being studied further in our laboratory.

[1] D.A.Peterson etal. "Stable pure sulfur discharges and associated Spectra" J.Chem. Phys. 73(4). 1551(1980);

[2] Yu Junhua et al. "Transverse-Optically Pumped Ultraviolet S_2 Laser" Proceeding of the Topical Meeting on LM&LS'88. p224;

[3] Yu Jun hua et al. "An Optically Pumped S_2 Blue-Green Laser" CHINESE PHYSICS LASERS. Vol.15. No.2. p107.1988
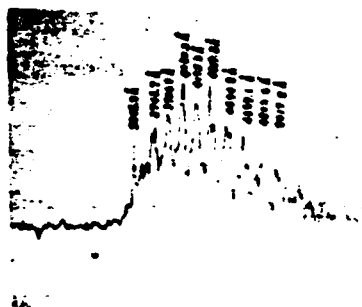
Fig.1 The S₂ fluorescence spectra

in 350-520nm range with 2 torr He-buffer
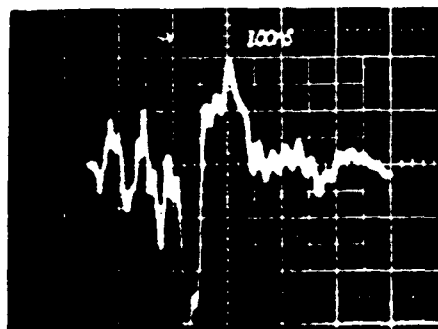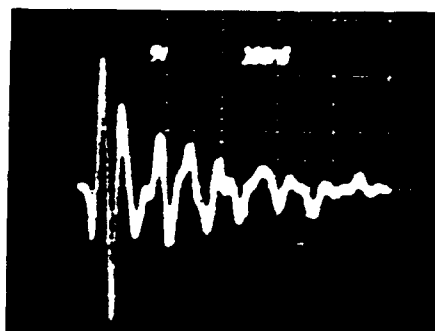

Fig.2 The first discharge current pulse profile

The second discharge current pulse profile

Frequency Conversion in Bulk Devices

FA   8:30am–10:30am
Anasazi South

William P. Risk, *Presider*
IBM Almaden Research Center

80% Nonlinear Conversion Efficiency: When?

Robert L. Byer

Stanford University

Improvements in the efficiency of cw second harmonic generation (SHG) and cw optical parametric oscillation depend on the ratio of the nonlinearity to the loss in the nonlinear medium. External resonant SHG in monolithic lithium niobate crystals has now reached 69% conversion efficiency. Progress for SHG to the ultraviolet in barium borate and for cw OPO operation will be reviewed.

Frequency–Doubled Diode Lasers

W. J. Kozlovsky
IBM Research Division
Almaden Research Center
San Jose, CA 95120
(408) 927–2133

Single–mode infrared diode lasers produce high output powers with long lifetimes, [1,2] and nonlinear optical processes can be used to convert the output of these sources to the blue. For instance, 430–nm light can be generated by frequency doubling the output from a GaAlAs diode laser in potassium niobate. To increase the efficiency of blue generation, an external enhancement resonator can be used to increase the fundamental intensity inside the nonlinear crystal.[3-8] For stable operation of such a system, a match of the output frequency of the diode laser and a resonant frequency of the external cavity must be maintained, since frequency differences will result in substantial fluctuations of the infrared power inside the resonator and thus in the blue output. Passive optical feedback has been used to lock the diode laser frequency to a resonator frequency,[3] with the requirement that the phase of the optical feedback be electronically controlled.[7] As an alternative, we have used an electronic feedback technique to frequency lock the diode laser frequency to a resonator frequency to produce 54 mW of stable blue output.[8]

The experimental set–up is shown in Figure 1. The GaAlAs diode laser generated 180 mW of single–spatial–mode, single–frequency 858–nm output at 23.3 °C. The collimator and prism beam expander produced a circular gaussian mode necessary for efficient excitation of the fundamental spatial mode of the enhancement resonator. The Faraday isolator prevented back–reflected and scattered light from reaching the diode laser, since this feedback would have disturbed the laser frequency stability. The final lens spatially mode–matched the diode–laser radiation to the nonlinear
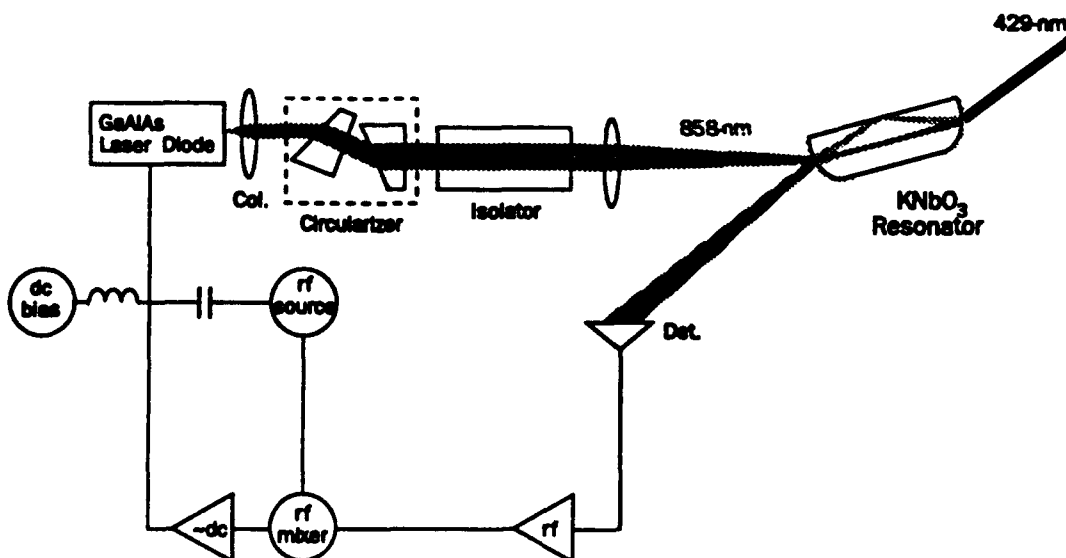
Figure 1. Experimental configuration for generation of 429–nm light by resonantly enhanced SHG of a GaAlAs laser diode.

resonator. The overall transmission of the optical components was 70% so that 125 mW of 858–nm power were incident on the KNbO3 crystal.

A monolithic ring resonator design was chosen to provide low cavity losses and good frequency stability. The ends of a 7–mm long crystal of potassium niobate were polished with 5–mm radius of curvature mirrors, and a TIR (total internal reflection) surface was polished along its length to complete the ring path.[5] Dielectric mirror coatings of high reflectivity were deposited onto the curved faces, with the input coupler reflectivity being chosen to impedance match the expected linear and nonlinear losses in the resonator.[6] The monolithic crystal resonator was placed on a Peltier element so that the crystal temperature could be maintained at 21.6 °C as required for noncritically phasematched frequency doubling.

In order to lock the laser frequency to the KNbO3 cavity resonance, we used a modified Pound–Drever[9] locking technique that exploited the convenient modulation and tuning properties of the semiconductor laser. For this method, FM–sidebands were produced around the ~5 MHz–wide laser emission line by superimposing a weak 300–MHz current on the dc injection current by capacitive coupling (see Figure 1). By using a double–balanced mixer for phase–sensitive detection of the heterodyne spectroscopy signal[10] contained in the light reflected from the input surface of the resonator, a strong servo signal indicative of the match of the laser and resonator frequencies was generated.[11] This servo signal was amplified and used to control the dc–current of the diode laser so that frequency stabilization was obtained by tuning of the laser frequency so that it tracked the cavity resonance.

With the servo loop closed the GaAlAs laser frequency remained locked to the nonlinear cavity resonance. As shown in Fig. 2, an output power of 54 mW at 429 nm was obtained with 125 mW of near–infrared power incident on the KNbO3 resonator, for an nonlinear conversion efficiency of 42%. The electrical input to the diode laser was ~440 mW, resulting in an overall electrical–to–blue conversion efficiency of ~12%.

Pulsing of the blue output was possible by switching the rf–current level to the diode laser. As the rf–current level was increased, the power in the FM–sidebands was increased at the expense of the carrier power level. Since only carrier
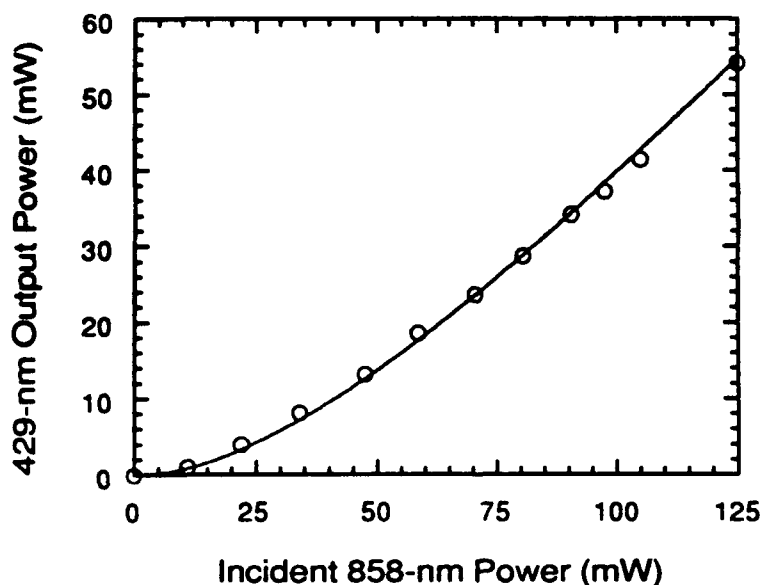

Figure 2. Generated blue power at 429 nm versus diode laser input power at 858 nm.

power can couple into the resonator, the decreased carrier power reduced the circulating power and therefore the blue output. Switching the rf–current between two levels thus produces blue pulses. Using this technique, pulses as short as 10 nsec were generated with several nanosecond rise times.

Resonator enhancement techniques can also be used to increase the efficiency of blue generation by sum frequency generation. In a separate experiment, a monolithic KTP resonator was used to enhance the power from both a 810–nm diode laser and a 1064–nm diode–pumped Nd:YAG laser, generating 4 mW of 459–nm light.[12] KTP permits sum–frequency mixing over a broad wavelength range that can be produced by GaAlAs diode lasers and InGaAs strained–layer diode lasers.

These results demonstrate that resonator–enhanced nonlinear frequency conversion techniques be used to efficiently produce blue light from presently available single–mode infrared diode lasers. Attractive output powers and performance characteristics can result from these compact blue sources.

REFERENCES

1. D. Welch, R. Craig, W. Streifer, and D. Scifres, "High Reliability, High Power, Single Mode Laser Diodes," *Electron. Lett.*, 26, pp. 1481–1483 (1990).

2. C. Harder, P. Buchmann, and H.P. Meier, "High–Power Ridge–Waveguide AlGaAs GRIN–SCH Laser Diode," *Electron. Lett.*, 22, pp. 1081–1082 (1986).

3. G. J. Dixon, Carrol E. Tanner, and Carl E. Wieman, "432–nm source based on efficient second–harmonic generation of GaAlAs diode–laser radiation in a self–locking external resonant cavity," *Opt. Lett.*, 14, pp. 731–733 (1989).

4. Lew Goldberg and Myuang Chun, "Efficient generation at 421 nm by resonantly enhanced doubling of GaAlAs laser diode array emission," *Appl. Phys. Lett.*, 55, pp. 218–220 (1989).

5. T. Baer, M. S. Keirstead, and D. F. Welch, "Efficient frequency doubling of a diode laser," Conference on Lasers and Electro–Optics, 1989 Technical Digest Series, Vol. 11 (Optical Society of America, Washington, D. C. 1989) p. 322.

6. W. J. Kozlovsky, C. D. Nabors, and R. L. Byer, "Efficient Second Harmonic Generation of a Diode–Laser–Pumped CW Nd:YAG Laser Using Monolithic MgO:LiNbO₃ External Resonant Cavities," *IEEE J. Quant. Electron.*, QE–24, pp. 913–919 (1988).

7. A. Hemmerich, C. Zimmerman, T. W. Hansch, "Second harmonic generation and optical stabilization of a diode laser in an external ring resonator," Conference on Lasers and Electro–Optics, 1990 Technical Digest Series, Vol. 7 (Optical Society of America, Washington, D. C. 1990) p. 20.

8. W. J. Kozlovsky, W. Lenth, E. E. Latta, A. Moser, and G. L. Bona, "Generation of 41 mW of blue radiation by frequency doubling of a GaAlAs diode laser," *Appl. Phys. Lett.*, 56, pp. 2291–2292 (1990).

9. R. W. P. Drever, J. L. Hall, F. V. Kowalski, J. Hough, G. M. Ford, A. J. Munley, and H. Ward, "Laser Phase and Frequency Stabilization Using an Optical Resonator," *Appl. Phys. B*, 31, pp. 97–105 (1983).

10. W. Lenth, "High Frequency Heterodyne Spectroscopy with Current–Modulated Diode Lasers," *IEEE J. Quant. Electron.*, QE–20, pp. 1045–1050 (1984).

11. Armin Sollberger, Arja Heinamaki, and Hans Melchior, "Frequency Stabilization of Semiconductor Lasers for Applications in Coherent Communication Systems," *J. Lightwave Tech.*, LT–5, pp. 485–491 (1987).

12. W. P. Risk and W. J. Kozlovsky, "Doubly resonant sum–frequency generation of 459–nm light in a monolithic KTP resonator," Conference on Lasers and Electro–Optics, 1991 Technical Digest Series, Vol. 10 (Optical Society of America, Washington, D. C. 1991) p. 218.

Miniature integrated SHG green laser

Hisashi MASUDA, Fumisada MAEDA, Michio OKA, Yushi KANEDA,
Minako SUGIURA, and Shigeo KUBOTA

Kubota Opto-Electronics Laboratory/
Opto-Electronics Research Department
Corporate Research Laboratories
Sony Corporation

6-7-35 Kitashinagawa, Shinagawa-ku,
Tokyo 141, JAPAN

Phone: 81-3-3448-5621
FAX: 81-3-3448-5634

Diode-pumped intracavity frequency doubled Nd:YAG lasers have been intensively investigated. Low noise characteristics of such a laser as well as its shorter wavelength than conventional laser diodes are attractive features for the higher density optical disk applications.[1]

We report miniature integrated diode-pumped SHG green lasers which are stabilized by a novel method. All components of this green laser including a laser diode (LD) chip, an imaging lens and a short resonator are mounted on a single TE (thermo-electric) cooler in a 28x38x16mm package (Fig.1). 5mW of TEMoo mode green output was derived from the LD pump power of 230mW (Fig.2). The retardation control of a KTP crystal combined with the insertion of a quarter wave plate (QWP) at 1064nm eliminated the instability caused by the sum-frequency mixing in the laser resonator.[2,3] The resultant noise level was lower than -140dB/Hz (RIN) at 5MHz. The laser operates just like a laser diode with the electric power supply and a temperature control circuit.

A miniature SHG green laser is composed of three blocks on a TE cooler, that is, a LD block, a lens block and a resonator block (Fig.1). The LD block and the resonator block are initially fixed with the mechanical fabrication accuracy. The alignment is achieved by the lens positioning. Temperature control of the LD and the resonator can be performed by a single TE cooler since the LD wavelength tuning range onto the Nd:YAG absorption lines is chosen to cover the stable temperature range of the resonator determined by the retardation of KTP. The LD used in this green laser is a 200mW commercial broad-area Sony SLD302. It has 50μm emission aperture which is imaged into the resonator through a glass aspheric mold lens with the magnification of M=1.5. The resonator is composed of a 0.5mm-thick quarter wave plate, a 1.5mm-Nd:YAG and a 2.5mm-KTP. A 3mm-long hollow extension was used between Nd:YAG and KTP crystals to extend the resonator length to 7.5mm for good mode overlap of this pump beam with the resonator mode. The resonator mode diameter is approximately 130μm at the Nd:YAG crystal. The input end of the QWP is spherically (radius of curvature r=10mm) ground

and polished with high reflectivity (HR) coating of R>99.9%. Similar HR coating is applied to the exit flat end of KTP to form a hemispherical standing wave resonator. Other flat surfaces of QWP and KTP in addition to the both ends of Nd:YAG are anti-reflection (AR) coated. These resonator parts are tightly glued on a metal block. Optical loss of all these components are evaluated with the accuracy of better than 0.1% by measuring the change of cavity finesse. The reduction of round-trip loss of the resonator is critical for this intracavity frequency doubled laser with low pump power. Due to high loss (~0.4%) of the AR coating of QWP used in this experiment it was necessary to raise the LD power to 230mW in order to obtain 5mW green output (Fig.2).

Instability due to the longitudinal mode coupling through sum frequency mixing in the resonator has been a serious problem in intracavity frequency doubled lasers.[2] Insertion of a rotated QWP at 45 degrees with respect to the c-axis of the type II phase-matched KTP successfully prohibited sum frequency mixing between longitudinal modes of different eigen-polarizations and enabled pure type II second harmonic generation of each eigen-polarization of the resonator.[3] However, sum frequency mixing between the longitudinal modes of the same polarization may still induce instability when the laser oscillates in multimode mainly due to the spatial hole burning of the gain medium. It was reported that two QWP's located at both sides of the gain medium with the relative orientation of their axes set at 45 degrees eliminated such spatial hole burning (twisted mode method).[4] We found a novel method to eliminate the spatial hole burning in Nd:YAG without using second QWP in order to let no more than one longitudinal mode of the same polarization oscillate, which is desired for stable operation of intracavity doubled lasers. When a KTP crystal having $\pm\pi/2$ retardation and a QWP with its axes rotated by 45 degrees with respect to c-axis of KTP are located at both sides of Nd:YAG, the eigen-polarizations defined at Nd:YAG are two orthogonal circular polarizations. The retardation was controlled by the transverse shift of a wedged KTP after its spatial retardation distribution was measured. Other advantages of this configuration compared with the conventional twisted mode method using two QWP's are the reduction of resonator loss owing to the use of less number of resonator parts and the linearly polarized green output because of the KTP location at the end of the resonator. Using this method and the temperature control within the range of several degrees to limit the the retardation error of KTP the miniature integrated SHG green lasers are stabilized.

1. M.Oka, T.Kashiwagi, and S.Kubota, Proc.SPIE **1139**, 149 (1989).
2. T.Baer, J.Opt.Soc.Am.B **3**, 1175 (1986).
3. M.Oka, and S.Kubota, Opt.Lett. **13**, 805 (1988).
4. V.Evtuhov, and A.E.Siegman, Appl.Opt. **4**, 142 (1965).
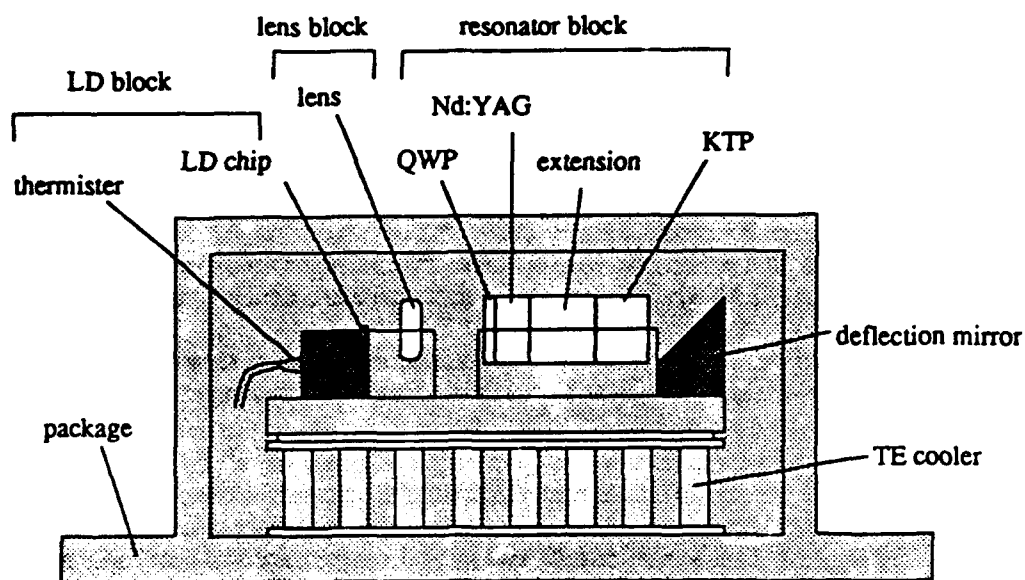
Fig.1   Configuration of a miniature integrated
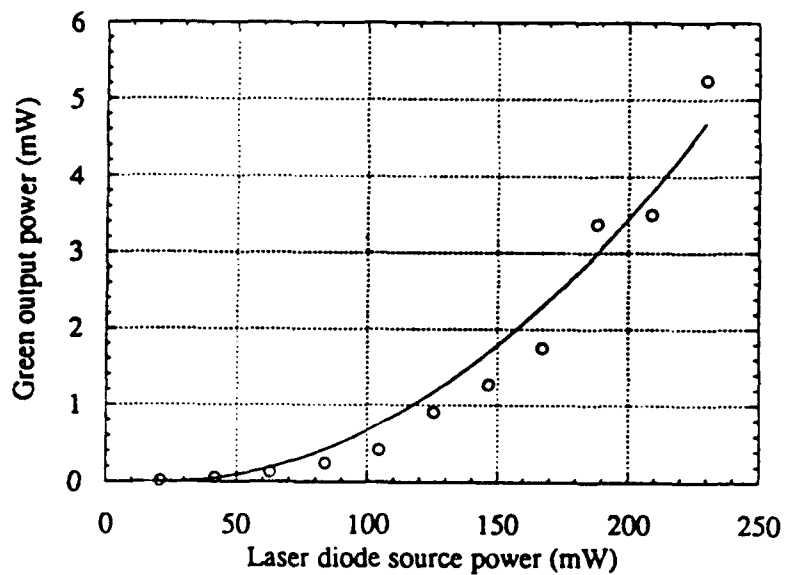   SHG green laser

Fig.2   Output power vs. LD source power

Seventy Percent Conversion Efficiency for Frequency-Doubling of a Diode-Pumped Continuous-Wave Single-Frequency Nd:YAG Laser

D.C. Gerstenberger, T.E. Olson, G.E. Tye and R.W. Wallace

LIGHTWAVE Electronics Corporation

1161 San Antonio Road

Mountain View, California 94043

(415)962-0755

The combination of diode pumped cw single-frequency Nd:YAG lasers and monolithic resonant frequency-doublers has lead to highly efficient and compact 532nm sources [1,2]. Using a diode-pumped 700 mW Nd:YAG laser, we have generated 500 mW of 532nm second harmonic with a monolithic magnesium-oxide-doped lithium niobate frequency-doubler. This corresponds to a conversion efficiency from 1064nm to 532nm of 72% and a conversion efficiency from the 2 W of 808.5nm diode pump light to the green of 25%.

The high-power Nd:YAG laser used in this work is similar to the laser described in Reference [3]. The output of an experimental high-brightness 2 W diode laser from Spectra Diode Labs was focussed onto an all-flat nonplanar ring Nd:YAG crystal using a spherical lens and cylinder lens pair. Approximately 70% of the diode laser output was collected and focussed onto the Nd:YAG crystal, producing 700 mW of single-frequency output at 1064nm. The output of the laser was an oval TEM_{00} spot with an aspect ratio of 1.2 to 1.

The frequency-doubler crystal geometry is shown schematically in Figure 1. The $MgO:LiNbO_3$ crystal was 6mm long by 4mm wide by 2mm thick. The front surface was curved with a radius of curvature of 16mm and coated to reflect 98.5% of 1064nm with s-polarization and transmit 97% of 532nm light of p-polarization. Two flat total-internal-

reflection (TIR) surfaces complete the ring resonator. The lithium niobate was obtained from Crystal Technology and had a nominal 5% magnesium-oxide concentration optimized to minimize sensitivity to photo-refractive damage. The doubler crystal used in this work was a factor of two smaller than the crystals used in earlier work [2]. The smaller geometry lead to lower intracavity losses and a factor of two broader phase-matching temperature range.

A schematic diagram of the frequency-locking and doubling arrangement is shown in Figure 2. The output of the Nd:YAG laser was focussed into the doubler with a 75mm focal length lens. Reflected 1064nm light and generated 532nm light were separated by a dichroic beam-splitter.

Frequency-locking of the laser to the doubler was accomplished using a modified Pound-Drever-Hall technique [4]. A 50 mV peak-to-peak 50 MHz dither signal was applied to the crystal. The phase shift introduced onto the reflected 1064nm light compared to the reference 50 MHz signal was detected by an RF mixer. The output of the mixer was filtered, amplified and fed to the laser to maintain frequency-locking.

Details of the system and results of lifetests of the device at 0.5 W power levels will be presented.

References

[1] W.J. Kozlovsky, C.D. Nabors and R.L. Byer, IEEE J. Quantum Electron.24, 913 (1988).
[2] D.C. Gerstenberger, G.E. Tye and R.W. Wallace, Opt. Lett. 16, 992 (1991).
[3] E.A.P. Cheng and T.J. Kane, Opt. Lett. 16, 478 (1991).
[4] R.W.P Drever, J.L. Hall, F.V. Kowalski, J. Hough, G.M. Ford, A.J. Munley and H. Ward, Appl. Phys. B 31, 97 (1983).
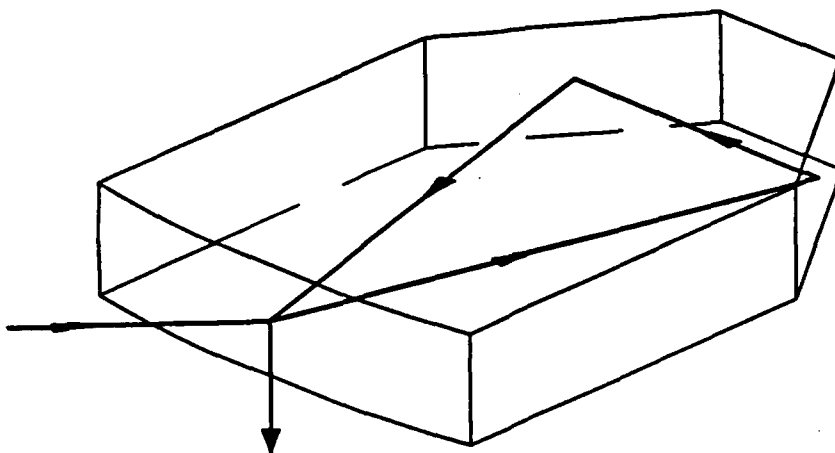
Figure 1: Monolithic Frequency-Doubler Crystal Geometry.
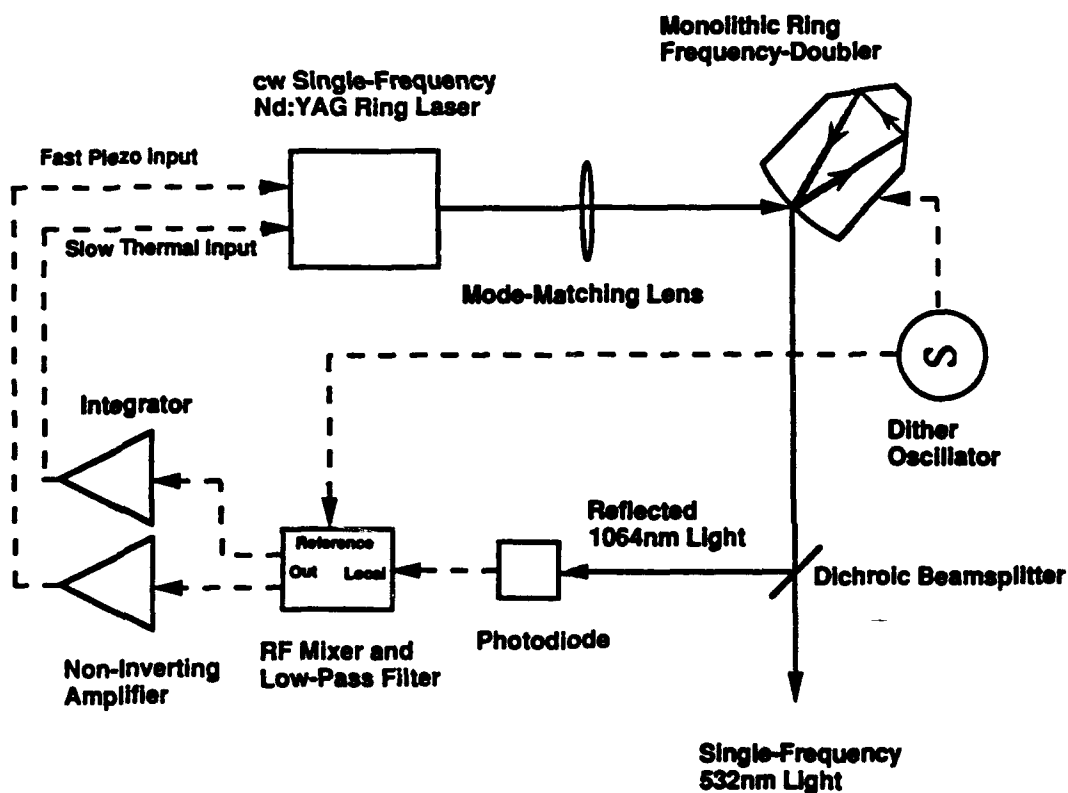
Figure 2: Schematic Diagram of Frequency-Locking Arrangement.

Harmonic Generation from 1.079 μm to 0.54 μm with 85% Efficiency

Z.Y. Ou, S.F. Pereira, E.S. Polzik, and H.J. Kimble

Norman Bridge Laboratory of Physics 12-33

California Institute of Technology

Pasadena, CA 91125

(818) 356-8342

For many years, potassium titanyl phosphate (KTP) has been a well known crystal for frequency doubling of Nd:YAG lasers (1.064 μm). The large nonlinear coefficient of KTP crystal together with the wide temperature width, large acceptance angle, and very low absorption loss make KTP a promising candidate for high conversion efficiency. One problem with the use of KTP is that phase matching at 1.064 μm is possible only by Type II angle tuning, so that walk-off of the ordinary and extraordinary beams inside the crystal limits its utility in situations involving high finesse resonators. Recently however, Garmash et al. [1] have reported that Type II 90° noncritical phase-matching is possible with an a-cut KTP at 1.079 μm, thus enhancing the possibilities for intracavity cw frequency doubling. Indeed by following this lead, we have achieved 85% nonlinear conversion efficiency for doubling of 1.079 μm radiation to 0.54 μm.

Our frequency doubling experiment consists of a 3x3x10 mm^3 a-cut flux-grown KTP inside a passive folded ring cavity, which is pumped by a frequency-stablized Nd:YAlO$_3$ laser operating at 1.079 μm. For our crystal, noncritical Type II 90° phase matching at 1.079 μm is achieved at 63°C with a temperature width of 30°C (note that this phase matching temperature is different from that reported in Ref. 2). The folded ring cavity consists of two curved mirrors of radii of curvature equal to 10 cm and two flat mirrors. A very small folding

angle for the cavity allows the extraordinary and ordinary beams to have the same reflectivity at the mirrors and the problem of astigmatism to be neglected. The KTP crystal is placed at the smaller waist between the two curved mirrors in the cavity, with the waist size being approximately 59 μm (which is about three times larger than the optimum waist for this crystal length). This geometry gives rise to a measured single pass nonlinear efficiency of 6.3×10^{-4} W^{-1}. One of the flat mirrors has a transmission of 97% and the other three are high reflectors at the fundamental frequency. The curved mirrors have transmission of 94% at the harmonic frequency. The total round trip loss of the cavity (excluding the input coupling mirror transmission) is 0.3% as inferred from measurements of the cavity finesse. Infrared light from a frequency-stabilized, TEM$_{00}$ mode Nd:YAlO3 laser was injected into the cavity with polarization of 45° relative to ordinary and extraordinary axes of KTP. Because of the difference in the indices of refraction, the two polarizations usually are not simultaneously resonant in the buildup cavity, and temperature tuning of the crystal is used for best circulating power of the two polarizations. Over a range of injected infrared power from 5 to 700 mW, the generated harmonic output has been recorded. For 700 mW input at 1.079 μm, 560 mW at 0.54 μm has been directly measured. After considering a correction for the curved cavity mirror transmission at 0.54 μm (94%), we thus infer an efficiency of 85% for the conversion of infrared to green light.

An absolute comparison between our experimental data and the theory based on Ref. 2 has been made and shows good agreement. This result is very promising for future experiments if we take into account that the beam waist inside the crystal has not been optimized and therefore the same efficiency should be achievable at lower input power. Once the cavity focusing and infrared input coupler are optimized, we expect that conversion efficiencies higher than 90% should be possible with the losses of the current arrangement.

References

[1] V. M.Garmash, G.A.Ermakov, N.I. Pavlova, and A.V. Tarasov, Sov. Tech. Phys. Lett., **12**, 505 (1986).

[2] E.S.Polzik and H.J.Kimble, Opt. Lett., **16**, 731 (1991).

Resonantly-pumped 459nm Sum-frequency Upconversion Laser.

P N Kean

Amoco Laser Company, 1251 Frontenac Rd, Naperville, Ill. 60540.

G J Dixon

CREOL, 12424 Research Parkway, Orlando, Fl. 32826.

Nonlinear frequency conversion of laser diodes and diode-pumped solid-state lasers provides potential sources of coherent laser radiation in the blue spectral region. Two efficient methods based on nonlinear frequency conversion are the direct doubling of laser diodes and intracavity doubling of the 946nm transition of Nd:YAG. Both of these methods however, require the use of Potassium Niobate. Although this crystal has a relatively large nonlinear coefficient, it is difficult to polish and depoles into multiple ferroelectric domains under slight stress or excessive temperature cycling. Reorientation of the domains lowers the effective crystal nonlinearity and produces domain walls which appear as 'cracks' within the bulk medium. These properties may well limit the application of $KNbO_3$ in commercial devices.

An alternative method for upconversion, that does not rely exclusively on $KNbO_3$, is intracavity sum-frequency mixing. Sum-frequency mixing of 1064nm and 809nm can be noncritically phase-matched at room temperature in KTP to give a wavelength of 459nm [1]. KTP has stable ferroelectric domains and is easily polished but unfortuantely, the output efficiencies of lasers using this approach have been much lower than those using $KNbO_3$ based methods. In order to improve the conversion efficiency of sum-frequency mixing, we have used the technique of resonant pumping [2]. In this case the pump power

within the laser resonator is significantly enhanced by making the cavity resonant at both the laser and pump wavelengths. The enhanced intracavity pump power greatly improves the efficiency the sum-frequency process. The experimental set-up is shown in figure 1. A thin plate of Nd:YAG forms one end of the near hemispherical cavity and is coated, on the input side, for high reflectivity at the laser wavelength and a small transmission at the pump wavelength. The 1cm radius mirror is HR for both wavelengths and all intracavity surfaces were AR coated. The Nd:YAG had a single pass absorption of 5% at the pump wavelength. With the pump beam mode-matched to the laser resonator, a large intracavity field is obtained which pumps the Nd:YAG laser and is also utilised in the sum-frequency process.

Our results with this system will be presented, where to date we have obtained 1.2mW at 459nm for an incident pump power of 50mW. The ouptut mirror had a measured transmission of 60% at 459nm and thus the actual unidirectional power generated was ≈2mW, representing a conversion efficiency of 4%. The pump build-up factor and conversion efficiency to the blue may be furthur improved by reducing the absorbtion of the gain medium. This will however, lead to a reduction in the intracavity 1064nm field and the output power at 459nm will to go through a maximum as the Nd:YAG absorption is reduced. Theoretical calculations (shown graphically in figure 2) indicate that the optimum absorption depends on the cavity parasitic losses but is in the region of 0.5% to 1% single pass. With an optimised design, a significant improvement in the output power at 459nm is expected.

References.

1. J C Baumert, FM Schellenberg, W Lenth, W P Risk, G C Bjorklund; *Appl. Phys. Lett.* **51**, 2192 (1987).

2. J P Cuthbertson, G J Dixon; *Opt. Lett.* **16**, 369 (1991).
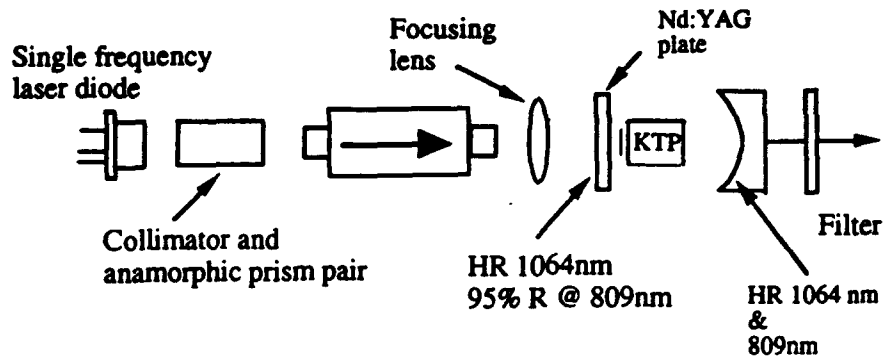
Figure 1. Schematic diagram of the experimental set-up for the resonantly pumped sum-frequency laser.
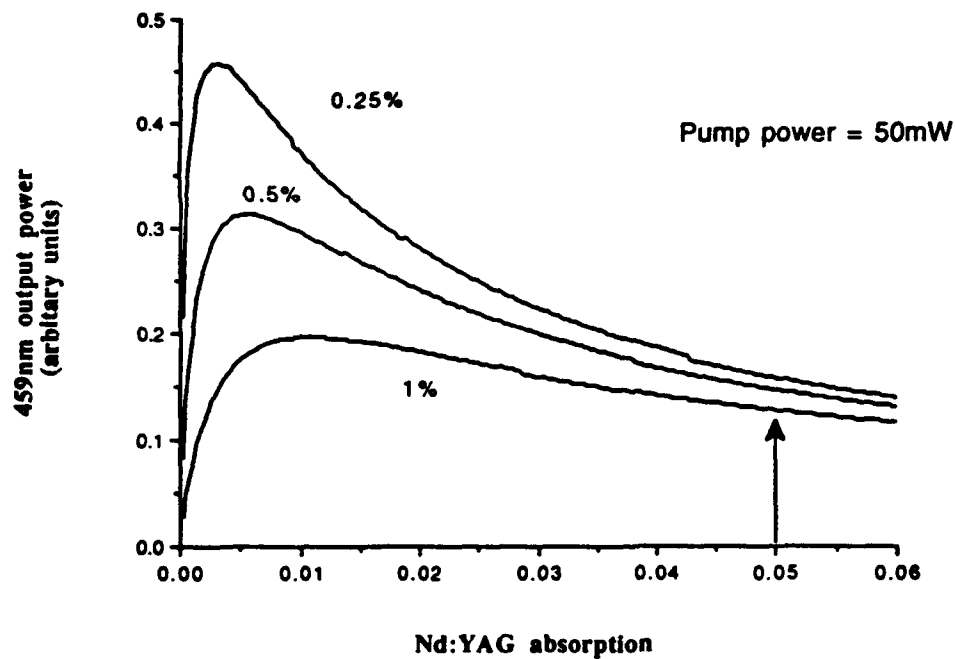
Figure 2. A theoretical plot of the relative output at 459nm as a function of the single pass Nd:YAG absorption for three values of the single pass parasitic loss. Our approximate operating point is indicated by the arrow.

Gas Lasers

FB   11:00am–12:00m
Anasazi South

J. Gary Eden, *Presider*
University of Illinois, Urbana-Champaign

AIR-COOLED NOBLE GAS ION LASERS
OPERATING PROPERTIES, CONSTRUCTION TECHNIQUES AND APPLICATIONS

S.M. JARRETT
SPECTRA-PHYSICS LASERS
1340 TERRA BELLA AVENUE
MOUNTAIN VIEW CA 94039
415/961-2550

In the early 1970's, a U.S. laser manufacture introduced a low power, air-cooled scientific argon ion laser. This laser was applied in the reprographics industry to color separators by manufacturers overseas within the next few years. Later, the same type laser was applied to high speed computer printers. By today's standards, these were primitive lasers. Their lifetime was not long, their power low and they required periodic maintenance. The lasers were fragile as well. Despite these drawbacks, these air-cooled lasers had some very desirable properties. As opposed to other ion lasers, they required no water cooling. Their power requirements were modest and the lasers and associated power supplies where small. They also operated in the blue-green with the superb optical properties and noise performance of low power gas lasers such as He-Ne.

The next major step occurred approximately ten years later when a Japanese manufacturer succeeded in building an air-cooled Ar ion laser with internal mirrors where the plasma tube itself formed the laser resonator structure. The Ar ion laser was reduced to almost the same level of simplicity, in an engineering sense, as the He-Ne laser. Of course, the basic discharge physics of these two different gas lasers remained: glow versus arc discharge, atomic versus ionic energy level inversion, red versus blue-green, etc. However, now, the air-cooled Ar ion laser was a true "hands off" laser. No longer was routine maintenance (cleaning) of laser intracavity space required, nor routine realignment. However, this technological advance, which included laser mirrors directly sealed to the plasma tube, did not come without a price. Namely, the intracavity Brewster or Littrow prisms which conveniently selected a particular laser line in the complex blue-green Ar ion spectrum could no longer be used.

At this juncture in the development of air-cooled Ar ion, two new technical advances were sought. First, a new way to select a single laser line from a complex spectrum of closely lying lines. Second, the fragile glass/ceramic technology built around a BeO laser bore had to be replaced by a more rugged construction. The later technical advance was obvious: glass/ceramic was replaced by metal/ceramic construction of plasma tube. However obvious this choice seemed, its implementation was difficult and expensive. The former technical advance was achieved with what is known as wavelength selective optics. Basically, these are very narrow band reflectors which discriminate between closely spaced groups of lines (488 nm vs 476 nm and 497 nm, as the most important example). These multilayer dielectric mirrors use pairs of coating materials which differ in refractive index by a small amount compared to the normal pairs used.

Following these two advances and with tube lifetimes in the thousands of hours and the development of reliable switching regulator power supplies, the applications for air-cooled Ar lasers blossomed, as did the number of manufacturers of the lasers themselves. Particularly interesting were the new bio-medical applications of DNA sequencing and clinical cell analysis, and applications in the semiconductor industry. At this period of time in the mid to late 1980's, the air-cooled Ar ion laser was limited to an input power of about 1 kW (a 90 V tube at 11 A). This meant in practice that a 5 to 50 mW 488 nm TEM_{00} polarized output could be obtained. A plasma tube of this size is shown below. This size tube was not powerful enough (with long tube lifetimes) at this input power level for some applications.

The next stage in the development explored higher input powers to larger tubes. Again, these are internal mirror tubes where the tube itself is the laser resonator structure. The input power to these tubes rose to 2.5 kW. These much larger tubes proved to be stable laser structures with good mode control. In addition, the wavelength selective optics continued to produce enough discrimination to yield single line operation (or in some cases two separated lines if desired, 458 nm and 515 nm as an example), TEM_{00}, with up to 150 mW of power. This power input level is a practical upper limit for the blowers used to air-cool these tubes. At these power levels, other possibilities are open for this type of laser. For example, they may be used with Kr in the red and also offer some ultraviolet capabilities. In addition, when operated in Ar, multimode, multiline, they are used in the entertainment industry for laser light shows.

Beyond the 2.5 kW level, pure air-cooling becomes difficult. Hybrid liquid to air cooling of tubes becomes a better choice. Recently, a large internal mirror, internal resonator tube based on BeO technology has been introduced. This tube is capable of more than 1 watt blue-green power.

In summary, the air-cooled Ar ion laser is a reliable, low cost, "hands off" laser. In its most modern form, the mirrors are internally sealed, wavelength selective and the tube body itself forms the resonator structure. Lifetimes are in the thousands of hours. Mode control and laser noise quality are excellent. Beyond the 2.5 kW level, the forced air-cooling technology looses its appeal and hybrid form of cooling becomes more attractive. Metal/ceramic technology has lead to high yield and low cost manufacturing. The use of BeO ceramic greatly simplifies this type of Ar ion laser.
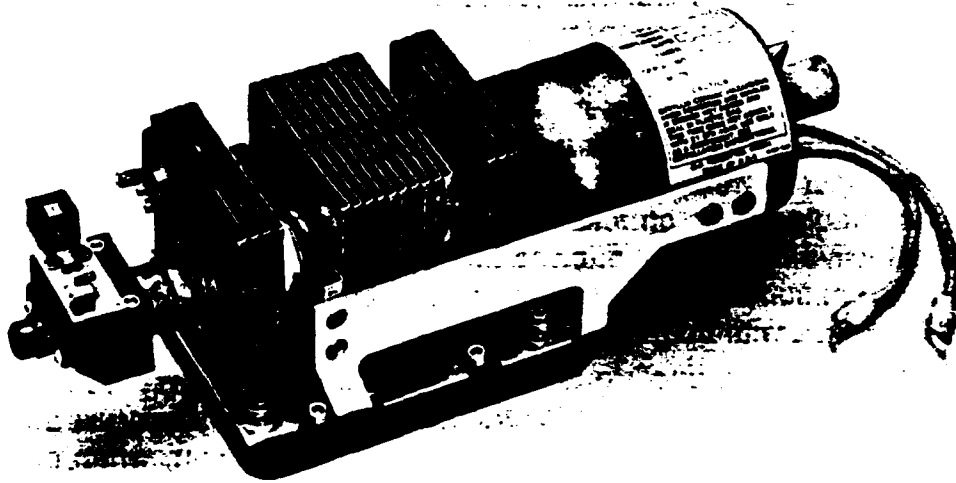
A compact blue-green Ar ion laser. All metal/ceramic construction with internal mirrors where the plasma tube itself is the laser resonator.

HeCd Lasers Present and Future
by
Mark W. Dowley

LiCONiX
3281 Scott Blvd. Santa Clara, CA 95054
(408) 496-0300

INTRODUCTION:
     The helium cadmium (HeCd) laser is a gas laser in which
the active species is ionized cadmium metal vapor in helium
buffer gas. It is similar in some respects to the HeNe
laser. Continuous wave emission occurs in the deep blue at
441.6nm and in the near uv at 325nm. Short wavelength output
of high spectral purity and excellent mode quality makes the
HeCd laser uniquely useful in many applications.

HISTORY OF COMMERCIAL DEVELOPMENT:
     CW lasing in cadmium metal vapor, which requires the
presence of helium gas, was first reported in 1966(1)
Commercial developments began in the early '70s. Commercial
models were first introduced by Spectra Physics and RCA.
Technical difficulties resulting in short lifetimes limited
the applications and market for early versions.
Current suppliers are LiCONiX, Omnichrome and Kimmon.

PRINCIPAL TECHNICAL PROBLEMS:
     1) Providing a uniform mix of cadmium metal vapor and
helium gas in a narrow capilliary bore.
     2) Control of metal vapor...preventing condensation on
critical optical surfaces.
     3) Helium gas clean up... various mechanisms.
     4) Discharge oscillations... giving rise to noise in
output.

     Solutions to these problems have been found with the
result that modern HeCd lasers are now extensively used in a
wide variety of applications.(2)

PERFORMANCE OF CURRENT LASERS....TYPICAL SPECIFICATIONS:

WAVELENGTH	441.6nm	325nm
SPECIFICATION		
Power in mw, TEMoo	7 to 100	1 to 20
Power in mw, multimode	20 to 100	5 to 40
Beam diameter, mm	1	1
Beam divergence, mrad	1	0.5
Pointing stability,μrads	25	25
Polarization	Plane or Random	
Optical noise %, pk-pk	3 tO 15, model dependent	
Lifetime, manufactures spec.	4,000 to 10,000 hours	
Lifetime, users experience	1,000 to 8,000 hours	
Power dissipation, watts	250 to 1,000 plus	
Price, unit quantity	$5,000 to $25,000	

APPLICATIONS:
The key to successful applications of the HeCd laser is to recognise that the short wavelength, continuous wave output of the device is uniquely useful for:
1) High resolution (diffraction limited spot size) inspection, imaging and microforming via photoresist
2) Efficient excitation of fluorescence in many organic, inorganic and biochemical materials.
3) Exposure under computer control of photopolymers, photoresist, photoconductors and other photosensitive materials.

Successful applications have been developed in:

1) High speed laser printing.........Xerox 9800   442nm
2) High resolution half-tone printing ....Purups   442nm
3) Accurate alignment in IC wafer stepper..Canon   442nm
4) Confocal scanning laser microscope... various   325nm
5) Pattern generators, IC fab masks.....Micronic   442nm
6) Solid modeling, stereolithography..3D Systems   325nm
7) CD mastering systems.........Philips and Sony   442nm
8) High density PCB inspection.........Optrotech   442nm

These are just a few of the many applications which have been developed and are being developed for HeCd lasers.

CURRENT AREAS OF DEVELOPMENT:
The vast majority of HeCd lasers sold over the past five years or so have been for OEM (system) application. The OEM customer demands reliability above all else. Reliability means many things but includes predictable long lifetime, performance within specifications, on-time delivery, fast response to orders and short service turn around time.

HeCd lasers in general have shorter and less predictable lifetimes than HeNe or low power air colled ion lasers. Customer experience ranges from a low of 1,000 hours to about 8,000 hours. OEMs would prefer a 5,000 to 6,000 hour mean life with a small standard deviation.
Manufacturers are making improvements in average lifetimes by focusing on process control and materials quality. Important considerations are:
1) Cleanliness of containers and purity of materials.
2) High temperature vacuum processing to minimize hydrocarbons and water vapor.
3) Elimination of early bird failures, due to process control problems.

Another area of current development is the achievement of higher power, particularly in the uv at 325nm. Greater than 100mw would be valuable for solid modeling. The goal is to achieve such power in a compact package with low power dissipation.

FUTURE POSSIBILITIES:
Market needs will dictate the future of HeCd laser development. For example longer lifetime with high reliability but without sacrifice of normally excellent beam quality will be available. The potential availability of isotopically pure cadmium at reasonable prices will result in greater power and efficiency. Higher power uv output may certainly be expected.

FUTURE APPLICATIONS:
The HeCd laser will continue to push lower the inspection and resolution limits of applications initially developed for HeNe and blue-green air cooled ion lasers. New applications which fully utilize the unique short wavelength of the 325 and 442nm emission lines will develop in industrial and medical diagnostics.

COMPETITION FROM SOLID STATE BLUE AND UV LASERS:
This conference will provide an update on the state-of-the-art of solid state blue-green lasers. Progress has been reported in the past few months on lasing at about 500nm in ZnCdSe diode lasers.(3) Also direct doubling of infrared diode lasers into the blue has been reported from several labs. These developments suggest the possibility of high efficiency, small size, extended life, solid state blue lasers. Consequently they pose a definite threat to traditional blue green gas lasers. Specifications such as power stability, beam quality and pointing stability have yet to be reported in detail for these new laser types. When operating specifications have been confirmed, reproducibility, availability and price will be the issues of interest to the OEM user.
If the history of the HeNe gas laser, when confronted with a competitive threat from the solid state infrared and red diode laser, may be used as a guide it can be assumed that a competitive solid state substitute for the HeCd laser is still some years in the future. By extension the uv laser will likely have a vigorous maturity and a graceful old age.

1) W.T.Silfvast et al. Appl. Phys.Lett. 8 318, 1966
2) M.W.Dowley, SPIE Vol. 741 p31, 1987
3) M.A.Hasse et al. Appl. Phys. Lett. 59, 1272, 1991

Frequency Conversion in Guided-Wave Devices

FC 1:30pm–3:30pm
Anasazi South

Martin M. Fejer, *Presider*
Stanford University

Second Harmonic Generation in Quasi-Phase-Matching Waveguides

Gunnar Arvidsson

Institute of Optical Research
S-100 44 Stockholm, Sweden

Use of integrated optical waveguides is advantageous for frequency conversion of light from low-power lasers. The light can be confined to a very small cross section area for a comparatively long distance so that high conversion efficiencies can be obtained with pump sources such as laser diodes and laser diode pumped solid state lasers.

Phase matching

A crucial issue for frequency conversion is phase-matching between the interacting waves. Birefringence is most commonly utilized, combined with temperature adjustments for fine tuning. For frequency doubling (second harmonic generation), it may thus be possible to obtain the same effective indices in the waveguide at the fundamental and second harmonic wavelengths, by using modes of different polarizations at the two wavelengths. The birefringence of the nonlinear crystal is thereby utilized to compensate for the material dispersion. The same phase-velocities is achieved at both wavelengths and efficient coupling of energy from the fundamental to the second harmonic can be obtained. A severe limitation is, however, that the phase-matching condition can only be fulfilled for a very restricted wavelength range determined by the magnitude of the birefringence of the crystal used. Generation of blue light by frequency doubling a laser diode is furthermore not possible because the birefringence in established waveguide materials is too small.

A more versatile method is to use a periodic structure for phase-matching, with the period choosen so that the phase-mismatch is compensated for (Quasi-phase-matching, QPM) [1,2]. See Fig 1.

Second harmonic intensity (arbitrary units)

Fig. 1 If the interaction is not phase-matched (curve A), the second harmonic is constructively built up only for a short distance (typically a few microns) and the energy is then coupled back again to the fundamental wave, etc. Curve B corresponds to a quasi-phase-matching technique, where the sign of the non-linear coefficient is periodically alternated along the path of the waves. At every point where the accumulated phase-difference between the waves has increased by 180°, the sign of the effective nonlinear coefficient is changed - corresponding to a phase-shift of 180°. Thereby the coupling of energy back to the fundamental can be avoided.
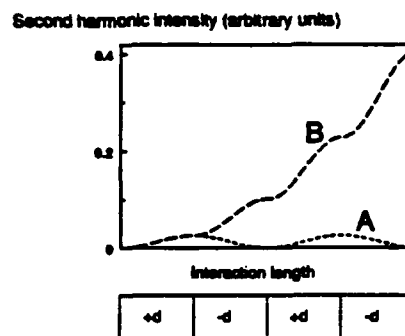
It turns out, however, that for an efficient interaction a periodic modulation of the optical nonlinearity is required. Such a modulation can be obtained by periodically alternating the crystal orientation, so that the effective nonlinearity alternates between two values $+ d_{eff}$ and $- d_{eff}$. The technique was early demonstrated by using a stack of differently oriented GaAs plates for freqency doubling of 10.6 μm radiation [3]. This implementation is however not very practical and has very seldom been used.

Quasi-phase-matching waveguides

Ferroelectric crystals as lithium niobate ($LiNbO_3$), lithium tantalate ($LiTaO_3$) and potassium titanyl phosphate ($KTiOPO_4$ or KTP), often used for frequency conversion, are normally used as single domain crystals, but may exist as multidomain crystals. Each ferroelectric domain may have two alternative orientations, corresponding to different sign of the effective nonlinearity. This offers a possibility to realize a waveguiding monolithic structure with period-ically alternating sign of the nonlinearity, as schematically shown in Fig 2.

A few years ago, fabrication of periodically domain-inverted waveguides was demonstrated by using two slightly different approaches [4,5]. In both cases photolithography, diffusion and heat treatment were applied to originally single-domain $LiNbO_3$ substrates. A periodic perturbation in the surface layer of the crystal (giving rise to a periodically varying Curie-temperature), com-bined with a heat treatment up to a temperature closely below the nominal Curie temperature, caused a domain inversion with periodically varying depth. Since then a number of different fabrication procedures have been reported, see Table 1. The underlying physics for the domain inversion processes has not been studied in any detail. A better understanding is expected to improve the fabri-cation techniques.

Fig 2. The ideal structure for a QPM waveguide. The waveguide passes through succesive regions in the crys-tal with alternating ferroelectric domain orientation.

The periodicity needed for generation of blue light is typically 3 - 4 μm, both in $LiNbO_3$, $LiTaO_3$, and KTP. Sometimes structures with longer periods, but used in 2nd or 3rd order, are utilized, since this facilitates the photolithographic procedure, even though it means a lower conversion efficiency.
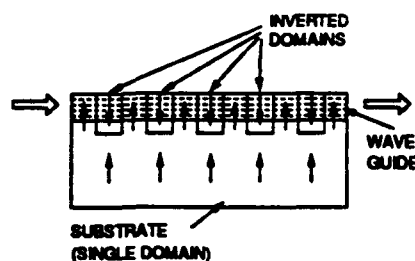
LiNbO₃	PERIODIC TITANIUM-PATTERN, HT [†]	[5,6,7,8,9]
	PERIODIC SiO₂-PATTERN, HT	[4,10]
	PERIODIC METAL ELECTRODE, PYROELECTRICALLY INDUCED E-FIELD	[11]
	PERIODIC MASK, E-FIELD, E-BEAM BOMBARDMENT, ELEVATED TEMP (580 C)	[12]
	E-BEAM WRITING AT ROOM TEMPERATURE	[13,14]
LiTaO₃	PERIODIC METAL ELECTRODE, EXTERNAL E-FIELD, HT	[15]
	PERIODIC PROTON EXCHANGE + HT	[16,17]
	LASER WRITING	[18]
KTiOPO₄	PERIODIC ION-EXCHANGE (Ba + Sr)	[19]
POLYMERS	PERIODIC POLING	[20]

[†] HT = HEAT TREATMENT

TABLE 1. Different methods for fabrication of QPM waveguides

QPM waveguides, fabricated utilizing photolithographic techniques, have the following advantages:

* Phase-matching can be obtained for *arbitrary wavelengths* by fabricating waveguide structures with the appropriate periodicity. The technique can be used for *frequency doubling, sum frequency generation, difference frequency generation* etc. The main limitation is the transparency range of the crystal.
* Potentially very *efficient* interactions can be obtained. For LiNbO₃ and many other crystals the largest nonlinear coefficient can be used, which is not accessible when using birefringence phase-matching.
* potentially cheap fabrication, mass-fabrication possible.
* waveguides with different periodicities on the same substrate.
* waveguides with chirped gratings [21] etc. to modifiy e.g. the acceptance bandwidth.

Conversion efficiency

In the ideal case the conversion efficiency η for frequency doubling increases linearly with the input power and with the square of the waveguide length, and is therefore sometimes normalized according to

$$\eta = P_{SH}/P_{FUND} = \eta_{NORM} \cdot L^2 \cdot P_{FUND}$$

and given in units of $\% W^{-1} cm^{-2}$. This value facilitates comparison between different experimental results, but the normalization must be handled with great care. Deviation from the scaling occurs due to e.g. photorefractive index changes at high power levels, difficulties to fabricate long homogeneous guides, waveguide losses etc. As can be seen in table 2, it has been demonstrated that milliwatts of blue light can be generated from IR power levels of the order of hundred milliwatt in several waveguide materials.

Substrate	P_{FUND}	P_{SH}	L	η	η_{NORM}		Order of	Refs
			cm		%	$W^{-1}cm^{-2}$	QPM	
LiNbO₃	15 mW	1 μW	0.1	6.4•10⁻⁵	37		3rd	[5]
	67 mW	0.56 mW	1.0	0.84%	11		1st	[9]
KTP	~50 mW	~0.5 mW	0.5	~1 %	80		1st	[19]
		~4 mW	0.5		100-400		1st	[22,23]
LiTaO₃	210 mW	12 mW	0.9	5.7 %	33		3rd	[16]
	145 mW	15 mW	0.9	10 %	86		1st	[24]

TABLE 2: Some examples of experimental results on generation of blue light in QPM waveguides.

Some issues of importance for high conversion efficiency and viable devices

The waveguides should be designed so that a high mode confinement and a good overlap betweeen the fundamental and the second harmonic mode is obtained.

When surface related processing technologies are used to realize the periodic domain inversion, the geometry of the structure that results (Fig 3) is material dependent and deviates from the optimal case of Fig 2. In KTP waveguide segments with inverted domain orientation is fabricated in one processing step [19]. In LiNbO₃ and LiTaO₃ the waveguide is normally fabricated separately after the domain inversion. The shape and depth for the domain-inverted regions has to be taken into account when evaluating the overlap integral for the interaction, and influences strongly the conversion efficiency [25,26]. For LiNbO₃ and LiTaO₃ some design guidelines have been derived. Various investigations have been carried out in order to find appropriate processing conditions to realize optimal performance.

For the choice of waveguide fabrication technique and processing parameters also factors as the following have to be taken into account: high index increase giving better mode confinement, photorefractive sensitivity, waveguide losses, risk of decreased nonlinearity in the crystal; and various compromises are necessary.

The phase-matching condition must be fulfilled along the whole length of the waveguide. Irregularities in the periodicity of the structure can therefore decrease the conversion efficiency. The influence of unintended irregularities when using photolithographic techniques to define the pattern, is, however, regarded to be negligible [27]. Variations in waveguide width and depth are more difficult to handle, but it is possible to minimize the influence of these inhomogeneities by appropriately choosing the waveguide parameters for noncritical phase-matching [6,28]. For annealed proton-exchanged waveguides in LiNbO$_3$ and LiTaO$_3$, detailed analysis on the changes in the refractive index profile during processing [29] is important in order to be able to fully apply this technique.

Although frequency doubling of laser diode radiation in a QPM waveguide, was demonstrated early [4], most work on optimization of the QPM waveguides have been using tunable dye- and Ti-sapphire lasers. Stable operation of a laser diode is more difficult due to feed-back from the waveguide. Optical isolators should be avoided in a compact device. Recent results on locking the laser diode to a Bragg-reflection from the waveguide [8,30], seem to be a solution to this problem.

Conclusions

The QPM technique is the most versatile and promising phase-matching technique for frequency conversion in waveguides. Although processing techniques can be improved and new fabrication techniques are under investigation, devices have already been fabricated with promising/high conversion efficiencies, in particular in LiTaO$_3$ and KTP. Initial results on on locking the laser diode to a Bragg-reflection from the waveguide, indicates one possibility to realize both compact, stable and efficient blue light sources based on this technology.
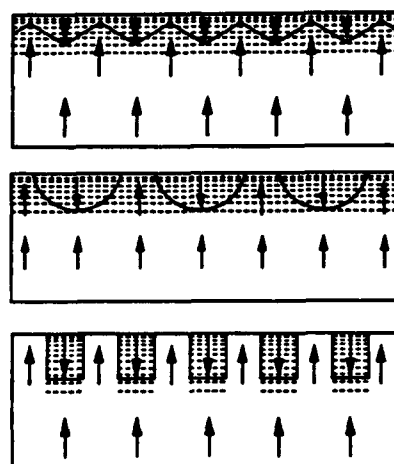
Fig. 3 Schematical illustration of actual QPM-waveguide-structures in (from top to bottom): LiNbO$_3$, LiTaO$_3$, and KTiOPO$_4$. Compare with the ideal structure of Fig 2.

References

1. A. Armstrong, N. Bloembergen, J. Ducuing, and P.S. Pershan, Phys. Rev. **127**, 1918-1939 (1962)
2. S. Somekh and A Yariv, Opt. Commun. **6**, 301-304 (1972)
3. D. E. Thompson, J.D. McMullen, and D.B. Anderson, Appl. Phys. Lett. **29**, 113-115 (1976)
4. J. Webjörn, F. Laurell and G. Arvidsson, IEEE Photonics Technol Lett **1**, 316-318 (1989)
5. E. J. Lim, M. M. Fejer, R. L. Byer and W. J. Kozlovsky, Electron. Lett. **25**, 731-732 (1989).
6. X. Cao, J Natour, R V Ramaswamy and R Srivastava, Appl Phys Lett **58**, 2331-2333 (1991)
7. Y Ishigame, T Suhara and H Nishihara, Opt. Lett. **16**, 375-377 (1991)
8. K Shinozaki, T Fukunaga, K Watanabe, and T. Kamijoh, Appl Phys Lett **59**, 510-512 (1991).
9. F Armani et al, "First order quasi phase matched second harmonic generation in LiNbO$_3$," ECOC 91, Postdeadline paper
10. M Fujimura, T. Suhara and H. Nishihara, Electron. Lett. **27**, 1207-1209 (1991).
11. H Seibert and W Sohler, Proc SPIE **1362**, 370-376 (1990).
12. R. W. Keys et al, Electron. Lett. **26**, 188-190 (1990)
13. M Yamada, K Kishima, Electron. Lett. **27**, 828-829 (1991)
14. H. Ito, C. Takyu, H. Inaba, Electron. Lett. **27**, 1221-1222 (1991)
15. S. Matsumoto, E. J. Lim, M. M. Fejer and H. M. Hertz, in *Integrated Photonics Research*, 1991 Technical Digest Series vol 8, (OSA, Washington, DC, 1991), p. 97.
16. K Yamamoto, K Mizuuchi, and T Taniuchi, *CLEO '91*, 1991 Technical Digest Series vol 10 (OSA 1991), postdeadline paper CPDP23, p. 616-617
17. H. Åhlfeldt, J. Webjörn, and G. Arvidsson, IEEE Photonics Technol. Lett. **3**, 638-639 (1991)
18. R A Rubino, D E Bossi, and J D Farina, "A novel thermal poling technique for fabricating QPM SHG structures in x-cut lithium tantalate", *OSA Topical Meeting on Compact Blue-Green Lasers*, Santa Fe, NM, Feb 1992
19. C. J. van der Poel, J. D. Bierlein, J. B. Brown and S. Colak, *Appl. Phys. Lett.*, vol. 57, pp. 2074-2076, 1990.
20. R. A. Norwood, and G. Khanarian, Electron. Lett. **26**, 2105-2106 (1990).
21. T. Suhara and H. Nishihara, IEEE J. Quantum Electron. QE-26, 1265-1276 (1990)
22. J. D. Bierlein, in *Integrated Photonics Research*, 1991 Technical Digest Series vol 8 (OSA 1991), p. 95
23. J. D. Bierlein, "Nonlinear optical properties of segmented KTP waveguides", *OSA Annual Meeting*, San Jose, Ca, USA, Nov 3-8, 1991 [Invited paper THK6]
24. K. Mizuuchi and K. Yamamoto, "Highly efficient quasi-phasematched second harmonic generation using a first-order periodically domain-inverted LiTaO$_3$ waveguide", *submitted to Appl. Phys. Lett.*
25. G. Arvidsson and B. Jaskorzynska, in *Materials for Non-linear and Electro-optics*, July 4-7, 1989, Cambridge, UK; Inst. Phys. Conf. Ser. No 103 (Inst. of Physics Publishing Ltd, Bristol, 1989) pp. 47-52
26. H. Åhlfeldt, G. Arvidsson, and B. Jaskorzynska, in *Nonlinear Guided Wave Phenomena*, 1991 Technical Digest Series vol 15 (OSA 1991), pp. 230-233
27. S. Helmfrid and G. Arvidsson, J. Opt. Soc. Amer. B **8**, 797-804 (1991)
28. E. J. Lim, S. Matsumoto, and M.M. Fejer, Appl. Phys. Lett. **57**, 2294-2296 (1990).
29. M.L. Bortz and M.M. Fejer, Optics Letters **16**, 1844-1846 (1991)
30. M. G. Roelofs, F. Laurell, and J. D. Bierlein, "Second harmonic generation from diode lasers in KTP waveguides," *OSA Topical Meeting on Compact Blue-Green Lasers*, Santa Fe, NM, Feb 1992

Second Harmonic Generation and Sum Frequency Generation in Optical Systems

John D. Bierlein
Du Pont
Experimental Station
Central Research & Development
PO Box 80356
Wilmington, Delaware 19880-0356

Optical waveguides offer potentially significant advantages to bulk
:tals for efficient second harmonic generation from relatively low power
rces because the fundamental optical beam can be tightly confined over
i interaction lengths. However, since channel waveguides must be used to
'eve this confinement, phase matching becomes a severe problem.
ause the channel orientation is predefined, birefringence angle tuning,
:h is commonly used with bulk crystals, cannot be used and temperature
ig, when it can be used, usually requires precise temperature control. Also,
ɔ the effective propagation constants depend on guide geometry, the
ɪguide dimensions must be tightly controlled over the entire optical path
h. Although guided second harmonic generation has been observed in
rm channel waveguides using both $LiNbO_3$ and $KTiOPO_4$ normalized
ɪrsion efficiencies have not exceeded about 5%/W-cm^2 and considerable
le-to-sample variation in efficiency and/or phase matching temperature is
ion.

Several techniques have been demonstrated that can improve overall
ncy and ease the phase matching problem. These include coupling
en a guided fundamental mode and a radiation second harmonic mode
ikov radiation), various quasi phase matching (QPM) schemes using both
uous and segmented channel waveguides, a new balanced phase
ng (BPM) process using segmented waveguides and external cavity
ɹide resonators. In addition to improved efficiency, the guide structure in
e QPM and BPM schemes can also be designed to significantly improve
ɹide fabrication tolerances.

rhe Cerenkov radiation scheme eases the phase matching problem but
ɔupling is difficult and special output beam shaping is required. High
:ion efficiencies have been demonstrated in $LiNbO_3$, $LiTaO_3$ and KTP
PM and in KTP using BPM. For QPM structures, normalized conversion
ɹes are in the 50% / W-cm^2 range for $LiNbO_3$, 100% /W-cm^2 for $LiTaO_3$
00%/W-cm^2 for KTP. Waveguide fabrication processes have been
ɹ to permit phase matched interaction lengths in excess of 5 mm which
ɪble output powers of greater than 1 mW. For KTP, the QPM guides
ɪduced outputs in excess of 4 mW average power in the 39C nm to 480
tral region from a 100 mW cw source without any evidence of optical

ɪs paper will generally review the various structures and will then give
ɪsults using KTP. Finally, some of the practical limitations of coupling
) waveguides and of stabilizing the diode against feedback will be
1.

Blue Second-harmonic Generation with Low Cerenkov Angles from
Ta_2O_5/$KTiOPO_4$ Waveguides

Hitoshi Tamada, Chiharu Isobe, Takaaki Murakami, and Masaki Saitoh
Sony Corporation Research Center
174 Fujitsuka-cho, Hodogaya-ku, Yokohama 240 Japan   (Tel:045-334-6868)

Summary

Efficient blue second-harmonic generation (SHG) with Cerenkov angles of
less than 1° has been observed for a Ta_2O_5/$KTiOPO_4$ channel waveguide [1].
In order to realize low (<1°) Cerenkov angles as well as a high SHG
efficiency, it is important to adjust waveguide parameters so that the
overlapping between a nonlinear polarization wave and a SH wave in the
$KTiOPO_4$ substrate becomes quite large as shown in Fig.1.

The conditions that the SHG efficiency of more than 1% is obtained for
Cerenkov angles of less than 1° with a fundamental power of 100mW and an
interaction length of 6mm are examined by calculations [2]. The calculated
relations among a fundamental wavelength, a Ta_2O_5 film thickness, a
channel width and a clad index are schematically shown in Fig.2. The
shaded area is a region covered by a particular Ta_2O_5 film thickness, and
the solid line traces the maximum of the SHG efficiency. The first most
important point is that there exist optimum values of a Ta_2O_5 thickness, a
channel width and a clad index for a given wavelength. This is because
field distributions like Fig.1 are functions of those waveguide
parameters. The second is that fundamental wavelengths ranged from about
860 to 818nm are satisfied by changing a clad index from 1 to 1.57 but no
more for other fundamental wavelengths. This feature is intrinsically
determined by refractive indexes and dispersions of Ta_2O_5 and $KTiOPO_4$. The
third is that the fundamental wavelength can be tuned over 6nm by changing
a channel width for a given Ta_2O_5 thickness, though the acceptance of a
fundamental wavelength for a particular channel width is less than about
3nm. The tunability of a fundamental wavelength by a clad index and a
channel width could be useful for device fabrications.

The effects of a clad index and a channel width were investigated
experimentally. The wavelength at which the maximum in the efficiency of
the SHG with low Cerenkov angles was obtained is summarized in Table 1.

The dependence of the fundamental wavelength on a clad index and a channel width is qualitatively quite consistent with calculated results as shown in Fig.2. This result also makes sure that a clad index and a channel width can be used to effectively tune a fundamental wavelength to a desired value after the deposition of a Ta_2O_5 film.

The SHG efficiency experimentally obtained for low Cerenkov angles is around 1mW with an interaction length of 5mm for an input Ti:sappire laser power of 50-100mW (guiding power). The wavelengths are ranged from about 430 to 410nm. The acceptance of a fundamental wavelength is 1-2nm. The theoretical limit of the SHG efficiency is not clear yet, so the device optimization is now proceeded to ensure the SHG efficiency limit.

References

1) H.Tamada, C.Isobe, and M.Saitoh, in Integrated Photonics Research 1991, Technical Digest Series, (Optical Society of America, Washington,DC 1991), pp.95-96.

2) H.Tamada, IEEE J.Quantum.Electron. QE-26, 1821 (1990).
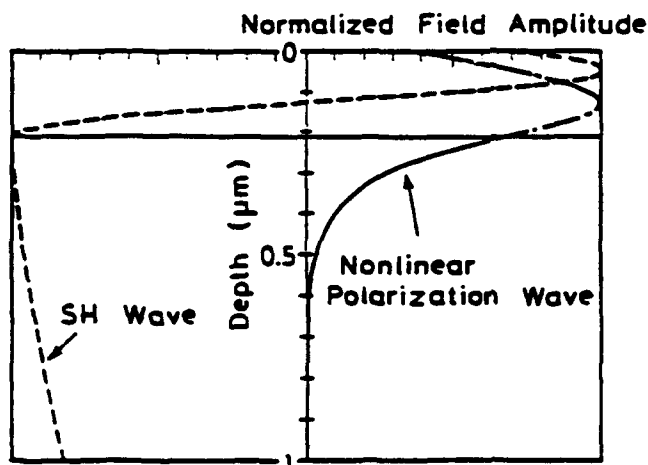
Fig.1. Typical example of normalized field distributions of a nonlinear polarization wave and a second-harmonic wave for Cerenkov angles of less than 1°.
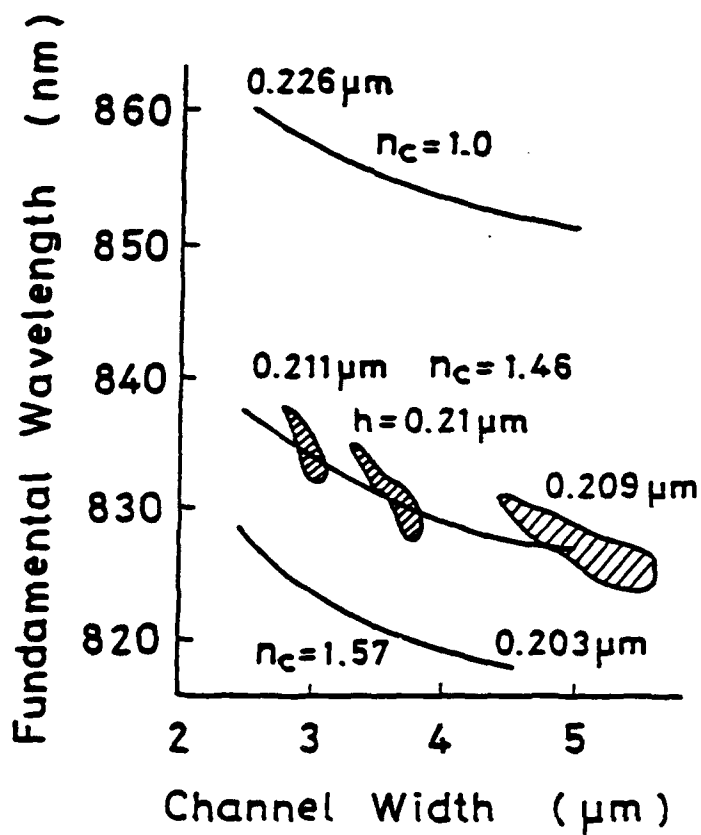
Fig.2. Relations among a fundamental wavelength,
a Ta_2O_5 film thickness, a channel width, and a clad
index calculated for the condition that the SHG
efficiency of more than 1% is obtained for Cerenkov
angles of less than 1° with a fundamental power of
100mW and an interaction length of 6mm.

Table 1. Experimental results.

n_c	h (μm)	λ_f (nm) / w (μm)			
1.00	0.2380			864.0 / 4	
1.46	0.2109	833.6 / 3		831.2 / 4	
1.57	0.2048	827.7 / 3	824.2 / 3.5	822.7 / 4	822.9 / 4.5

n_c:clad index, h:Ta2O5 thickness, λ_f:fundamental wavelength
W:channel width

Efficient Direct Diode Laser Frequency Doubling
in Quasi-Phase Matched LiNbO$_3$ Waveguide

Xiaofan Cao, Ramu V. Ramaswamy, and Ramakant Srivastava

Photonics Research Laboratory

Department of Electrical Engineering

University of Florida

Gainesville, Fl 32611

We report efficient (22%/W) blue light generation by direct diode laser frequency doubling in second order quasi-phase matched LiNbO$_3$ channel waveguides.

Guided wave second harmonic generation (SHG) by quasi-phase matching (QPM) is an attractive method to obtain highly efficient frequency conversion of the infrared semiconductor laser output into blue light, mainly due to the fact that QPM at an arbitrary wavelength may be achieved by appropriate periodic modulation of the nonlinear polarization. Using this method, efficient blue light generation was recently obtained in annealed proton exchanged $LiNbO_3$[1,2] and $LiTaO_3$[3] waveguides. However, in most of the SHG experiments reported, narrow linewidth tunable solid state and dye lasers were used instead of diode lasers. While several milliwatts of blue light has been generated with efficiency of 24%/W with a Ti:Sapphire laser source,[3] extension of these nonlinear waveguides to efficient doubling of diode laser remains a difficult task.

In this paper, we report efficient direct diode frequency doubling using a second order QPM $LiNbO_3$ waveguide. We also address the issue of high power diode laser output spectrum and its effect on the SHG conversion efficiency. By comparing the QPM waveguide SHG performance of single-and multi-mode (longitudinal) diode laser and single mode Ti-Sapphire laser, we show experimentally that the SHG conversion efficiency strongly depends on the pump laser mode structure.

The periodically domain-inverted structure was fabricated by diffusing titanium stripes on $LiNbO_3$ substrate at 1050 °C with a period of 6.6 µm. The channel waveguides were fabricated by annealed proton exchange (APE) technique described elsewhere.[4] SHG experiment was performed using a SDL-5422 high power diode laser and a Ti-Sapphire laser. The diode laser output (with a far field angle of $10°/40°$) was first collected and collimated with a 20X microscopic objective (N.A. =0.5), then its TE polarization was rotated to TM by a half wave plate, and finally another identical lens was used to focus the beam into the $LiNbO_3$ channel waveguide. Using such a coupling setup the laser output power can be coupled into the waveguide with 28% throughput efficiency. This coupling efficiency represents a factor of 1.5 improvement over the case of Ti-Sapphire laser experiment. This is a result of better matching between the laser output mode and the channel waveguide mode. With the Ti-Sapphire laser, the QPM waveguide was found to be phase matched at 850.2 nm with a phase matching bandwidth of 0.11 nm (indicating an effective phase matching length of 6 mm). The diode laser output wavelength can be temperature tuned from 842 nm to 855 nm. To study the spectral mode structure dependence of the SHG conversion efficiency, we monitor the spectrum of the IR diode output as a function of output power. It was observed that for laser power below 112 mW, single longitudinal mode operation is obtained. When the laser power exceed 112 mW, two –

four longitudinal modes with mode spacing of about 0.27 nm are observed (Fig. 1). Fig.2 shows the second harmonic power as a function of the transmitted diode power. The results for Ti:Sapphire laser case are also presented for comparison. The SHG conversion efficiency of 22%/W was observed for diode laser power range of 10 ~ 130 mW when one or two axial modes are present. This conversion efficiency is comparable with that obtained with the Ti-Sapphire laser. However, when the diode output power exceeds 130 mW (3–4 modes), the SHG conversion efficiency is reduced to 12%/W. These results can be explained by considering two competing processes: sum frequency enhancement and the phase mismatching degradation due to multimode operation at higher diode powers.

In conclusion, we have demonstrated the generation of 0.3 mW blue SHG radiation from a diode laser with conversion efficiency of 22%/W using second order QPM in $aLiNbO_3$ waveguide. We show that a double mode pump source with mode spacing up to 3 times the phase matching bandwidth is as efficient as a single mode source. However, a 3 dB degradation occurs when additional modes begins to oscillate at higher powers.

References

[1]   E. J. Lim, M. M. Fejer, R. L. Byer, and W. J. Kozlovsky, Electron. Lett. **25**, 731 (1989).

[2]   J. Webjörn, F. Laurell, and G. Arvidsson, IEEE Photon. Technol. Lett. **1**, 316 (1989).

[3]   K. Yamamoto, K. Mizuuchi, and T. Taniuchi, Opt. Lett. **16**, 1156 (1991).

[4]   X. F. Cao, J. Natour, R. V. Ramaswamy, and R. Srivastava, Appl. Phys. Lett. **58**, 2331 (1991).

Figure Caption

Fig. 1   Output power dependence of the diode laser spectrum.

Fig.2   Second harmonic power as a function of the transmitted fundamental power for the case of diode laser (o) and Ti:Sapphire laser (Δ).

Fig. 1
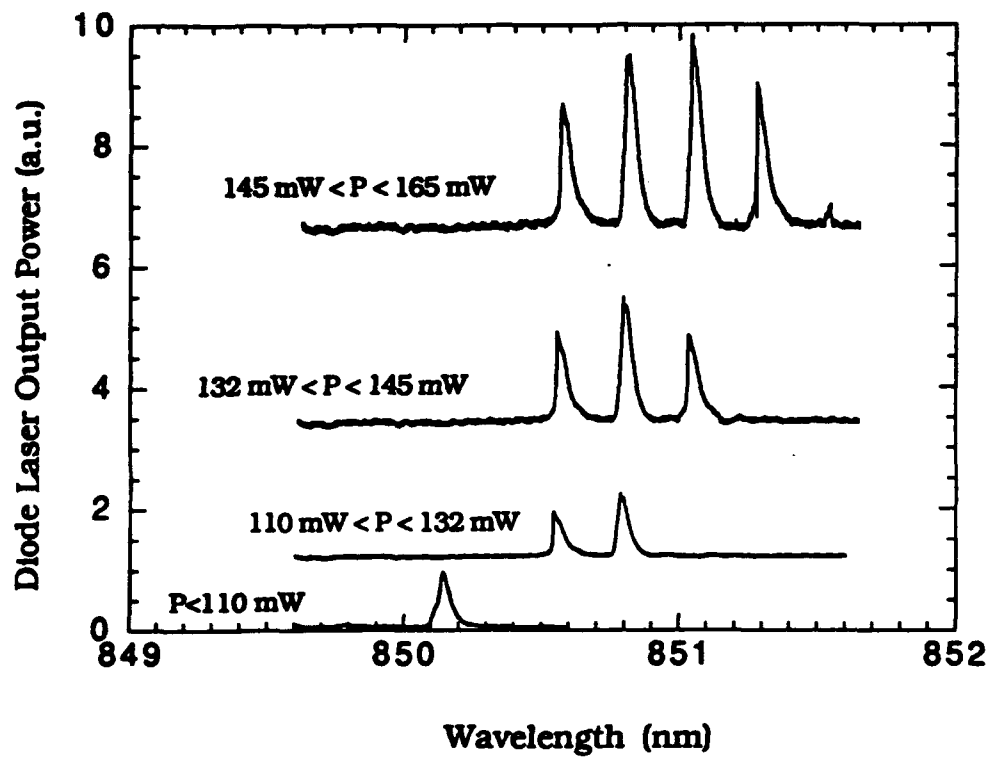
Fig. 2
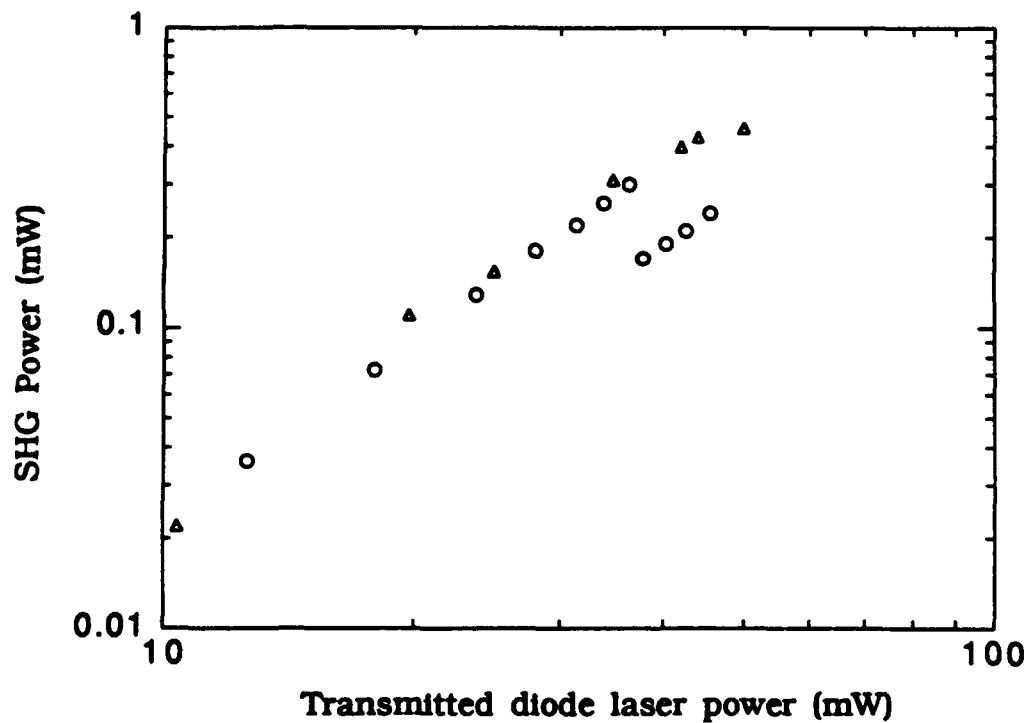
Second harmonic generation from diode lasers in KTP waveguides[1]

M. G. Roelofs[*], F. Laurell[†], J. D. Bierlein[*]

[*]E. I. du Pont de Nemours & Co., Central Research & Development,
  P. O. Box 80328, Wilmington, DE 19880-0328 USA

[†]Institute of Optical Research, S-100 44 Stockholm, Sweden

Segmented optical waveguides in $KTiOPO_4$ were coupled to single mode diode lasers for blue light generation using QPM. The KTP waveguide consists of an ~4 μ periodic domain-inverted array of Rb/Ba diffused and non-diffused areas. This grating produces a narrow Bragg peak in reflected light at a specific wavelength. The reflected light was used to lock the diode laser, forcing it to remain narrow-band even in the presence of reflected light from the end faces of the waveguide. Temperature tuning of the KTP brought the SHG peak into coincidence with the Bragg-locked laser, with 5 °C bandwidth. The blue power obtained at 422 nm was 0.3 mW for a 5 mm long waveguide, using 113 mW IR at the focusing objective, and with 39 mW IR emerging from the waveguide. This technique eliminates the need for an optical isolator between diode and waveguide.

Blue-green light generation from a neodymium fiber laser

K.S.Buritskii, V.P.Gapontsev[*], E.M.Dianov, V.A.Maslov,
I.E.Samartsev[*], V.A.Chernykh, E.A.Shcherbakov.
General Physics Institute
38 Vavilov Str., 117942 Moscow, USSR
Phone: (095) 132 82 31
[*]R&D Center IRE-POLUS
1 Vvedenskogo Sq., Fryazino, 141120 Moscow, USSR
Phone: (095) 526 90 83

Much interest has been attracted recently to the problem of design compact blue-green light sources. Most the activity is concentrated around the frequency doubling of semiconductor lasers with the wavelengths of 0.8-0.9 μm. On the other hand rare-earth doped fiber lasers are an interesting alternative to diode lasers due to their tunability, high quality output beam etc [1]. Such lasers are compatible with channel KTP-waveguides [2] which are very promising for the nonlinear frequency conversion from the near-IR to green and blue. The phase-matched type II interaction or quasi- phase-matched type I interaction can be used depending on the fundamental wavelength [3].

In this paper we report for the first time the phase-matched (type II) nonlinear frequency conversion of Nd^{3+}-doped fiber laser radiation in the channel Rb:Ba:KTP waveguide.

Channel waveguides were fabricated on the z-cut flux-grown KTP substrates to be directed along the y-axis by ion exchange from pure $RbNO_3$ or mixed $RbNO_3/Ba(NO_3)_2$ melts at 340°C (see Fig.1) [3]. The duration of process was 15 min. In the experiment we used the fiber laser in the tunable configuration as shown in Fig.2. The tuning curve is plotted in Fig.3. The tunability has allowed us to observe the variety of nonlinear interactions. The fiber cavity configuration enabled to couple the output endface of fiber laser directly to the input one of KTP waveguide. Coupling efficiency was about 30% because of the mode mismatch of fiber and waveguide. It can be sufficiently

increased due to small eccentricity of channel KTP waveguide mode field distribution [4]. Second harmonic generation has been observed in Rb:Ba:KTP waveguide (the phase-matching fundamental wavelength λ=1.115 μm is marked in Fig.2 with an arrow). At the same time no phase-matched SHG has been observed in Rb:KTP waveguide in the tuning range of Nd^{3+}-fiber laser. We explain the phase matching availability in a Rb:Ba:KTP waveguide by a large value of refractive index increase in such waveguides. If the light from fiber laser (λ_1=1.06 μm) and pumping laser diode (λ_2=0.8 μm) have been coupled simultaneously to the Rb:KTP waveguide, blue sum-frequency generation has occured. In the Rb:Ba:KTP waveguide phase-matched SFG has been also observed when the fiber laser double wave (1.12 μm and 1.06 μm) lasing occured.

While the waveguide parameters were not optimized in this experiment, useful amounts of green light were nevertheless observed. The SH power, achieved in Rb:Ba:KTP waveguide, was about 45 μW under the conditions of 5 mW pump power in the waveguide. When SFG occuring in this waveguide, the output "green" power of 78 μW was achieved for total pumping power of 7 mW. The optimization of the fiber laser and the waveguide parameters is now in progress. We expect to observe substantial increase in the conversion efficiency in the optimized device. Further results will be given in the talk.

References.

1. V.P.Gapontsev, I.E.Samartsev, A.A.Zayats, R.R.Loryan. Techn.Dig. Advanced Solid State Lasers (OSA, Washington, D.C.,1991), paper WC1.

2. J.D.Bierlein, A.Ferretti, L.H.Brixner, W.Y.Hsu. Appl.Phys.Lett., 50, 1216 (1987).

3. C.J.van der Poel, J.D.Bierlein, J.B.Brown, S.Colak. Appl.Phys.Lett., 57, 2074 (1990).

4. K.S.Buritskii, E.M.Dianov, Yu.M.Grjaznov, N.G.Dobrjakova, V.A.Maslov, V.A.Chernykh, E.A.Scherbakov. Sov.Lightwave Commun., 1, 107 (1991).
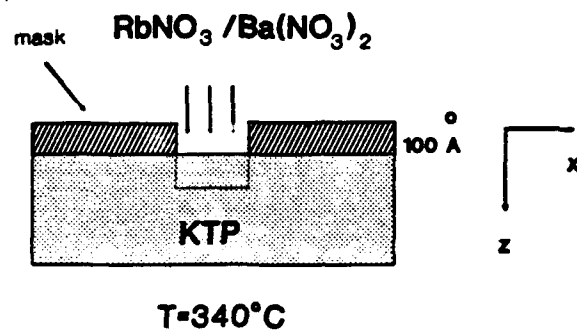
Fig.1. Waveguide fabrication technique.
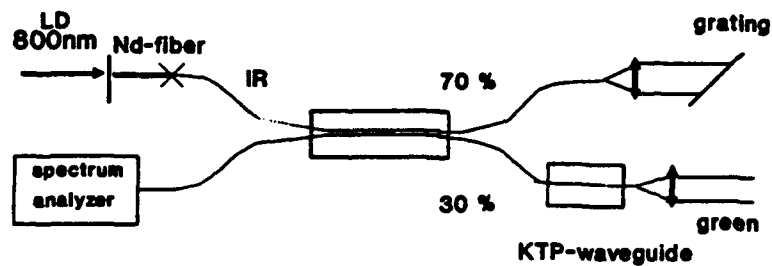
Fig.2. Tunable fiber laser configuration.
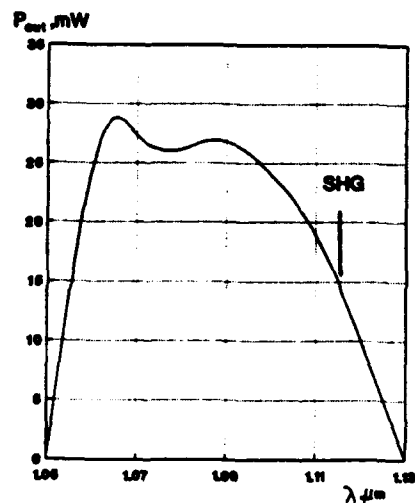
Fig.3. Fiber laser output response.

Shcherbakov, E.A. — FC6
Sipes, Donald L. — ThA
Sklar, Larry A. — ThA2
Snow, Judith B. — ThE2
Srivastava, Ramakant — ThE9, FC4
Stafsudd, Oscar M. — ThE1
Stone, R.E. — ThE5
Sugiura, Minako — FA3

Tamada, Hitoshi — FC3
Thrash, R.J. — ThB3
Tropper, Anne C. — ThB1
Tye, G.E. — FA4

Wallace, R.W. — FA4
Wang, Pu — ThE6
Wang, S.C. — ThE5

Xie, W. — ThC3
Xue, Jing — ThE6

Yu, Jun-hua — ThE12

Zhang, Qinqing — ThE6
Zhang, Zhong-hua — ThE12
Zhang, hua — ThE12
Zhou, Bingkun — ThE6
Zhu, Zhong-wei — ThE12
Zory, Peter S. — ThC, ThE3
Zysset, B. — ThE7

COMPACT BLUE-GREEN LASERS

**ADDENDUM AND
POSTDEADLINE PAPERS**

**FEBRUARY 20–21, 1992
SANTA FE, NEW MEXICO**

11:45am-12:00m
ThB4   Rare-earth-doped waveguide devices: the potential for
         compact blue-green lasers, N. A. Sanford, K. J. Malone,
         D. R. Larson, M. J. McCollum, National Institute of
         Standards and Technology.

Rare-earth-doped channel waveguide devices have been demonstrated
to lase in the infrared. The possibility for upconversion visible
lasing is also being explored.

POSTDEADLINE PAPERS

Thursday, February 20, 1992

6:00pm-7:30pm

PD1   Optically pumped blue lasing in ZnSe/ZnMgSSe double
         heterostructures, H. Okuyama, F Hiei, K. Akimoto,
         Sony Corp., Japan.

Photopumped blue laser oscillation has been achieved at room
temperature in a ZnSe/ZnMgSSe double heterostructure. ZnMgSSe is
a promising material for the cladding layer of blue laser diodes.

PD2   Remarks about quasi phase matching in periodically
         poled LiNbO3 waveguides, D. Delacourt, F. Armani,
         Michel R. Papuchon, Thomson-CSF, France.

We have analyzed how the involved modes convert via the overlap
integral, the image of ferro-electric polarization into an
effective periodic non-linear coefficient.

Rare-Earth-Doped Waveguide Devices: The Potential For Compact Blue-Green Lasers

N.A. Sanford, J.A. Aust, D.R. Larson, and K.J. Malone

National Institute of Standards and Technology

Optical Electronic Metrology Group, 814.02

325 Broadway, Boulder, Colorado 80303

Tel: (303) 497-5239

Fax: (303) 497-3387

Optically-pumped rare-earth-doped waveguide lasers have been demonstrated in glass[1] and lithium niobate[2] host materials. This technology is attractive since complex multi-waveguide circuits with a variety of possible rare-earth dopants can be fabricated by VLSI techniques. A recently reported Nd-doped Y-branch laser[3] is an example of such integration. Devices formed in LiNbO$_3$ have been demonstrated to lase near 1550 nm with Er used as a dopant and near 1060 nm with Nd used as a dopant (see Ref. 2 and references therein). The recent reports[4,5] of visible upconversion lasing in Pr and Er doped fluorozirconate fibers have not yet been duplicated in a planar waveguide geometry. Visible green and red upconversion luminescence has, however, been observed from an Er-doped LiNbO$_3$ waveguide laser[2] which operated near 1550 nm and was pumped at 1477 nm. In this paper, we will expand on these latter results and show that the visible green upconversion luminescence efficiency is approximately 0.3% for Er-doped Ti:LiNbO$_3$ waveguides pumped at 973 nm.

20 nm thick films of Er were e-beam deposited on the surfaces of Z-cut LiNbO$_3$ plates. One set of samples was annealed (in air) at 1080 °C for 70 hours; a second set was annealed for 140 hours. For the experimental results which follow, both sets of samples yielded essentially the same results. This

processing should give[4] a surface concentration of Er of approximately 1×10^{19} cm^{-3} and a 1/e depth of 5 - 7 μm. Following the Er diffusion, Ti stripes 8 μm wide and 100 nm thick were patterned on the surfaces of the samples. The individual stripes were separated by 200 μm. The waveguide channels were then formed by annealing the samples at 1060°C for 9 hours. The samples were then cut and polished for end-fire pumping to finished lengths of 10 mm and 20 mm.

Optical pumping was carried out at 973 nm with a Ti:sapphire laser. Absorption takes place from the $^4I_{15/2}$ state to the $^4I_{11/2}$ state followed by additional absorption to the $^4F_{7/2}$ state. Subsequent relaxation to the $^2H_{11/2}$ and the $^4S_{3/2}$ levels results in radiative decay to the ground state. A schematic energy level diagram showing this process is illustrated in Fig. 1. Excitation involving cooperative ion-ion upconversion is also possible. The luminescence conversion efficiency, defined as the ratio of absorbed pump power to total integrated green emission (both guided and unguided), is approximately 0.3%. The luminescence spectra for polarization parallel to the optic axis (TM) and perpendicular to the optic axis (TE), for both ~ 550-nm and ~ 1550-nm emission, is shown in Fig. 2.

Transient excitation decay for the ~ 550-nm and the ~ 1550-nm emission is shown in Fig. 3. In these measurements the pump input was gated with an acousto-optic modulator. The visible transient luminescence is characterized by a two step process: an initial spiking followed by a 0.55-ms (1/e) decay to an equilibrium level. When the pump pulse is switched off the signal falls with a 0.03-ms time constant. Two-photon pumping at 805 nm produces green emission with roughly the same conversion efficiency but without the transient spiking. The decay lifetime observed for the 1550-nm emission is 2.64 ms which is shorter than the 2.9 ms reported in ref. 2. These results are illustrated in Fig. 3.

Although upconversion lasing has not yet been achieved with these samples the results are encouraging. 54 mW of absorbed pump power at 973 nm in a 1-cm long sample simultaneously gave 1.2 μW of guided green luminescence and 1.6 μW of guided luminescence near 1550 nm. Upconversion experiments using Er-doped LiNbO$_3$ are continuing and experiments with Ho and Pr as active dopants

2

are currently underway.

References

1.   H. Aoki, O. Maruyama, and Y. Asahara, Electron. Lett. 26, 1910 (1990).

2.   R. Brinkmann, W. Sohler, and H. Suche, Electron. Lett. 27, 415 (1991).

3.   N.A. Sanford, K.J. Malone and D.R. Larson, Opt. Lett. 16, 1168 (1991).

4.   J.Y. Allain, M. Monerie, and H. Poignant, Electron. Lett. 27, 189 (1991).

5.   J.Y. Allain, M. Monerie, and H. Poignant, Electron. Lett. 28, 111 (1992).

Figure Captions

Figure 1.   Approximate energy level diagram for erbium showing possible two-photon excitation
and resulting photoluminescence schemes for 973-nm and 805-nm pumping. Only the
observed emission is shown.

Figure 2(a).   Spectrum of guided green luminescence under 973-nm pump for polarization parallel
to the crystal c axis (TM) and polarization perpendicular to the c axis (TE).

Figure 2(b).   TE and TM spectra for guided luminescence near 1550 nm. Same pump condition as
2(a).

Figure 3(a).   Transient excitation decay for visible green luminescence.

Figure 3(b).   Transient excitation decay for luminescence near 1550 nm.

3

Luminescence Spectrum for a 973nm pump

Figure 2.

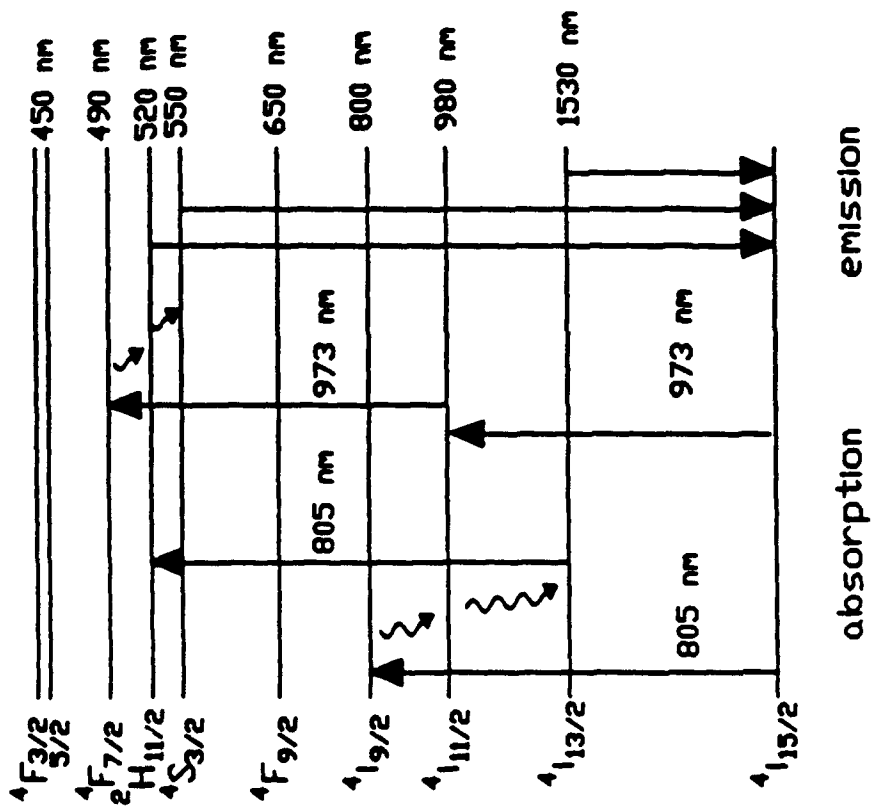Excitation Decay for a 973nm pump

Figure 3.

Figure 1.

Optically Pumped Blue Lasing in ZnSe/ZnMgSSe Double Heterostructures

H. Okuyama, F. Hiei and K. Akimoto

Sony Corporation Research Center, Fujitsuka 174, Hodogaya, Yokohama 240,

Japan

Telephon 045-334-6856, Fax. 045-334-6934

Abstract

Photopumped blue laser oscillation has been achieved at room temperature in a ZnSe/ZnMgSSe double heterostructure. ZnMgSSe is a promising material for the cladding layer of blue laser diodes.

Optically Pumped Blue Lasing in ZnSe/ZnMgSSe Double Heterostructures

H. Okuyama, F. Hiei and K. Akimoto

Sony Corporation Research Center, Fujitsuka 174, Hodogaya, Yokohama 240,

Japan

Telephone 045-334-6856, Fax. 045-334-6934

Summary

ZnSe has been regarded as a suitable material for the active layer of blue laser diodes. However, there have not been candidates for a cladding layer material, that is lattice-matched to the substrate and has sufficient band-gap energy. Recently, we found a new material $Zn_xMg_{1-x}S_ySe_{1-y}$, whose band-gap energy can be varied from 2.8 to near 4 eV, and maintains lattice-matching to a (100)GaAs substrate.

Double heterostructures composed of ZnSe and ZnMgSSe have been grown on (100)GaAs substrates by molecular beam epitaxy. Figure 1 shows the structure of the sample. Composition x and y of ZnMgSSe were 0.94 and 0.12,

respectively. The band-gap energy between ZnSe and ZnMgSSe is 0.13 eV. Based on the discussion of the common cation and common anion rule, the most probable structure for the heterojunction is Type I.

The sample was cleaved to $400\mu m \times 600\mu m$, and was mounted on a heat sink. The sample was excited by a pulsed N_2 laser, whose maximum output power, pulse width and repetition rate were 800 kW, 5 ns and 10 Hz, respectively.

Figure 2 shows the intensity of the light output at room temperature from the cleaved edge of the sample against the input intensity. The intensity of the light output rapidly increased above the threshold intensity suggesting a lasing action. The threshold intensity was estimated to be about 150 kW/cm^2.

The emission spectra at room temperature excited below and above the threshold intensity are shown in Fig. 3. For the excitation intensity below the threshold, two peaks were observed. The emission peak at 457 nm is due to the spontaneous emission from the ZnSe layer and the peak at 438 nm is due to the spontaneous emission from the ZnMgSSe layer. For the excitation intensity above the threshold, a sharp peak was observed at 470.5 nm. The full width at half-maximum of the peak is about 2.5 nm, and the peak position is shifted to a longer wavelength than the spontaneous emission peak where the gain peak would normally be expected.

The polarization dependence of the light-output characteristic is shown in Fig. 4. The emission was predominantly TE-polarized. This result is further evidence of the lasing action in this double heterostructure.
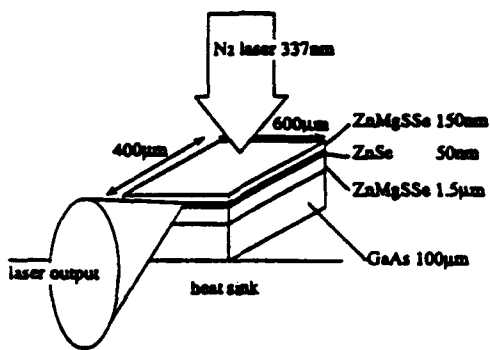
Fig. 1 Schematic structure of ZnSe/ZnMgSSe
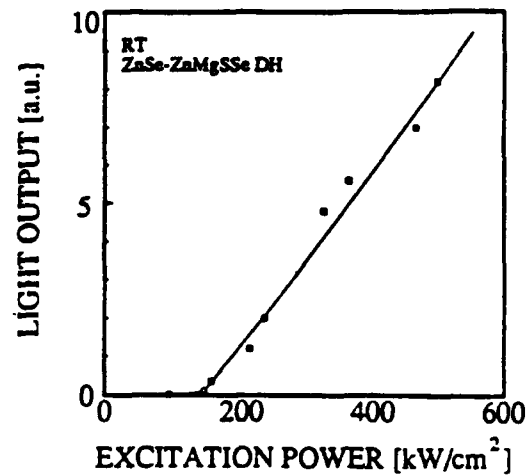   double heterostructure.

Fig. 2 Light output vs excitation
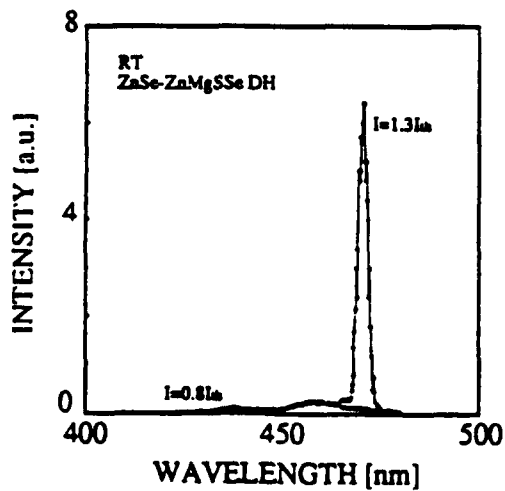   power characteristics.

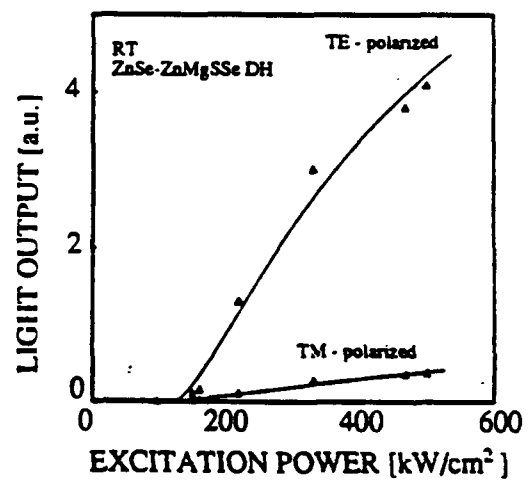Fig. 3 Emission spectra above
       and below the lasing threshold.

Fig. 4 Polarization dependence of the
       light output characteristics.

REMARKS ABOUT QUASI PHASE MATCHING IN PERIODICALLY POLED LiNbO$_3$ WAVEGUIDES

D. DELACOURT, F. ARMANI, M. PAPUCHON

Thomson-CSF / LCR

Domaine de Corbeville, 91404 Orsay Cedex (France)

Abstract

We have analyzed how the involved modes convert via the overlap integral, the image of ferro-electric polarization into an effective periodic non-linear coefficient.

REMARKS ABOUT QUASI PHASE MATCHING IN PERIODICALLY POLED LiNbO₃ WAVEGUIDES

D. DELACOURT, F. ARMANI, M. PAPUCHON
Thomson-CSF / LCR
Domaine de Corbeville, 91404 Orsay Cedex (France)

As regards blue generation from near-infrared laser diodes, the Quasi-Phase Matching (QPM) technique gives the possibility to use highly non-linear materials such as KTP (1), LiTaO₃ (2) and LiNbO₃ (3), (4), in which standard methods could fail. This QPM consists in periodically perturbating the non-linear interaction to compensate the difference Δk due to refractive index dispersion.

$$\Delta k = k_{2\omega} - 2k_{\omega}$$

where $k_{2\omega}$ and k_{ω} are the propagation vectors of the harmonic and fundamental modes. This periodic perturbation can be achieved by a modulation of the :

- refractive index
- refractive index dispersion
- overlap between the nonlinear polarization and harmonic wave
- non-linear coefficient

Among these different methods which can be combined (5), one of the most efficient is the periodic modulation of the non-linear coefficient d involved in the interaction. In that case, d can be written as :

$$d(x) = \sum_{n=-\infty}^{+\infty} d_n \, e^{-inKx}$$

with n integer, $K = 2\pi/\Lambda$ where Λ is the period of the modulation. To achieve QPM in the order m, is necessary that Λ and the modulation shape of d is such as a spatial harmonic m of the Fourier ecomposition of d satisfies :

$$\Delta k = mK$$

The conversion efficiency is thus closely related to the value of the d_m coefficient and in general the gher the order m, the lower the conversion efficiency. As an other consequence, QPM is possible to achieve in the mth order with a modulation which does not contain the corresponding atial harmonic mK ($d_m = 0$), as it is the case with a sine shaped modulation using an order gher than one.

ferro-electric material such as KTP, LiTaO₃ and LiNbO₃, this modulation can be obtained by a riodic reversal of the spontaneous polarization. In LiNbO₃, a common way to get this reversal is indiffuse a Titanium grating on the z+ face of the crystal near its Curie temperature. fortunately this technique does not lead to abrupt regions in which the non-linear coefficient is inged in sign. Fig.1 schematizes what is the image of polarization which is commonly obtained 1 typical diffusion conditions, for periods compatible with low order QPM and for a 50 %/50 %

duty cycle of the Titanium stripe grating. In fact, this process leads to two homogeneous and opposite polarization regions separated by a periodic triangle shaped boundary which oscillates in the thickness M. As a consequence the resulting modulation of the non-linear coefficient effectively involved in the frequency doubling, will depend directly on the overlap between this boundary and the fundamental and harmonic modes, the corresponding fields of which can be written (according to the notations of fig. 1), as follows :

$$E_\omega (x, y, z) = A_\omega F_\omega (y) G_\omega (z) e^{i(\omega t - k_\omega x)}$$

$$E_{2\omega} (x, y, z) = A_{2\omega} (x) F_{2\omega} (y) G_{2\omega} (z) e^{i(2\omega t - k_{2\omega} x)}$$

A_ω and $A_{2\omega}$ represent the amplitudes of the fundamental (ω) and harmonic (2ω) modes.

$$\left[\frac{\partial A_\omega (x)}{\partial x} = 0, \ A_\omega (0) = 0 \right]$$

$F_\omega(y)$, $G_\omega(z)$, $F_{2\omega}(y)$, $G_{2\omega}(z)$ represent their profiles in the two direction (z, y) perpendicular to the propagation axis (x).

F and G satisfy :

$$\int_{-\infty}^{\infty} F_{\omega/2\omega} (y) . F^{*}_{\omega/2\omega} (y) \, dy = 1 \qquad \text{and} \qquad \int_{-\infty}^{\infty} G_{\omega/2\omega} (z) . G^{*}_{\omega/2\omega} (z) \, dz = 1$$

Using usual assumptions, $A_{2\omega}$ is found to verify :

(1)
$$\frac{\partial A_{2\omega}(x)}{\partial x} = -i \, e^{i\Delta k.x} . I(x)$$

(2)
$$I(x) = B_1 \ B_2 \int_{-\infty}^{\infty} d (x, z) \, G_\omega^2 (z) \, G^{*}_{2\omega} (z) \, dz$$

$$B_1 = \frac{\omega}{n_{2\omega}.c} A_\omega^2 \qquad\qquad B_2 = \int_{-\infty}^{\infty} F_\omega^2 (y) \, F^{*}_{2\omega} (y) \, dy$$

ω is the pulsation of the fundamental mode, $n_{2\omega}$, the effective index of the harmonic mode and c the velocity of light in vacuum. Because of the shape shown in fig.1, the non-linear coefficient d, which is either equal to d_{33} or to -d_{33}, depends on x and z (d is constant in the y direction because the Titanium stripes are much longer than the waveguide width).

The solution (1) indicates clearly that the periodic element that effectively gives the possibility to satisfy the QPM condition, is the integral I(x) that can be written as follows :

$$I(x) = d_{eff}(x).E^2$$

where E is a constant which can be identified to an equivalent electric field, and d_{eff} is a periodic effective non-linear coefficient, the modulation shape of which is the only one to take into account

to predict the conversion efficiency. This shape can be much different from the triangular shape of the boundary between the two opposite polarization. As a matter of fact, let us consider very confined fundamental and harmonic modes centered in the thickness M as it is illustrated in figure 2.a. It can be easily demonstrated that in that case, d_{eff} presents a square shaped modulation, as shown in fig. 2.b. At the opposite for modes so weakly confined that one can consider that their amplitude is constant in the thickness M (see fig. 3.a), the triangle shaped modulation of d_{eff} clearly appears (see fig.3.b). As we have seen above, this modulation shape influences directly the values of the Fourier coefficient corresponding to the harmonic mK that has to be used for QPM in the mth order. To illustrate this point it is convenient to calculate the ratio R between the harmonic power obtained in the third order and the harmonic power obtained in the first order for the same interaction length. It is well known that in the case of figure 2 we obtain R = 1/9 and R = 1/81 in the case of figure 3. Then let's consider a more realistic intermediate case, for example gaussian profile modes centered in the modulation thickness M and with waists of the order of magnitude of M. In that type of case, our numerical calculation shows that the ratio R can be out of the interval [1/81, 1/9] and much lower than 1/81, that means nearly 0. As a matter of fact, in these cases, it can be calculated that the effective non-linear coefficient is close to a sine shaped function which does not present the third spatial harmonic needed to reach QPM in the third order (see figure 4).

This confirms that the image of polarization in the crystal after the reversal process is converted by the involved modes into an effective non-linear coefficient the modulation shape of which is directly related to the profiles of these modes via the overlap integral and can be far from the triangular shape of the boundary between the two opposite polarization regions. This shows also how carefully it is necessary to design these devices especially when the goal is to reach QPM in an order higher than one to benefit by a higher modulation M.

References

(1) C.J. Van der Poel, J.D. Bierlein, J.B. Brown and S. Colak, Appl. Phys. Lett. 57 (20), 12 November 1990, p.2074.

(2) K. Yamamoto, K.Mizuuchi and T.Taniuchi, Optics Lett., vol. 16, n°15, 1 August 1991, p.1156.

(3) E.J. Lim, M.M. Feper, R.L. Byer and W.J. Kozlovski, Electronics Lett. vol.25, 25 May 1989, p.731.

(4) J. Webjörn, F. Laurell and G. Arvidsson, IEEE Photonetics Tech. Lett., vol. 1, n°10, October 1989, p.316.

(5) J. Khurgin, S. Colak, R. Stolzenberger and R. N. Bhargava, Appl. Phys. lett. 57 (24), 10 December 1990, p.2540.
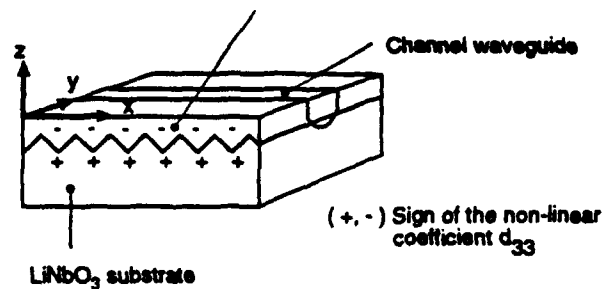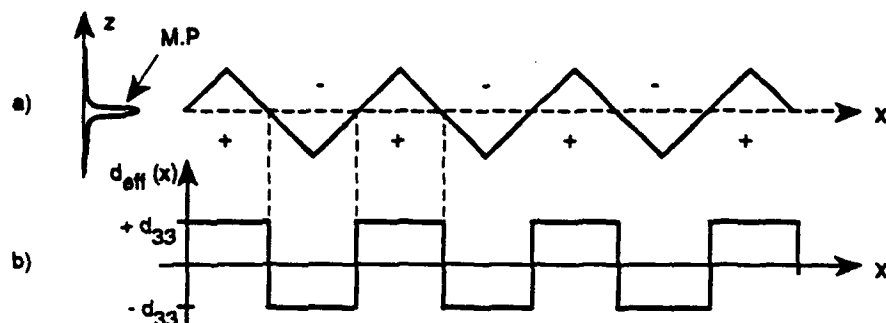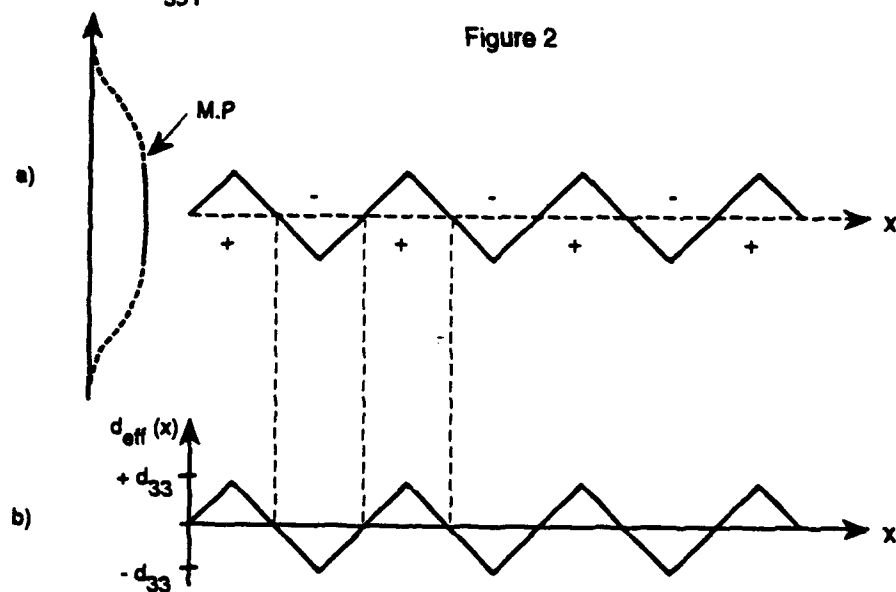
Channel waveguide

(+, -) Sign of the non-linear coefficient d_{33}

LiNbO$_3$ substrate

Figure 1

a)

M.P

$d_{eff}(x)$

+ d_{33}

b)

- d_{33}

Figure 2

a)

M.P

$d_{eff}(x)$

+ d_{33}

b)

- d_{33}

Figure 3

a)

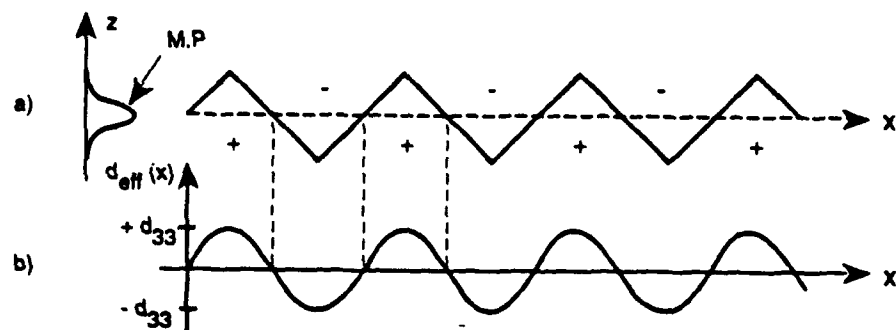M.P

$d_{eff}(x)$

+ d_{33}

b)

- d_{33}

Figure 4

(M.P = Schematic representation of the fundamental and harmonic mode profiles)

Pd2-5

COMPACT BLUE-GREEN LASERS
KEY TO AUTHOR-POSTDEADLINE

Akimoto, K.   PD1

Armani, F.   PD2

Delacourt, D.   PD2

Hiei, F.   PD1

Okuyama, H.   PD1

Papuchon, Michel   PD2

COMPACT BLUE-GREEN LASERS

ADDENDUM AND
POSTDEADLINE PAPERS

FEBRUARY 20–21, 1992
SANTA FE, NEW MEXICO

11:45am-12:00m
ThB4   Rare-earth-doped waveguide devices: the potential for
          compact blue-green lasers, N. A. Sanford, K. J. Malone,
          D. R. Larson, M. J. McCollum, <u>National Institute of
          Standards and Technology</u>.

Rare-earth-doped channel waveguide devices have been demonstrated
to lase in the infrared. The possibility for upconversion visible
lasing is also being explored.

                        POSTDEADLINE PAPERS

<u>Thursday, February 20, 1992</u>

6:00pm-7:30pm

PD1   Optically pumped blue lasing in ZnSe/ZnMgSSe double
          heterostructures, H. Okuyama, F Hiei, K. Akimoto,
          Sony Corp., Japan.

Photopumped blue laser oscillation has been achieved at room
temperature in a ZnSe/ZnMgSSe double heterostructure. ZnMgSSe is
a promising material for the cladding layer of blue laser diodes.

PD2   Remarks about quasi phase matching in periodically
          poled LiNbO3 waveguides, D. Delacourt, F. Armani,
          Michel R. Papuchon, Thomson-CSF, France.

We have analyzed how the involved modes convert via the overlap
integral, the image of ferro-electric polarization into an
effective periodic non-linear coefficient.

Rare-Earth-Doped Waveguide Devices: The Potential For Compact Blue-Green Lasers

N.A. Sanford, J.A. Aust, D.R. Larson, and K.J. Malone

National Institute of Standards and Technology

Optical Electronic Metrology Group, 814.02

325 Broadway, Boulder, Colorado 80303

Tel: (303) 497-5239

Fax: (303) 497-3387

Optically-pumped rare-earth-doped waveguide lasers have been demonstrated in glass[1] and lithium niobate[2] host materials. This technology is attractive since complex multi-waveguide circuits with a variety of possible rare-earth dopants can be fabricated by VLSI techniques. A recently reported Nd-doped Y-branch laser[3] is an example of such integration. Devices formed in LiNbO$_3$ have been demonstrated to lase near 1550 nm with Er used as a dopant and near 1060 nm with Nd used as a dopant (see Ref. 2 and references therein). The recent reports[4,5] of visible upconversion lasing in Pr and Er doped fluorozircona e fibers have not yet been duplicated in a planar waveguide geometry. Visible green and red upconversion luminescence has, however, been observed from an Er-doped LiNbO$_3$ waveguide laser[2] which operated near 1550 nm and was pumped at 1477 nm. In this paper, we will expand on these latter results and show that the visible green upconversion luminescence efficiency is approximately 0.3% for Er-doped Ti:LiNbO$_3$ waveguides pumped at 973 nm.

20 nm thick films of Er were e-beam deposited on the surfaces of Z-cut LiNbO$_3$ plates. One set of samples was annealed (in air) at 1080 °C for 70 hours; a second set was annealed for 140 hours. For the experimental results which follow, both sets of samples yielded essentially the same results. This

processing should give[4] a surface concentration of Er of approximately 1×10^{19} cm^{-3} and a $1/e$ depth of 5 - 7 μm. Following the Er diffusion, Ti stripes 8 μm wide and 100 nm thick were patterned on the surfaces of the samples. The individual stripes were separated by 200 μm. The waveguide channels were then formed by annealing the samples at 1060°C for 9 hours. The samples were then cut and polished for end-fire pumping to finished lengths of 10 mm and 20 mm.

Optical pumping was carried out at 973 nm with a Ti:sapphire laser. Absorption takes place from the $^4I_{15/2}$ state to the $^4I_{11/2}$ state followed by additional absorption to the $^4F_{7/2}$ state. Subsequent relaxation to the $^2H_{11/2}$ and the $^4S_{3/2}$ levels results in radiative decay to the ground state. A schematic energy level diagram showing this process is illustrated in Fig. 1. Excitation involving cooperative ion-ion upconversion is also possible. The luminescence conversion efficiency, defined as the ratio of absorbed pump power to total integrated green emission (both guided and unguided), is approximately 0.3%. The luminescence spectra for polarization parallel to the optic axis (TM) and perpendicular to the optic axis (TE), for both $\sim$550-nm and $\sim$1550-nm emission, is shown in Fig. 2.

Transient excitation decay for the $\sim$550-nm and the $\sim$1550-nm emission is shown in Fig. 3. In these measurements the pump input was gated with an acousto-optic modulator. The visible transient luminescence is characterized by a two step process: an initial spiking followed by a 0.55-ms $(1/e)$ decay to an equilibrium level. When the pump pulse is switched off the signal falls with a 0.03-ms time constant. Two-photon pumping at 805 nm produces green emission with roughly the same conversion efficiency but without the transient spiking. The decay lifetime observed for the 1550-nm emission is 2.64 ms which is shorter than the 2.9 ms reported in ref. 2. These results are illustrated in Fig. 3.

Although upconversion lasing has not yet been achieved with these samples the results are encouraging. 54 mW of absorbed pump power at 973 nm in a 1-cm long sample simultaneously gave 1.2 μW of guided green luminescence and 1.6 μW of guided luminescence near 1550 nm. Upconversion experiments using Er-doped LiNbO$_3$ are continuing and experiments with Ho and Pr as active dopants

2

ThB4--

are currently underway.

References

1. H. Aoki, O. Maruyama, and Y. Asahara, Electron. Lett. 26, 1910 (1990).

2. R. Brinkmann, W. Sohler, and H. Suche, Electron. Lett. 27, 415 (1991).

3. N.A. Sanford, K.J. Malone and D.R. Larson, Opt. Lett. 16, 1168 (1991).

4. J.Y. Allain, M. Monerie, and H. Poignant, Electron. Lett. 27, 189 (1991).

5. J.Y. Allain, M. Monerie, and H. Poignant, Electron. Lett. 28, 111 (1992).

Figure Captions

Figure 1.   Approximate energy level diagram for erbium showing possible two-photon excitation

and resulting photoluminescence schemes for 973-nm and 805-nm pumping. Only the

observed emission is shown.

Figure 2(a).   Spectrum of guided green luminescence under 973-nm pump for polarization parallel

to the crystal c axis (TM) and polarization perpendicular to the c axis (TE).

Figure 2(b).   TE and TM spectra for guided luminescence near 1550 nm. Same pump condition as

2(a).

Figure 3(a).   Transient excitation decay for visible green luminescence.

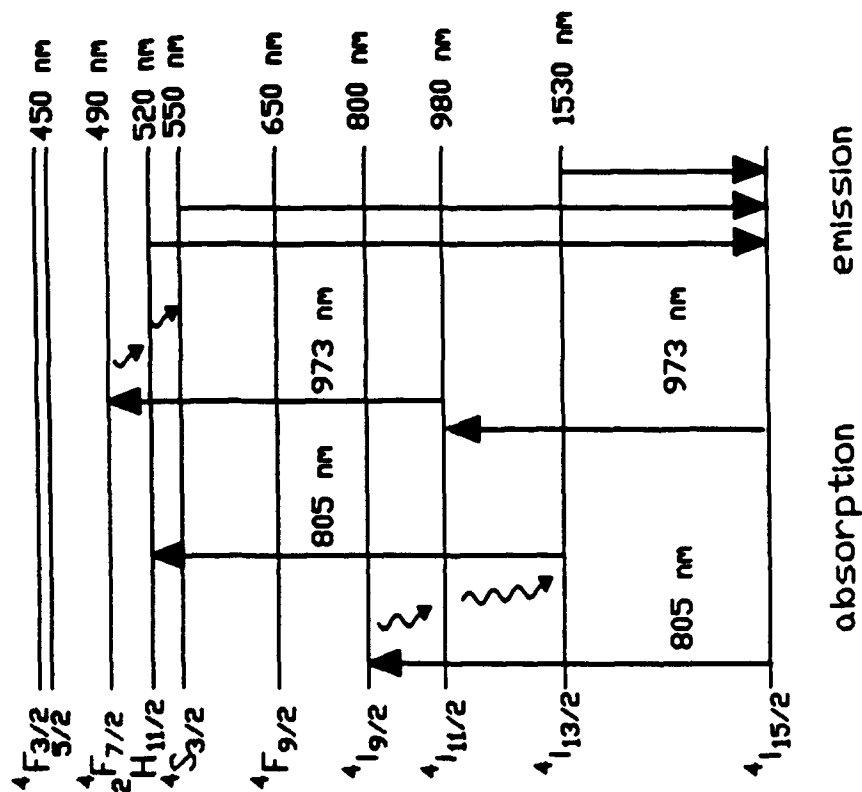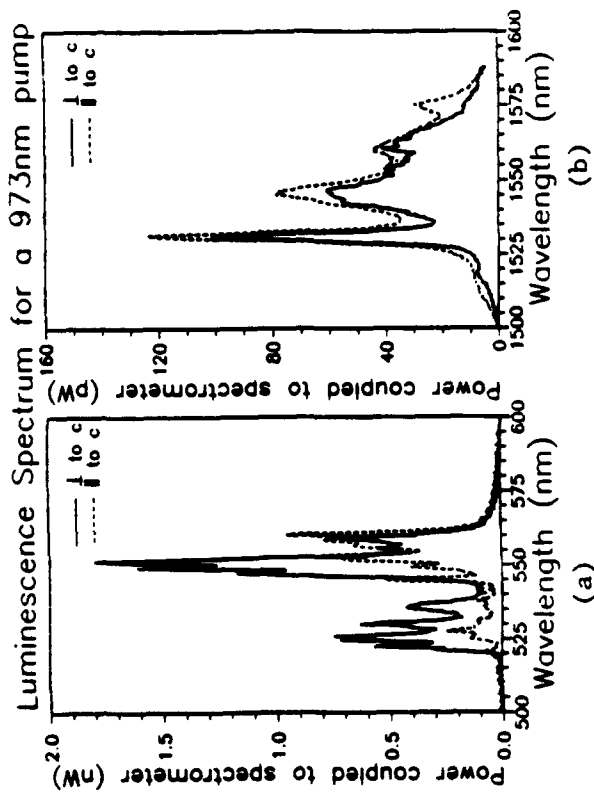Figure 3(b).   Transient excitation decay for luminescence near 1550 nm.

3

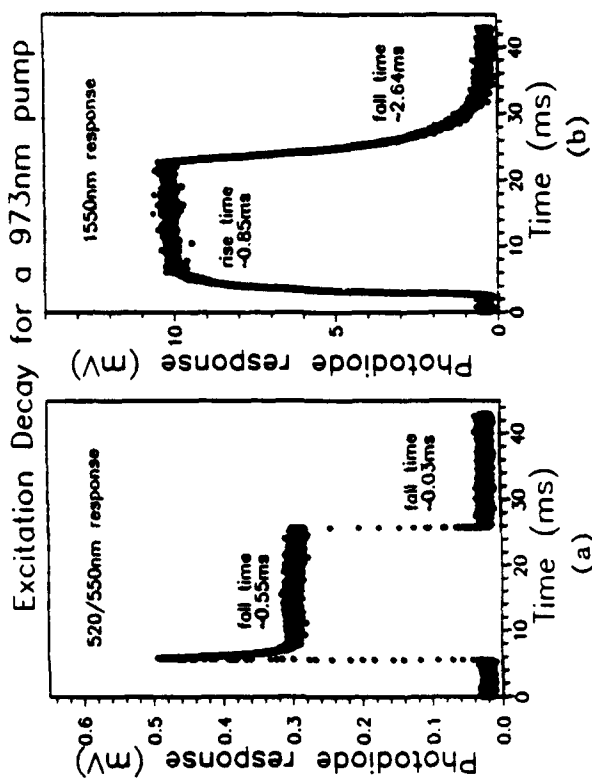Luminescence Spectrum for a 973nm pump

⊥ to c
‖ to c

Power coupled to spectrometer (nW)

Wavelength (nm)

(a)

Power Spectrum for a 973nm pump

⊥ to c
‖ to c

Power coupled to spectrometer (pW)

Wavelength (nm)

(b)

Figure 2.

Excitation Decay for a 973nm pump

520/550nm response

fall time ~0.55ms

fall time ~0.03ms

Photodiode response (mV)

Time (ms)

(a)

1550nm response

rise time ~0.85ms

fall time ~2.64ms

Photodiode response (mV)

Time (ms)

(b)

Figure 3.

$^4F_{3/2}$ $_{5/2}$

$^4F_{7/2}$

$^2H_{11/2}$

$^4S_{3/2}$

$^4F_{9/2}$

$^4I_{9/2}$

$^4I_{11/2}$

$^4I_{13/2}$

$^4I_{15/2}$

450 nm

490 nm

520 nm

550 nm

650 nm

800 nm

980 nm

1530 nm

973 nm

805 nm

973 nm

805 nm

emission

absorption

Figure 1.

ThB4-4

Optically Pumped Blue Lasing in ZnSe/ZnMgSSe Double Heterostructures

H. Okuyama, F. Hiei and K. Akimoto

Sony Corporation Research Center, Fujitsuka 174, Hodogaya, Yokohama 240,

Japan

Telephon 045-334-6856, Fax. 045-334-6934

Abstract

Photopumped blue laser oscillation has been achieved at room temperature in a ZnSe/ZnMgSSe double heterostructure. ZnMgSSe is a promising material for the cladding layer of blue laser diodes.

Optically Pumped Blue Lasing in ZnSe/ZnMgSSe Double Heterostructures

H. Okuyama, F. Hiei and K. Akimoto

Sony Corporation Research Center, Fujitsuka 174, Hodogaya, Yokohama 240,

Japan

Telephone 045-334-6856, Fax. 045-334-6934

Summary

ZnSe has been regarded as a suitable material for the active layer of blue laser diodes. However, there have not been candidates for a cladding layer material, that is lattice-matched to the substrate and has sufficient band-gap energy. Recently, w⁻ found a new material $Zn_xMg_{1-x}S_ySe_{1-y}$, whose band-gap energy can be varied from 2.8 to near 4 eV, and maintains lattice-matching to a (100)GaAs substrate.

Double heterostructures composed of ZnSe and ZnMgSSe have been grown on (100)GaAs substrates by molecular beam epitaxy. Figure 1 shows the structure of the sample. Composition x and y of ZnMgSSe were 0.94 and 0.12,

respectively. The band-gap energy between ZnSe and ZnMgSSe is 0.13 eV. Based on the discussion of the common cation and common anion rule, the most probable structure for the heterojunction is Type I.

The sample was cleaved to 400μm × 600μm, and was mounted on a heat sink. The sample was excited by a pulsed N_2 laser, whose maximum output power, pulse width and repetition rate were 800 kW, 5 ns and 10 Hz, respectively.

Figure 2 shows the intensity of the light output at room temperature from the cleaved edge of the sample against the input intensity. The intensity of the light output rapidly increased above the threshold intensity suggesting a lasing action. The threshold intensity was estimated to be about 150 kW/cm².

The emission spectra at room temperature excited below and above the threshold intensity are shown in Fig. 3. For the excitation intensity below the threshold, two peaks were observed. The emission peak at 457 nm is due to the spontaneous emission from the ZnSe layer and the peak at 438 nm is due to the spontaneous emission from the ZnMgSSe layer. For the excitation intensity above the threshold, a sharp peak was observed at 470.5 nm. The full width at half-maximum of the peak is about 2.5 nm, and the peak position is shifted to a longer wavelength than the spontaneous emission peak where the gain peak would normally be expected.

The polarization dependence of the light-output characteristic is shown in Fig. 4. The emission was predominantly TE-polarized. This result is further evidence of the lasing action in this double heterostructure.
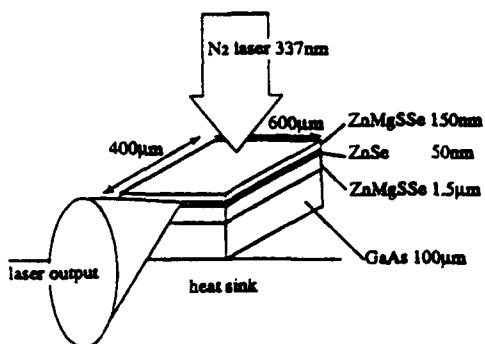
Fig. 1 Schematic structure of ZnSe/ZnMgSSe
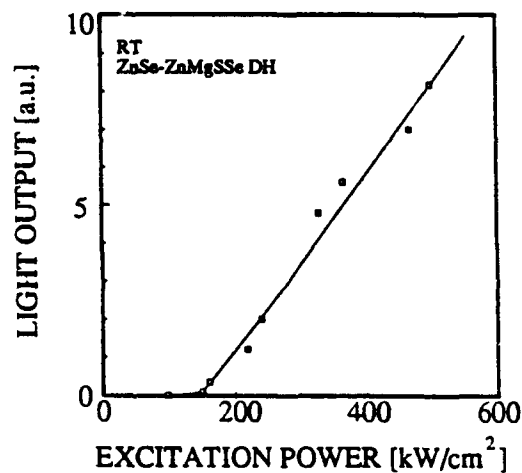double heterostructure.

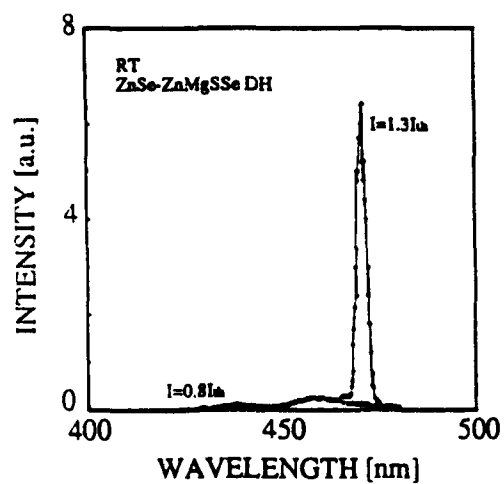Fig. 2 Light output vs excitation
power characteristics.

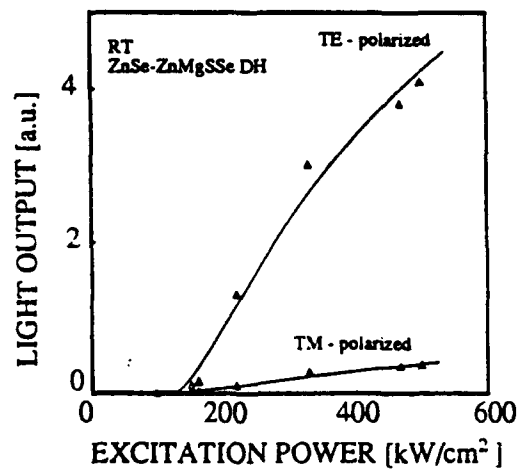Fig. 3 Emission spectra above
and below the lasing threshold.

Fig. 4 Polarization dependence of the
light output characteristics.

REMARKS ABOUT QUASI PHASE MATCHING IN PERIODICALLY POLED LiNbO$_3$ WAVEGUIDES

D. DELACOURT, F. ARMANI, M. PAPUCHON

Thomson-CSF / LCR

Domaine de Corbeville, 91404 Orsay Cedex (France)

Abstract

We have analyzed how the involved modes convert via the overlap integral, the image of ferro-electric polarization into an effective periodic non-linear coefficient.

REMARKS ABOUT QUASI PHASE MATCHING IN PERIODICALLY POLED LiNbO$_3$ WAVEGUIDES

D. DELACOURT, F. ARMANI, M. PAPUCHON
Thomson-CSF / LCR
Domaine de Corbeville, 91404 Orsay Cedex (France)

As regards blue generation from near-infrared laser diodes, the Quasi-Phase Matching (QPM) technique gives the possibility to use highly non-linear materials such as KTP (1), LiTaO$_3$ (2) and LiNbO$_3$ (3), (4), in which standard methods could fail. This QPM consists in periodically perturbating the non-linear interaction to compensate the difference Δk due to refractive index dispersion.

$$\Delta k = k_{2\omega} - 2k_{\omega}$$

where $k_{2\omega}$ and k_{ω} are the propagation vectors of the harmonic and fundamental modes. This periodic perturbation can be achieved by a modulation of the :

-   refractive index
-   refractive index dispersion
-   overlap between the nonlinear polarization
    and harmonic wave
-   non-linear coefficient

Among these different methods which can be combined (5), one of the most efficient is the periodic modulation of the non-linear coefficient d involved in the interaction. In that case, d can be written as :

$$d(x) = \sum_{n=-\infty}^{+\infty} d_n \, e^{-inKx}$$

with n integer, $K = 2\pi/\Lambda$ where Λ is the period of the modulation. To achieve QPM in the order m, it is necessary that Λ and the modulation shape of d is such as a spatial harmonic m of the Fourier decomposition of d satisfies :

$$\Delta k = mK$$

The conversion efficiency is thus closely related to the value of the d_m coefficient and in general the higher the order m, the lower the conversion efficiency. As an other consequence, QPM is impossible to achieve in the mth order with a modulation which does not contain the corresponding spatial harmonic mK ($d_m = 0$), as it is the case with a sine shaped modulation using an order higher than one.

In ferro-electric material such as KTP, LiTaO$_3$ and LiNbO$_3$, this modulation can be obtained by a periodic reversal of the spontaneous polarization. In LiNbO$_3$, a common way to get this reversal is to indiffuse a Titanium grating on the z+ face of the crystal near its Curie temperature. Unfortunately this technique does not lead to abrupt regions in which the non-linear coefficient is changed in sign. Fig.1 schematizes what is the image of polarization which is commonly obtained with typical diffusion conditions, for periods compatible with low order QPM and for a 50 %/50 %

duty cycle of the Titanium stripe grating. In fact, this process leads to two homogeneous and opposite polarization regions separated by a periodic triangle shaped boundary which oscillates in the thickness M. As a consequence the resulting modulation of the non-linear coefficient effectively involved in the frequency doubling, will depend directly on the overlap between this boundary and the fundamental and harmonic modes, the corresponding fields of which can be written (according to the notations of fig. 1), as follows :

$$E_\omega (x, y, z) = A_\omega F_\omega (y) G_\omega (z) e^{i(\omega t - k_\omega x)}$$

$$E_{2\omega} (x, y, z) = A_{2\omega} (x) F_{2\omega} (y) G_{2\omega} (z) e^{i(2\omega t - k_{2\omega} x)}$$

A_ω and $A_{2\omega}$ represent the amplitudes of the fundamental (ω) and harmonic (2ω) modes.

$$\left[\frac{\partial A_\omega (x)}{\partial x} = 0, A_\omega (0) = 0 \right]$$

$F_\omega(y)$, $G_\omega(z)$, $F_{2\omega}(y)$, $G_{2\omega}(z)$ represent their profiles in the two direction (z, y) perpendicular to the propagation axis (x).

F and G satisfy :

$$\int_{-\infty}^{+\infty} F_{\omega/2\omega} (y).\overset{*}{F}_{\omega/2\omega} (y) \, dy = 1 \qquad \text{and} \qquad \int_{-\infty}^{+\infty} G_{\omega/2\omega} (z).\overset{*}{G}_{\omega/2\omega} (z) \, dz = 1$$

Using usual assumptions, $A_{2\omega}$ is found to verify :

(1) $$\frac{\partial A_{2\omega} (x)}{\partial x} = -i \, e^{i\Delta k.x} .I(x)$$

(2) $$I(x) = B_1 \; B_2 \int_{-\infty}^{+\infty} d (x, z) \, G_\omega^2 (z) \, \overset{*}{G}_{2\omega} (z) \, dz$$

$$B_1 = \frac{\omega}{n_{2\omega}.c} A_\omega^2 \qquad\qquad B_2 = \int_{-\infty}^{+\infty} F_\omega^2 (y) \, \overset{*}{F}_{2\omega} (y) \, dy$$

ω is the pulsation of the fundamental mode, $n_{2\omega}$, the effective index of the harmonic mode and c the velocity of light in vacuum. Because of the shape shown in fig.1, the non-linear coefficient d, which is either equal to d_{33} or to $-d_{33}$, depends on x and z (d is constant in the y direction because the Titanium stripes are much longer than the waveguide width).

The solution (1) indicates clearly that the periodic element that effectively gives the possibility to satisfy the QPM condition, is the integral I(x) that can be written as follows :

$$I(x) = d_{eff}(x).E^2$$

where E is a constant which can be identified to an equivalent electric field, and d_{eff} is a periodic effective non-linear coefficient, the modulation shape of which is the only one to take into account

to predict the conversion efficiency. This shape can be much different from the triangular shape of the boundary between the two opposite polarization. As a matter of fact, let us consider very confined fundamental and harmonic modes centered in the thickness M as it is illustrated in figure 2.a. It can be easily demonstrated that in that case, d_{eff} presents a square shaped modulation, as shown in fig. 2.b. At the opposite for modes so weakly confined that one can consider that their amplitude is constant in the thickness M (see fig. 3.a), the triangle shaped modulation of d_{eff} clearly appears (see fig.3.b). As we have seen above, this modulation shape influences directly the values of the Fourier coefficient corresponding to the harmonic mK that has to be used for QPM in the mth order. To illustrate this point it is convenient to calculate the ratio R between the harmonic power obtained in the third order and the harmonic power obtained in the first order for the same interaction length. It is well known that in the case of figure 2 we obtain R = 1/9 and R = 1/81 in the case of figure 3. Then let's consider a more realistic intermediate case, for example gaussian profile modes centered in the modulation thickness M and with waists of the order of magnitude of M. In that type of case, our numerical calculation shows that the ratio R can be out of the interval [1/81, 1/9] and much lower than 1/81, that means nearly 0. As a matter of fact, in these cases, it can be calculated that the effective non-linear coefficient is close to a sine shaped function which does not present the third spatial harmonic needed to reach QPM in the third order (see figure 4).

This confirms that the image of polarization in the crystal after the reversal process is converted by the involved modes into an effective non-linear coefficient the modulation shape of which is directly related to the profiles of these modes via the overlap integral and can be far from the triangular shape of the boundary between the two opposite polarization regions. This shows also how carefully it is necessary to design these devices especially when the goal is to reach QPM in an order higher than one to benefit by a higher modulation M.

References

(1) C.J. Van der Poel, J.D. Bierlein, J.B. Brown and S. Colak, Appl. Phys. Lett. 57 (20), 12 November 1990, p.2074.

(2) K. Yamamoto, K.Mizuuchi and T.Taniuchi, Optics Lett., vol. 16, n°15, 1 August 1991, p.1156.

(3) E.J. Lim, M.M. Feper, R.L. Byer and W.J. Kozlovski, Electronics Lett. vol.25, 25 May 1989, p.731.

(4) J. Webjörn, F. Laurell and G. Arvidsson, IEEE Photonetics Tech. Lett., vol. 1, n°10, October 1989, p.316.

(5) J. Khurgin, S. Colak, R. Stolzenberger and R. N. Bhargava, Appl. Phys. lett. 57 (24), 10 December 1990, p.2540.
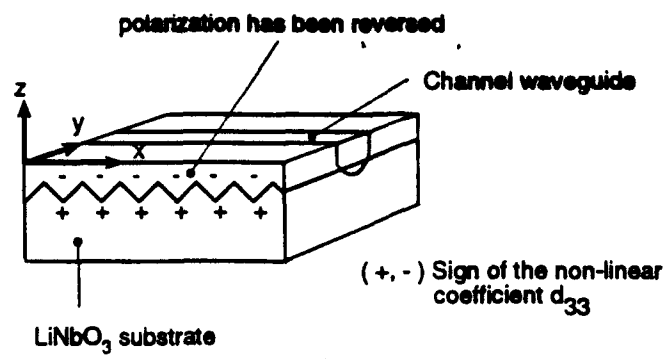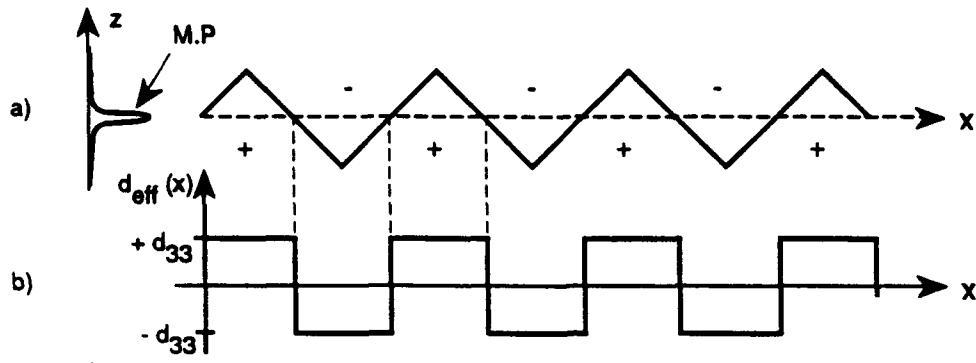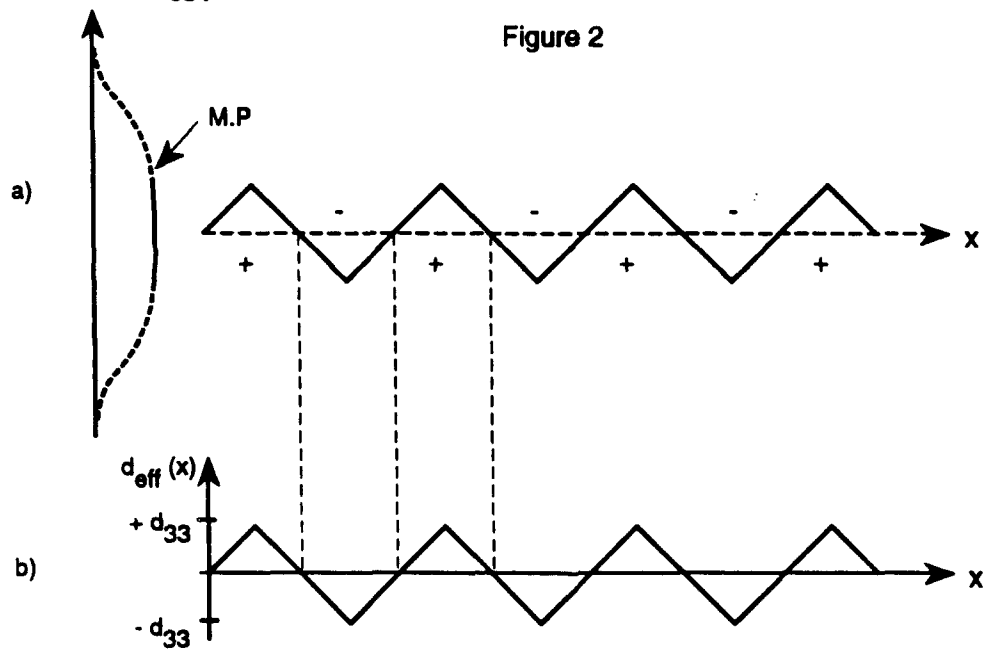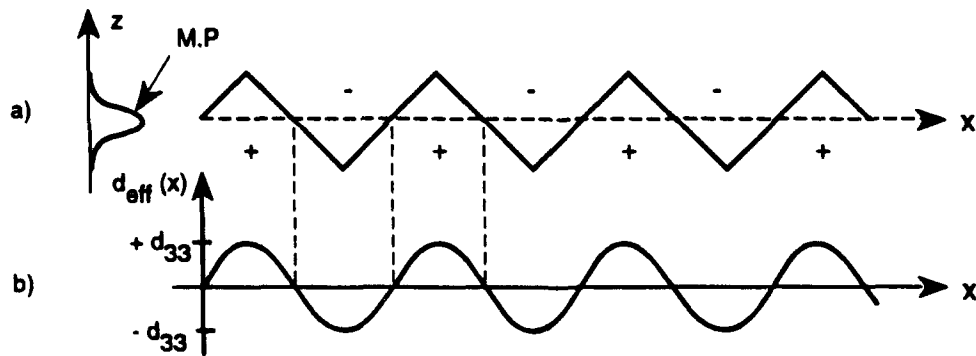
Figure 1

Figure 2

Figure 3

Figure 4

(M.P = Schematic representation of the fundamental and harmonic mode profiles)

Key To Author - Postdeadline

:imoto, K. - PD1
rmani, F. - PD2

:lacourt, D. - PD2

_ei, F - PD1

:uyama, H. - PD1

apuchon, Michel - PD2

TECHNICAL PROGRAM COMMITTEE

END

FILMED

DATE:

10-92

DTIC